A UNITED STATES DEPARTMENT OF COMMERCE PUBLICATION

SECTION A

JOURNAL OF RESEARCH

of the NATIONAL BUREAU OF STANDARDS

JNBAAR 76A (4) 321-373, July–Aug. 1972

Physics and Chemistry

U.S. DEPARTMENT OF COMMERCE
National Bureau of Standards

Journal of Research

of the

National Bureau of Standards

A. Physics and Chemistry

July–Aug. • 1972

VOLUME • 76A

NUMBER • 4

Editor: C. W. Beckett

Associate Editor: D. D. Wagman

Publication dates:
Feb. 1, Apr. 1, June 1, Aug. 1, Oct. 1, Dec. 1, 1972

J. Res. Nat. Bur. Stand. (U.S.), A

JOURNAL OF RESEARCH

The National Bureau of Standards Journal of Research reports research and development in the fields of activity shown at right. Also included from time to time are survey articles on topics closely related to the Bureau's scientific and technical program.

The Journal is published in two separate sections as follows:

A. Physics and Chemistry

Contains papers of interest primarily to scientists working in these fields. Issued six times a year. Annual subscription: domestic, $9.50; foreign $11.75. Single copy, varies.

B. Mathematical Sciences

Presents studies and compilations designed mainly for the mathematician and the theoretical physicist. Issued quarterly. Annual subscription: domestic, $5.00; foreign, $6.25. Single copy, $1.25.

The National Bureau of Standards[1] was established by an act of Congress March 3, 1901. The Bureau's overall goal is to strengthen and advance the Nation's science and technology and facilitate their effective application for public benefit. To this end, the Bureau conducts research and provides: (1) a basis for the Nation's physical measurement system, (2) scientific and technological services for industry and government, (3) a technical basis for equity in trade, and (4) technical services to promote public safety. The Bureau consists of the Institute for Basic Standards, the Institute for Materials Research, the Institute for Applied Technology, the Center for Computer Sciences and Technology, and the Office for Information Programs.

THE INSTITUTE FOR BASIC STANDARDS provides the central basis within the United States of a complete and consistent system of physical measurement; coordinates that system with measurement systems of other nations; and furnishes essential services leading to accurate and uniform physical measurements throughout the Nation's scientific community, industry, and commerce. The Institute consists of a Center for Radiation Research, an Office of Measurement Services and the following divisions:

Applied Mathematics—Electricity—Heat—Mechanics—Optical Physics—Linac Radiation[2]—Nuclear Radiation[2]—Applied Radiation[2]—Quantum Electronics[3]—Electromagnetics[3]—Time and Frequency[3]—Laboratory Astrophysics[3]—Cryogenics[3].

THE INSTITUTE FOR MATERIALS RESEARCH conducts materials research leading to improved methods of measurement, standards, and data on the properties of well-characterized materials needed by industry, commerce, educational institutions, and Government; provides advisory and research services to other Government agencies; and develops, produces, and distributes standard reference materials. The Institute consists of the Office of Standard Reference Materials and the following divisions:

Analytical Chemistry—Polymers—Metallurgy—Inorganic Materials—Reactor Radiation—Physical Chemistry.

THE INSTITUTE FOR APPLIED TECHNOLOGY provides technical services to promote the use of available technology and to facilitate technological innovation in industry and Government; cooperates with public and private organizations leading to the development of technological standards (including mandatory safety standards), codes and methods of test; and provides technical advice and services to Government agencies upon request. The Institute also monitors NBS engineering standards activities and provides liaison between NBS and national and international engineering standards bodies. The Institute consists of the following technical divisions and offices:

Engineering Standards Services—Weights and Measures—Flammable Fabrics—Invention and Innovation—Vehicle Systems Research—Product Evaluation Technology—Building Research—Electronic Technology—Technical Analysis—Measurement Engineering.

THE CENTER FOR COMPUTER SCIENCES AND TECHNOLOGY conducts research and provides technical services designed to aid Government agencies in improving cost effectiveness in the conduct of their programs through the selection, acquisition, and effective utilization of automatic data processing equipment; and serves as the principal focus within the executive branch for the development of Federal standards for automatic data processing equipment, techniques, and computer languages. The Center consists of the following offices and divisions:

Information Processing Standards—Computer Information—Computer Services—Systems Development—Information Processing Technology.

THE OFFICE FOR INFORMATION PROGRAMS promotes optimum dissemination and accessibility of scientific information generated within NBS and other agencies of the Federal Government; promotes the development of the National Standard Reference Data System and a system of information analysis centers dealing with the broader aspects of the National Measurement System; provides appropriate services to ensure that the NBS staff has optimum accessibility to the scientific information of the world, and directs the public information activities of the Bureau. The Office consists of the following organizational units:

Office of Standard Reference Data—Office of Technical Information and Publications—Library—Office of International Relations.

[1] Headquarters and Laboratories at Gaithersburg, Maryland, unless otherwise noted; mailing address Washington, D.C. 20234.
[2] Part of the Center for Radiation Research.
[3] Located at Boulder, Colorado 80302.

U.S. DEPARTMENT OF COMMERCE
Peter G. Peterson, Secretary
National Bureau of Standards,
Lawrence M. Kushner, Acting Director

Order all publications from the Superintendent of Documents
U.S. Government Printing Office, Washington, D.C. 20402

Use of funds for printing this publication approved by the Director of the Bureau of the Budget (June 22, 1966).

JOURNAL OF RESEARCH of the National Bureau of Standards—A. Physics and Chemistry
Vol. 76A, No. 4, July–August 1972

The EMF-Temperature Coefficient of "Acid" Standard Cells of the Saturated Cadmium Sulfate Type from 15 to 40° C

Walter J. Hamer, Anna Skapars, and Bruce F. Field

Institute for Basic Standards, National Bureau of Standards, Washington, D.C. 20234

(February 9, 1972)

This paper gives the results of new measurements of the effect of temperature on the electromotive force of standard cells of the saturated cadmium sulfate type. Measurements were made over the temperature range of 15 to 40 °C. Twelve cells of NBS manufacture and twenty-four cells supplied by two different commercial manufacturers were used in the studies. Final results were analyzed by the method of least squares using computer programs. The relation between emf and temperature for NBS, company 1, and company 2 cells was found to be given, respectively, by:

$$E_t = E_{20\,°C} - [40.44\,(t-20) + 0.921\,(t-20)^2 - 0.00866\,(t-20)^3] \times 10^{-6}\ \text{V},$$
$$E_t = E_{20\,°C} - [40.14\,(t-20) + 0.888\,(t-20)^2 - 0.00668\,(t-20)^3] \times 10^{-6}\ \text{V},$$
$$E_t = E_{20\,°C} - [39.28\,(t-20) + 0.986\,(t-20)^2 - 0.00943\,(t-20)^3] \times 10^{-6}\ \text{V}.$$

Values for the entropy and heat-capacity changes for the cell reaction in "acid" standard cells are also given.

Key words: EMF-temperature coefficients of standard cells; standard cells; entropy changes in standard cells; heat-capacity changes in standard cells; effect of acid on standard cells.

1. Introduction

In a recent paper [1][1] the thermodynamics of standard cells of the saturated cadmium sulfate type were given. That paper dealt with so-called "neutral" standard cells to which no sulfuric acid is intentionally added when the cell is constructed. The electromotive forces (emfs) were known in terms of the legal volt maintained by the National Bureau of Standards and the emf-temperature coefficient was that derived from the international formula [2, 3, 4] but converted to the V_{69} and t_{68} scales of voltage and temperature [1], respectively.

It is now common practice to add sulfuric acid in small amounts, between approximately 0.03 and 0.1 N (or 0.015 and 0.05 M), to standard cells to reduce the formation of the basic mercurous sulfate, $Hg_2O \cdot Hg_2SO_4$ which is formed in the hydrolysis of mercurous sulfate according to the equation:

$$2\,Hg_2SO_4(s) + H_2O(l) \rightleftharpoons Hg_2O \cdot Hg_2SO_4(s) + H_2SO_4(aq) \qquad (1)$$

where s = solid, l = liquid, and aq = aqueous. Gouy [5] and Hager and Hulett [6] found that the equilibrium concentration of H_2SO_4 formed in the hydrolysis of mercurous sulfate (eq (1)) was 0.002 N while Craig and Vinal [7] found it to be 0.00198 N at 0 °C and 0.00216 N at 28 °C thus showing that it did not change appreciably with temperature. Cadmium sulfate, the solute used to prepare the solution in a standard cell also hydrolyzes to form sulfuric acid, the equilibrium concentration being 0.00092 N at 25 °C [8]. This concentration is insufficient to prevent hydrolysis of mercurous sulfate although sometimes cadmium sulfate, especially if prepared from cadmium nitrate and sulfuric acid or digested with sulfuric acid, contains occluded sulfuric acid in sufficient amount to prevent the hydrolysis of mercurous sulfate and is therefore present through inadvertance. Usually, however, sulfuric acid in small amount is added to the cadmium sulfate electrolyte when the cells are constructed. Solutions 0.03 to 0.06 N with respect to sulfuric acid are generally used because mercurous sulfate exhibits a minimum solubility in the range from 0.04 to 0.08 N. Higher concentrations of acid cause excessive gassing at the cadmium-amalgam electrode.

Although the effect of the addition of sulfuric acid on the emf of saturated standard cells is well known [8, 9, 10, 11, 12, 13] published results do not agree as to the effect of the addition of sulfuric acid on the emf-temperature coefficient. Obata and Ishibashi [14] determined the emf-temperature coefficient of acid cells over a wide range of acidities, namely, 0.078 to 0.756 N and for temperatures from 15.67 to 29.57 °C and concluded that "the use of the acid electrolyte

[1] Figures in brackets indicate the literature references at the end of this paper.

has very little effect on the temperature coefficient of the cell; the cell containing an electrolyte acidified to 0.76 *N* [too high for emf stability] has a temperature coefficient only 11 percent larger than the neutral one." For 0.078 *N* their value of -42.5 μV for dE/dT at 20 °C may be compared with -40.64 μV for the neutral cell [1]; it is evident, therefore, that their results even for low acidity show that addition of acid increases the emf-temperature coefficient.

However, Vosburgh and Eppley [15] stated that a cell made with saturated cadmium sulfate to which 0.015 *M* sulfuric acid was added had the same emf-temperature coefficient as the neutral cell, while they later [16] stated that the change in emf between 25 and 35 °C for *some* cells with electrolytes containing 0.01 mol sulfuric acid per liter of solution is slightly less than that of neutral cells. Also later, Vosburgh [17] after measuring the emf of acid cells from 15 to 40 °C stated that "Wolff's temperature formula was found to hold for all [cells], the presence of acid being found to have little or no effect on the temperature coefficient." Vosburgh had used cells with sulfuric acid concentrations of 0.021, 0.035, 0.048, 0.064, and 0.078 mol per liter. Also the National Physical Laboratory [18] stated that the temperature coefficients of standard cells of acidities from 0.05 to 0.5 *N* show no particular correlation with the acidity.

At about the same time this latter work was done, the Electrotechnical Laboratory of Japan [12] also investigated the effect of acid on the emf-temperature coefficient of saturated standard cells; acidities ranged from 0.008 to 1.0 *N* and the temperature range was 15 to 30 °C. Ishibashi and Ishizaki [12] who conducted the investigation found that the emf-temperature coefficients of cells with electrolytes of low acidity were irregular and some of them were smaller than those for neutral cells. They also stated that "the cells acidified up to 0.08 mol/liter (0.16 *N*) have practically the same temperature coefficient of emf as given by Wolff and Waters' equation, so far as the accuracy of only 0.005 percent is required [i.e., the same as neutral cells]. The coefficient for separate cells, however, must be determined whenever the accuracy of about 0.001 percent is required."

Vigoureux and Watts [19] also measured the emf of "acid" cells as a function of temperature over the range of -20 to 40 °C. The solvent for the electrolyte, $CdSO_4 \cdot \frac{8}{3} H_2O$, in these cells was decinormal sulfuric acid; therefore, the cell acidity was 0.077 *N*. Vigoureux and Watts did not, however, give comparisons with "neutral" cells except to cite reference [18] to the effect that the acidity of the electrolyte does not affect the temperature coefficient to an appreciable extent.

2. Experimental Detail

Owing to the various results reported above on the emf-temperature coefficients of "acid" standard cells of the saturated cadmium sulfate type and the increased use of "acid" cells it was decided to make new measurements of the emf-temperature coefficient of the "acid" type of cell. Accordingly, 12 cells made at NBS in December 1955 were selected for the study. These cells were made with 10 percent cadmium amalgam, electrolytic mercurous sulfate, and crystals of $CdSO_4 \cdot \frac{8}{3} H_2O$ having a diameter of about 2 to 4 mm. The saturated solution of cadmium sulfate was acidified to 0.021 *N* by the addition of sulfuric acid. The cells were of the H-form and were assembled as outlined in reference [8]; see also references [20] and [21] for descriptions of the preparations of saturated standard cells at the National Bureau of Standards. These cells were also used in 1966 in the transfer of the "volt standard" from the old NBS site in Washington to the new NBS site in Gaithersburg, Md. [22, 23].

In addition two different manufacturers of standard cells each supplied 12 "acid" saturated standard cells for the study. These are subsequently referred to as commercial 1 cells or C1 cells and as commercial 2 cells or C2 cells. These cells were about 2 years old at the start of the study. They were also of the H-form and were made with 10 percent cadmium amalgam and electrolytic mercurous sulfate. The C1 cells had a stated acidity of 0.061 *N* (except cell C1B which was replaced by one of acidity of 0.044 *N* for the measurements in Gaithersburg, Md.; the former one of acidity of 0.061 *N* was broken in transit from Washington, D.C. to Gaithersburg, Md.) and were made with crystals of $CdSO_4 \cdot \frac{8}{3} H_2O$ of 4, 8, and 10 mm in diameter. The C2 cells had a stated acidity of 0.025 *N* and the crystals of $CdSO_4 \cdot \frac{8}{3} H_2O$ over the mercurous sulfate paste had a consistency of granulated sugar while those over the amalgam consisted of a mixture of crystals of the consistency of granulated sugar and of larger crystals about 8 mm in diameter. The depth of mercurous paste was about 1.3 cm in NBS cells, 1.5 cm in C1 cells, and 1.7 cm in C2 cells.

Studies of the effect of temperature on the emf of these 36 cells were started in December 1961. The cells were housed in an oil bath maintained within ± 0.001 °C at each of the temperatures used in the study on the day measurements of the emf were made. The temperatures were read with a calibrated Pt-resistance thermometer and the emfs were measured to 0.1 μV with a Brooks comparator [24]. After a change in temperature the cells were maintained at least one week at the new temperature before readings of the emf were taken. At least ten readings over a period of two weeks were made at each temperature. The sequence of the temperatures, the groups of cells used at each temperature, and the time interval from the termination of the last of the initial readings at 28 °C to the time of the last readings at subsequent temperatures are given in table 1.

Various interruptions, most notably the move of NBS from Washington, D.C. to Gaithersburg, Md., in 1966, delayed completion of the study until September,

TABLE 1. *Sequence of measurements*

Sequence of temperatures	Groups of cells	Time intervals (days)* for		
		NBS cells	C1 cells	C2 cells
Washington, D.C.				
28 °C	NBS, C1, C2	0	0	0
32 °C	NBS, C1, C2	42	59	44
35 °C	NBS, C1, C2	108	105	108
38 °C	NBS, C1, C2	147	147	147
40 °C	NBS, C1, C2	190	197	190
35 °C	NBS, C1, C2	253	266	265
28 °C	NBS, C1, C2	351	352	351
20 °C	NBS, C1, C2	506	507	506
20 °C	NBS, C1, C2	625	629	628
25 °C	NBS, C1, C2	741	742	741
Gaithersburg, Md.				
15 °C	C1, C2	.....	1938	1937
25 °C	NBS	2246	.....	.....
20 °C	NBS	2303	.....	.....
15 °C	NBS	2414	.....	.....

*From final date at one temperature to final date at subsequent temperature.

1968. Owing to the time period, about 7 years, consumed in the study, the cells showed slight drifts in emf with time. These were made evident by comparing the mean emf of the 12 cells of each group at those temperatures where second sets of measurements were made. The average changes or drift rates were found to be 3.62×10^{-9} V/day for the NBS cells,[2] 2.71×10^{-9} V/day for the C1 cells, and 9.6×10^{-10} V/day for the C2 cells.

First the observed emfs without drift-rate corrections were fitted to the third-order equation:[3]

$$E_t = E_{20\,°C} + \alpha(t-20) + \beta(t-20)^2 + \gamma(t-20)^3 \tag{2}$$

by the method of least squares using a computer program: $E_{20\,°C}$ is the emf at 20 °C and α, β, and γ are constants. The values of α, β, and γ for the NBS, C1, and C2 cells are given, respectively, in tables 2, 3, and 4. The mean standard deviations are given for α, β, and γ and the uncertainties in the fit, 1σ, are standard deviations of the fit of the data to equation (2). Corrections for drifts in emf with time were then made for each cell. These were obtained from the equation:

$$E' - E = \Delta E = \alpha'(t-20) + \beta'(t-20)^2 + \gamma'(t-20)^3 \tag{3}$$

where E' is the corrected emf and $\alpha' = \alpha+\Delta$, $\beta' = \beta+\Delta$, and $\gamma' = \gamma+\Delta$ with Δ being the correction to the constants of eq (2). The final values for the constants for each cell and the averages are given within the parentheses in tables 2, 3, and 4.

Final recommended values for α, β, and γ for each type of cell are given at the bottom of tables 2, 3, and 4; data for cell C2J were omitted in arriving at a final value owing to the large standard deviation of the fit to eq (2). Thus, for NBS cells of 0.021 N acidity,

$$E_t = E_{20\,°C} - [40.44(t-20) + 0.921(t-20)^2 - 0.00866(t-20)^3] \times 10^{-6}\text{V} \tag{4}$$

TABLE 2. *Coefficients in the equation:* $E = E_{20°C} + \alpha(t-20) + \beta(t-20)^2 + \gamma(t-20)^3$ *for National Bureau of Standards cells*

Cell No.	$E_{20\,°C}$ V	(On V_{69} and t_{68} scales)			
		α μV	β μV	γ μV	σ μV
NBS1157	#[a] 1.0186569(4)	*– 40.4096(.01)	*– 0.9271(.008)	*0.0077(.00070)	1.3194
NBS1158	1.0186598(3)	– 40.4076(.01)	– 0.9498(.003)	.0086(.00061)	1.2891
NBS1159	1.0186597(3)	– 40.4971(.01)	– 0.9304(.007)	.0080(.00069)	1.3941
NBS1160	1.0186599(4)	– 40.4061(.01)	– 0.9260(.005)	.0077(.00063)	1.0890
NBS1161	1.0186619(6)	– 40.7635(.02)	– 0.9221(.010)	.0080(.00136)	1.9925
NBS1162	1.0186507(3)	– 40.2162(.01)	– 0.9216(.003)	.0075(.00060)	1.0133
NBS1163	1.0186528(2)	– 40.3923(.01)	– 0.9194(.002)	.0077(.00054)	1.4056
NBS1164	1.0186580(6)	– 40.6369(.01)	– 0.9221(.008)	.0081(.00099)	1.7193
NBS1165	1.0186529(4)	– 40.6680(.01)	– 0.8893(.008)	.0069(.00070)	1.5041
NBS1166	1.0186549(1)	– 40.7567(0)	– 0.8840(0)	.0067(.00032)	1.3328
NBS1167	1.0186602(6)	– 40.1705(.01)	– 1.0128(.009)	.0114(.00104)	2.3725
NBS1168	1.0186537(2)	–40.1258(0)	– 0.9170(.001)	.0071(.00035)	0.5679
mean	1.0186564(4)	– 40.4542(.01)	– 0.9268(.005)	.0080(.00071)	.....
σ_m	.....	0.0630	0.0093	.00035	1.4847
final	.....	– 40.44	– 0.921	0.00866	1.5

Values within parentheses are negative.
* All values within parentheses are positive corrections for drift in emf with time.
[a] Values in parentheses for this column are corrections for the last decimals in the emf or should be multiplied by 10^{-7}.

[2] Earlier observations, from December 1955 to December 1961 also gave this drift rate for these cells.

[3] Inspections showed that a second-order equation was inadequate whereas a fourth-order equation gave no better fit to the experimental data than a third-order equation.

TABLE 3. *Coefficients in the equation:* $E = E_{20\,°C} + \alpha\,(t-20) + \beta\,(t-20)^2 + \gamma\,(t-20)^3$ *for Company 1 cells*

Cell No.	$E_{20\,°C}$ V	(On V_{69} and t_{68} scales)			
		α μV	β μV	γ μV	σ μV
C1A	# [a] 1.0186005(8)	*−40.1148(0)	*−0.8902(.001)	*0.0061(.00008)	0.4947
C1B	1.0185969(24)	−40.5868(0)	−0.8039(.001)	.0031(.00033)	.4359
C1C	1.0185995(27)	−40.1137(.01)	−0.8963(.001)	.0064(.00035)	.6385
C1D	1.0186021(43)	−40.2768(.01)	−0.8933(.003)	.0065(.00050)	.8085
C1E	1.0185992(45)	−40.4774(.01)	−0.8608(.003)	.0055(.00054)	.6251
C1F	1.0186026(51)	−40.3271(.01)	−0.9174(.004)	.0073(.00058)	.7664
C1G	1.0186006(32)	−40.0042(.01)	−0.9063(.001)	.0067(.00042)	.2867
C1H	1.0186011(61)	−40.1528(.01)	−0.8850(.007)	.0060(.00059)	.3872
C1I	1.0186007(40)	−39.9425(.01)	−0.9064(.002)	.0067(.00050)	.4037
C1J	1.0186000(32)	−39.8191(.01)	−0.9244(.001)	.0072(.00042)	.7741
C1K	1.0185987(37)	−39.9253(.01)	−0.9095(.002)	.0067(.00046)	.7795
C1L	1.0185999(67)	−40.0702(.01)	−0.9015(.008)	.0067(.00062)	.5839
mean	1.0186002(38)	−40.1509(.01)	−0.8913(.003)	.0062(.00044)	.....
σ_m	.....	0.0662	0.0093	0.00029	0.6067
final	.....	−40.14	−0.888	0.00668	0.6

Values within parentheses are negative
*All values within parentheses are positive corrections for drift in emf with time.
[a] Values in parentheses for this column are corrections for the last decimals in the emf or should be multiplied by 10^{-7}.

TABLE 4. *Coefficients in the equation:* $E = E_{20\,°C} + \alpha\,(t-20) + \beta\,(t-20)^2 + \gamma\,(t-20)^3$ *for Company 2 cells*

Cell No.	$E_{20\,°C}$ V	(On V_{69} and t_{68} scales)			
		α μV	β μV	γ μV	σ μV
C2A	[a] 1.0186219(52)	*−38.8723(.01)	−1.0420(.005)	0.0109(.00060)	1.9416
C2B	#1.0186231(21)	−39.6109(0)	−0.9413(.001)	.0075(.00031)	1.1653
C2C	1.0186221(4)	−39.4001(0)	−0.9683(0)	.0084(.00007)	1.5217
C2D	#1.0186220(10)	−40.2280(0)	−0.8616(0)	#.0051(.00018)	0.8837
C2E	1.0186223(31)	−38.9803(.01)	−1.0480(.001)	.0112(.00045)	1.7775
C2F	1.0186214(31)	−39.3767(.01)	−0.9904(.001)	.0095(.00045)	1.3334
C2G	1.0186254(15)	−39.2822(0)	−0.9942(.001)	.0094(.00020)	1.6330
C2H	1.0186199(23)	−38.9568(.01)	−1.0350(.001)	.0106(.00031)	1.8220
C2I	#1.0186169(42)	−40.2187(.01)	−0.8390(.003)	.0040(.00053)	2.0724
C2J	#1.0186041(368)	#−39.9149(1.45)	#−0.7728(.240)	.0008(.00950)	7.2131
C2K	1.0186217(46)	−38.5832(.01)	−1.0853(.004)	.0124(.00054)	2.5660
C2L	#1.0186218(4)	−38.7256(0)	−1.0649(0)	#.0115(.00007)	2.3618
mean	#1.0186202(20)	#−39.3458(.12)	#−0.9702(.019)	.0084(.00035)	.....
σ_m	.....	0.1669	0.0262	.00101	2.7024
mean-C2J	1.0186217(11)	−39.2941(.01)	−0.9882(.002)	.0091(.00029)	.....
σ_m	.....	0.1669	0.0243	.00081	1.7991
final	.....	−39.28	−0.986	.00943	1.8

Values within parentheses are negative.
*All values within parentheses are positive corrections for drift in emf with time unless noted.
[a] Values in parentheses for this column are corrections for the last decimals in the emf or should be multiplied by 10^{-7}.

for C1 cells of 0.061 *N* acidity,

$$E_t = E_{20\,°C} - [40.14(t-20) + 0.888(t-20)^2 - 0.00668(t-20)^3] \times 10^{-6}\text{V} \quad (5)$$

for C2 cells of 0.025 *N* acidity,

$$E_t = E_{20\,°C} - [39.28(t-20) + 0.986(t-20)^2 - 0.00943(t-20)^3] \times 10^{-6}\text{V}. \quad (6)$$

At about the same time covered by this investigation, Froehlich and Melchert, with the assistance of Steiner, in the laboratories of the Physikalisch-Technische Bundesanstalt, also carried out a study of the emf-temperature coefficient of "acid" standard cells over the range of 10 to 30 °C and published their results in April, 1971 [25]. The pH of the electrolyte used in the cells was 1.4 ± 0.2; the hydrogen-ion activity was, therefore, of the order of 0.04. No concentration value was given; from known values of the activity coefficient of saturated cadmium sulfate solution, namely, 0.03641 [1] and of sulfuric acid of the same ionic strength, namely, 0.208 [26], and the density of the saturated solution [27] the normality calculated from the pH value given by Froehlich and Melchert would appear to be about 0.26 *N*. However, the emfs given for 20 °C by Froehlich and Melchert indicate

that the acidity was about 0.03–0.04 *N*. Ten cells were used in the study, two each of about three, four, five, seven, and nine years old at the time of the measurements. The emfs at 20 °C ranged from 1.0186053 V to 1.0186457 V; no correlation with pH was given, however, a relation between E and dE/dT may be calculated from their data and is shown later.

From the results obtained for the ten cells over a temperature range of 10 to 30 °C and taking cognizance of drifts in emf with time, Froehlich and Melchert [25] arrived at:

$$E_t = E_{20\,°C} - [39.78(t-20) + 0.936(t-20)^2 - 0.0086(t-20)^3] \times 10^{-6}\text{V} \quad (7)$$

for the relation between emf and temperature.

In table 5, values for dE/dT from 15 to 40 °C are given for NBS, C1, and C2 cells. The standard deviation, σ, of an individual value and the standard deviation of the mean, σ_m, are also given. The values of dE/dT given by the international formula (Int), the equation of Vigoureux and Watts (VW), and of Froehlich and Melchert (FM) are given for comparison. Also the mean emfs are given at the bottom of the table.

Inspection of the data shows that there is no correlation between dE/dT and the normality of the solution. This is clearly shown in figure 1 for values of dE/dT at 20 °C; similar results are found for the other temperatures. It is evident, as was stated earlier by Ishibashi and Ishizaki [12] that the emf-temperature coefficients of cells with electrolytes of low acidity are irregular. Since the emf is decreased by the addition of acid it remains that dE/dT may be a function of the emf. This is shown not to be the case in figure 2 where dE/dT at 20 °C is plotted against the emf at 20 °C; 10.5 μV (see ref. [8] for this factor) were subtracted from the emfs of Ishibashi and Ishizaki to place their emfs on the United States of America base of reference for the volt. It is evident from figure 2 that there is no clear correlation between E and dE/dT over the acidity range of 0 to 0.06 *N*. As also stated earlier by Ishibashi and Ishizaki for a precision of 0.005 percent the addition of acid has little or no effect on dE/dT while for a precision of 0.001 percent the individual values of dE/dT must be experimentally determined. Furthermore, drift rates must be determined if the highest precision is required.

One point is significant in figure 2, namely, that some of the emf data of NBS and ETL at 20 °C exceed that normally attributed to "neutral" cells and that some of the emfs reported by Froehlich and Melchert are very close to that for the so-called "neutral" cell. The international value of the emf of "neutral" cells was based on the measurements made with cells with chemically prepared and with dc-electrolytic mercurous sulfate. Wolff and Waters [2] showed that dc-electrolytic mercurous sulfate, on the average, gave cells with emfs exceeding by 16.8 μV those made with chemically prepared mercurous sulfate. Since dc-electrolytic mercurous sulfate was used in the cells discussed herein, this value of 16.8 μV was added to the international value and is designated as "corrected emf" in figure 2. With this correction the emfs of the NBS cells approximate that of the so-called "neutral" cell; apparently, the acid in the cells is largely neutralized by the alkaline constituent of the glass container during the aging period (this is exhibited by the upward drift in emf with time, as mentioned earlier in this paper).

Finally in table 6 values of the second derivative, d^2E/dT^2, and in table 7 values of the entropy and heat-capacity changes for the cell reaction in "acid"

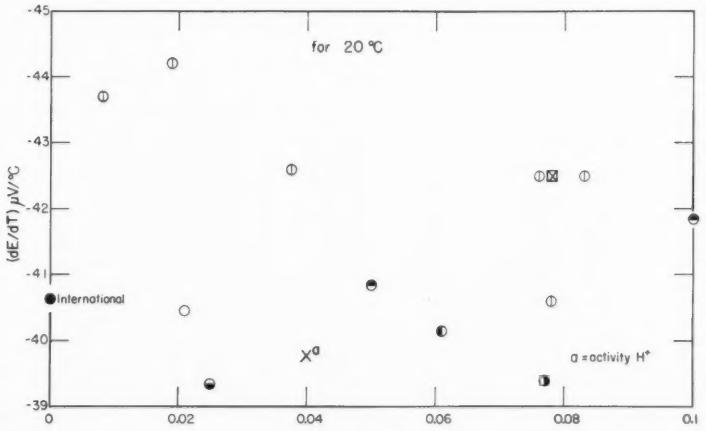

FIGURE 1. *Emf-temperature coefficients of saturated standard cells and the normality of sulfuric acid in the electrolyte in the cell.*

○—National Bureau of Standards [1].
◓—National Physical Laboratory [18].
◑—Electrotechnical Laboratory, Tokyo [12].
×—Physikalisch-Technische Bundesanstalt [25].
◑—Vigoureux and Watts [19].
⊠—Obata and Ishibashi [14].
◐—Company 1.
◒—Company 2.
●—International formula [2,3,4].

TABLE 5. *Emf-temperature coefficients of "acid" standard*

No.*	15 °C			20 °C			25 °C		
	NBS	C1	C2	NBS	C1	C2	NBS	C1	C2
1	−30.60	−30.76	−27.63	−40.42	−40.11	−38.86	−48.98	−48.54	−48.37
2	−30.24	−32.30	−29.62	−40.40	−40.59	−39.61	−49.17	−48.36	−48.43
3	−30.60	−30.64	−29.08	−40.49	−40.10	−39.40	−49.07	−48.55	−48.45
4	−30.56	−30.84	−31.24	−40.40	−40.27	−40.23	−48.98	−48.64	−48.48
5	−30.92	−31.44	−27.63	−40.74	−40.47	−38.97	−49.16	−48.59	−48.57
6	−30.41	−30.59	−28.73	−40.21	−40.32	−39.37	−48.78	−48.86	−48.51
7	−30.59	−30.41	−28.63	−40.38	−39.99	−39.28	−48.94	−48.51	−48.49
8	−30.80	−30.87	−27.79	−40.63	−40.14	−38.95	−49.09	−48.43	−48.47
9	−31.28	−30.35	−31.51	−40.66	−39.93	−40.21	−48.90	−48.44	−48.23
10	−31.39	−30.00	[c](−30.46)	−40.76	−39.81	[c](−41.36)	−49.07	−48.47	[c](−50.72)
11	−29.19	−30.30	−26.79	−40.16	−39.92	−38.57	−49.27	−48.45	−48.42
12	−30.41	−30.58	−27.22	−40.13	−40.06	−38.73	−48.73	−48.45	−48.52
mean	−30.58	−30.76	[c]−28.72	−40.45	−40.14	[c]−39.29	−49.01	−48.52	[c]−48.45
σ	0.557	0.410	1.559	0.216	0.232	0.554	0.159	0.092	0.090
σ_m	.161	.118	.470	.062	.067	.167	.046	.027	.027
Int.		[a]−30.39(.04)			−40.64(.04)			−40.39(.04)	
VW		[b]−29.79(.71)			−39.40(.55)			−48.02(.55)	
FM		[a]−29.78(.06)			−39.78(.05)			−48.50(.03)	
E(NBS)		1.0188353			1.0186572			1.0184331	
E(C1)		1.0187817			1.0186040			1.0183819	
E(C2)		[c]1.0187934			[c]1.0186228			[c]1.0184029	
FM		1.0187982			1.0186238			1.0184026	
Int.		1.0188224			1.0186442			1.0184185	

* Numbers are in sequence for cells NBS, C1, and C2 given in tables 2, 3, and 4.
[a] Values in parentheses are σ_m, standard deviation of the mean.
[b] Maximum uncertainty of deviations from given formula.
[c] Eleven cells only; data for cell No. 10 omitted.
[d] Vigoureux and Watts gave only the differences between emfs at a particular temperature and emfs of reference cells at 20 °C.

TABLE 6. *The second derivative,* d^2E/dT^2

No.*	15 °C			20 °C			25 °C		
	NBS	C1	C2	NBS	C1	C2	NBS	C1	C2
1	−2.090	−1.964	−2.419	−1.838	−1.778	−2.074	−1.586	−1.593	−1.729
2	−2.170	−1.711	−2.115	−1.894	−1.606	−1.881	−1.617	−1.501	−1.646
3	−2.108	−1.993	−2.191	−1.847	−1.791	−1.937	−1.586	−1.588	−1.683
4	−2.092	−1.991	−1.871	−1.842	−1.781	−1.723	−1.592	−1.571	−1.676
5	−2.105	−1.897	−2.444	−1.824	−1.716	−2.094	−1.543	−1.534	−1.745
6	−2.080	−2.063	−2.277	−1.837	−1.827	−1.979	−1.594	−1.590	−1.680
7	−2.082	−2.024	−2.274	−1.835	−1.811	−1.986	−1.588	−1.597	−1.698
8	−2.101	−1.954	−2.395	−1.828	−1.756	−2.068	−1.556	−1.558	−1.741
9	−1.991	−2.025	−1.808	−1.763	−1.809	−1.672	−1.535	−1.593	−1.536
10	−1.979	−2.075	(−2.335)	−1.768	−1.847	(−2.026)	−1.557	−1.618	(−1.717)
11	−2.381	−2.030	−2.551	−2.008	−1.815	−2.163	−1.634	−1.600	−1.774
12	−2.056	−2.004	−2.473	−1.832	−1.787	−2.130	−1.509	−1.570	−1.787
mean	−2.103	−1.978	[c]−2.256	−1.843	−1.777	[c]−1.973	−1.575	−1.576	[c]−1.709
σ	0.088	0.096	0.212	0.058	0.064	0.159	0.036	0.031	0.070
σ_m	.025	.028	.067	.017	.019	.048	.010	.009	.021
Int.		[a]−2.200(.005)			−1.900(.003)			−1.600(.003)	
VW		[b]−2.049(.08)			−1.806(.06)			−1.653(.06)	
FM		−2.130(.007)			−1.872(.004)			−1.614(.007)	

*Numbers are in sequence for cells NBS, C1, and C2 given in tables 2, 3, and 4.
[a] Values in parentheses are σ_m, standard deviation of the mean.
[b] Maximum uncertainty of deviations from given formula.
[c] Eleven cells only; data for cell No. 10 omitted.

cells of the saturated cadmium sulfate type, μV/°C

30 °C			35 °C			40 °C		
NBS	C1	C2	NBS	C1	C2	NBS	C1	C2
− 56.28	− 56.04	− 56.15	− 62.32	− 62.62	− 62.21	− 67.10	− 68.27	− 66.54
− 56.57	− 55.62	− 56.07	− 62.58	− 62.36	− 62.55	− 67.22	− 68.59	− 67.85
− 56.35	− 55.98	− 56.23	− 62.32	− 62.41	− 62.73	− 67.00	− 67.82	− 67.97
− 56.32	− 55.97	− 55.98	− 62.40	− 62.25	− 62.76	− 67.24	− 67.48	− 68.79
− 56.18	− 55.81	− 56.42	− 61.79	− 62.12	− 62.52	− 66.00	− 67.53	− 66.87
− 56.15	− 56.22	− 56.17	− 62.30	− 62.40	− 62.33	− 67.23	− 67.40	− 67.00
− 56.08	− 55.96	− 56.27	− 62.34	− 62.35	− 62.60	− 67.19	− 67.66	− 67.49
− 56.18	− 55.73	− 56.35	− 61.91	− 62.03	− 62.60	− 66.28	− 67.35	− 67.21
− 56.00	− 55.86	− 55.57	− 61.97	− 62.20	− 62.23	− 66.79	− 67.47	− 68.21
− 56.33	− 55.99	[c](− 58.53)	− 62.54	− 62.37	[c](− 64.80)	− 67.69	− 67.60	[c](− 69.52)
− 56.50	− 55.92	− 56.32	− 61.88	− 62.31	− 62.28	− 66.75	− 67.62	− 66.30
− 56.21	− 55.76	− 56.59	− 62.58	− 61.98	− 62.96	− 67.83	− 67.12	− 67.61
− 56.26	− 55.91	[c]− 56.19	− 62.24	− 62.28	[c]− 62.52	− 67.03	− 67.66	[c]− 67.44
0.165	0.160	0.262	0.284	0.179	0.241	0.521	0.405	0.688
.048	.046	.079	.082	.052	.073	.150	.117	.297
	− 56.63(.04)			− 62.37(.06)			− 66.60(.09)	
	[e]− 56.10(.63)			[e]− 64.08(.70)			[e]− 72.41(.70)	
	− 55.92							
Electromotive forces [d]								
	1.0181694			1.0178726			1.0175493	
	1.0181205			1.0178246			1.0174994	
	[c] 1.0181408			[c] 1.0178436			[c] 1.0175182	
	1.0181410							
	1.0181528			1.0178547			1.0175317	

[e] Based on four cells only; Vigoureux and Watts considered their results above 28 °C to be less reliable than those for lower temperatures.
Int. International formula [2, 3, 4].
VW Vigoureux and Watts [19].
FM Froehlich and Melchert [25].

for saturated standard cells, μV/°C/°C

30 °C			35 °C			40 °C		
NBS	C1	C2	NBS	C1	C2	NBS	C1	C2
− 1.334	− 1.408	− 1.384	− 1.082	− 1.222	− 1.039	− 0.830	− 1.037	− 0.694
− 1.341	− 1.396	− 1.412	− 1.065	− 1.291	− 1.078	− 0.788	− 1.186	− 0.943
− 1.325	− 1.386	− 1.428	− 1.065	− 1.183	− 1.174	− 0.804	− 0.981	− 0.920
− 1.342	− 1.361	− 1.428	− 1.092	− 1.151	− 1.280	− 0.842	− 0.941	− 1.133
− 1.263	− 1.353	− 1.395	− 0.982	− 1.172	− 1.046	− 0.701	− 0.991	− 0.696
− 1.351	− 1.354	− 1.381	− 1.108	− 1.118	− 1.083	− 0.865	− 0.881	− 0.784
− 1.340	− 1.383	− 1.410	− 1.093	− 1.170	− 1.122	− 0.846	− 0.956	− 0.834
− 1.283	− 1.361	− 1.413	− 1.010	− 1.163	− 1.086	− 0.737	− 0.965	− 0.759
− 1.307	− 1.377	− 1.400	− 1.079	− 1.161	− 1.264	− 0.851	− 0.945	− 1.128
− 1.347	− 1.390	(− 1.408)	− 1.136	− 1.161	(− 1.099)	− 0.926	− 0.932	(− 0.790)
− 1.261	− 1.385	− 1.386	− 0.888	− 1.171	− 0.998	− 0.515	− 0.956	− 0.610
− 1.385	− 1.353	− 1.444	− 1.162	− 1.136	− 1.101	− 0.938	− 0.919	− 0.758
− 1.323	− 1.392	− 1.408	− 1.072	− 1.177	− 1.116	− 0.804	− 0.974	− 0.842
0.038	0.080	0.020	0.068	0.044	0.105	0.113	0.077	0.172
.011	.023	.006	.020	.013	.032	.033	.022	.052
	− 1.300(.003)			− 1.000(.005)			− 0.700(.008)	
	− 1.590(.07)			[d]− 1.617(.08)			[d]− 1.734(.09)	
	− 1.356(.013)							

[d] Vigoureux and Watts gave only differences between emfs at a particular temperature and emf of reference cells at 20 °C.
Int. International formula [2, 3, 4].
VW Vigoureux and Watts [19].
FM Froehlich and Melchert [25].

TABLE 7. *Entropy and heat-capacity changes for the reaction in "acid" standard cells of the saturated cadimum sulfate type*

	Entropy changes, J K^{-1} mol^{-1}						
	Acidity N	15 °C	20 °C	25 °C	30 °C	35 °C	40 °C
International [2,3,4]	0.00092	−5.86	−7.84	−9.53	−10.93	−12.04	−12.85
NBS	.021	−5.90	−7.81	−9.46	−10.86	−12.01	−12.94
FM	*	−5.75	−7.68	−9.36	−10.79		
C2	.025	−5.54	−7.58	−9.35	−10.84	−12.06	−13.01
C1	.061	−5.94	−7.75	−9.36	−10.79	−12.02	−13.06
VW	.077	−5.75	−7.60	−9.27	[a](−10.83)	[a](−12.37)	[a](−13.97)
Thermochemical [1]	0			−9.58			
		Heat-capacity changes, J K^{-1} mol^{-1}					
International [2,3,4]	0.00092	−122.33	−107.48	−92.06	−76.05	−59.46	−42.30
NBS	.021	−116.94	−104.26	−90.62	−77.40	−63.75	−48.59
FM	*	−118.44	−105.90	−92.86	−79.33		
C2	.025	−125.45	−111.71	−98.33	−82.37	−66.36	−50.88
C1	.061	−109.99	−101.64	−90.68	−81.43	−69.99	−58.96
VW	.077	−113.94	−102.17	−95.10	[a](−93.02)	[a](−96.15)	[a](−104.79)
Thermochemical [1]	0			−93.72			

* pH = 1.4 ± 0.2; $a_{H^+} \approx 0.04$.
[a] Based on four cells only [19].

International—International formula [2,3,4].
FM Froehlich and Melchert [25].
VW Vigoureux and Watts [19].

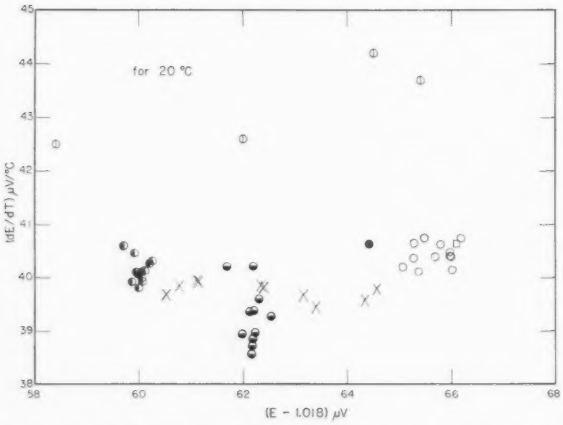

FIGURE 2. *Emf-temperature coefficients of saturated standard cells and the emf of the cell.*

○—National Bureau of Standards [1].
◐—Electrotechnical Laboratory, Tokyo [12].
×—Physikalisch-Technische Bundesanstalt [25].
◑—Company 1.
◒—Company 2.
●—International formula [2,3,4].
□—Corrected international emf.

standard cells are given. The entropy change for the "acid" cells is in all cases less than those observed for the so-called "neutral" cell while the heat-capacity change for "acid" cells relative to the "neutral" cell is less well defined.

3. References

[1] Hamer, W. J., J. Res. Nat. Bur. Stand. (U.S.), 76A (Phys. and Chem.), No. 3, 185–205 (May-June 1972).
[2] Wolff, W. A., and Waters, C. E., Bull. BS **4,** 70 (1907).
[3] Wolff, W. A., Bull. BS **5,** 309 (1908).
[4] International conference on electrical units and standards, Appendix to report: Notes to the specifications as to the methods adopted in various standardizing laboratories to realize the international ohm and the international ampere, and to prepare the Weston Normal Cell (Darling & Sons, Ltd., London, 1908).
[5] Guoy, M., Compt. rendu. **130,** 1399 (1900).
[6] Hager, O. B., and Hulett, G. A., J. Phys. Chem. **36,** 2095 (1932).
[7] Craig, D. N., and Vinal, G. W., J. Res. NBS **17,** 709 (1936)RP939.
[8] Hamer, W. J., Standard cells, their construction, maintenance, and characteristics, NBS Monograph 84, 1965.
[9] Smith, F. E. (Sir Frank), A Dictionary of Applied Physics, p. 268, Ed. Sir Richard Glazabrook, (Macmillan and Co., Ltd., London, 1911).
[10] Report of Natl. Phys. Lab., Electrician **75,** 463 (1915).
[11] Obata, J., Proc. Math. Phys. Soc. (Japan), (3), **2,** 232 (1920).
[12] Ishibashi, V., and Ishizaki, T., Researches Electrotechnical Lab., No. 318 (1931).
[13] Vosburgh, W. C., J. Am. Chem. Soc. **47,** 1255 (1925).
[14] Obata, J., and Ishibashi, V., Researches Electrotechnical Lab., No. 88 (1921).
[15] Vosburgh, W. C., and Eppley, M., J. Am. Chem. Soc. **45,** 2268 (1923).
[16] Vosburgh, W. C., and Eppley, M., J. Am. Chem. Soc. **46,** 110 (1924).
[17] Vosburgh, W. C., J. Opt. Soc. & Rev. Sci. Instrument **12,** 511 (1926).
[18] Rapport, Comité Consultatif d'Electricité Procès-Verbaux des Séances de 1930, in Procès-Verbaux des Séances, Comité International des Poids et Mesures Deuxième Série-Tome XIV, p. 171, 1931.
[19] Vigoureux, P., and Watts, S., Proc. Phys. Soc. (London) **45,** 172 (1933).
[20] Brickwedde, L. H., Compt. rendus Quatorzième Conférence IUPAC, p. 105, London, 1947.
[21] Hamer, W. J., and Law, C. A., Comité Consultatif d'Electricité, **11**e Ses, Doc. No. 5, May 10–12, 1965.
[22] Hamer, W. J., J. Wash. Acad. Sci. **56,** 101 (1966).
[23] Hamer, W. J., Inst. Soc. Am., M2–1–Mestind–67, 1967.
[24] Brooks, H. B., BS J. Res. **11,** 211 (1933).
[25] Froehlich, M., and Melchert, F., with Steiner, O., Metrologia **7,** No. 2, 58 (1971).
[26] Harned, H. S., and Hamer, W. J., J. Am. Chem. Soc. **57,** 27 (1935).
[27] International critical tables **3,** 66 (1928).

(Paper 76A4–723)

JOURNAL OF RESEARCH of the National Bureau of Standards — A. Physics and Chemistry
Vol. 76A, No. 4, July–August 1972

Pulse Radiolysis of Neopentane in the Gas Phase*

R. E. Rebbert and P. Ausloos

Institute for Materials Research, National Bureau of Standards, Washington, D.C. 20234

(February 9, 1972)

The pulse radiolysis of gaseous neopentane has been investigated in the absence and presence of electron scavengers (SF_6, CD_3I, CCl_4). Deuterium labeling experiments show that the stable product molecules can be accounted for by (a) radical combination reactions involving mainly CH_3 and H; (b) hydride ion transfer reactions involving $C_2H_3^+$, $C_2H_5^+$, and $C_3H_5^+$; (c) neutralization reactions of $C_4H_9^+$ and $C_5H_{11}^+$; and (d) unimolecular dissociation of the parent ion ($C_5H_{12}^+$) and of electronically excited neopentane. Neutralization of the t-$C_4H_9^+$ ion, which is the major positive ion in the system occurs as follows: (a) $t\text{-}C_4H_9^+ + e \rightarrow i\text{-}C_4H_8 + H$ and (b) $t\text{-}C_4H_9^+ + e \rightarrow 2CH_3 + C_3H_6$. It is shown that $C_5H_{11}^+$ produced in hydride ion transfer reaction $C_nH_m^+ + \text{neo-}C_5H_{12} \rightarrow C_nH_{m+1} + C_5H_{11}^+$ (where $C_nH_m^+ = C_2H_3^+$, $C_2H_5^+$, and $C_3H_5^+$) rearranges to the $CH_3C^+(CH_3)CH_2CH_3$ structure prior to neutralization. A detailed accounting of all products produced in the unimolecular and bimolecular reactions led to the conclusion that the ratio of neutral electronically excited molecules to parent ions (N_{ex}/N_+) is 0.28.

Key words: Electron scavengers; gas phase; ion-molecule reactions; neopentane; neutralization; pulse radiolysis.

1. Introduction

Although nearly 500 papers dealing with pulse radiolysis have appeared in the literature, pulse radiolysis studies of alkanes in the gas phase are nonexistent, with the exception of two cursory studies of methane [1].[1] The reason for this is that it has become customary to associate direct detection techniques with pulse radiolysis experiments, and these techniques can not be readily applied to hydrocarbon gases. Actually, in the case of hydrocarbons (with the exception of aromatics), the absorption spectra of most of the fragment ions and free radicals, which are known to be present, have never been observed [2].

The limitations of optical absorption techniques for these systems do not, however, rule out pulse radiolysis as a powerful tool in the elucidation of the chemical changes brought about by high energy irradiation of hydrocarbon gases. Indeed, the pulse irradiation of judiciously selected hydrocarbons, or hydrocarbon-containing mixtures, followed by chemical analysis of the end products, may yield a wealth of information which will contribute to our overall understanding of radiolytic phenomena.

The main distinguishing feature of high dose rate pulse radiolysis experiments is the short lifetime of the charged species. Neutralization will be entirely homogeneous and reactions of ions with minor impurities or accumulated products will be negligible. Furthermore, the absence of long ionic chain reactions simplfies the interpretation of the initial unimolecular and bimolecular reactions.

The present study which is the first in a series devoted to the pulse radiolysis of alkanes deals with neopentane. This molecule was chosen for the present exploratory study, because of the relatively limited number of reactive intermediates produced and because the low dose rate radiolysis has been investigated [3]. In the discussion which follows, the unimolecular and bimolecular reactions contributing to the formation of the products will be examined, by taking advantage of the same diagnostic isotopic labeling techniques which were successfully employed in earlier low dose rate investigations [3].

2. Experimental Procedure

2.1. Pulsed Electron Beam Sources

Two different electron pulse instruments, the Febetron 705 and 706,[2] were used in this study. These pulse sources are capacitor-discharge type instruments which use the field emission effect to obtain a high current of electrons from fine tungsten needles in a vacuum tube. The Febetron 705 has a half-maximum pulse duration of about 55 ns at maximum output (35 kV charging voltage, 4000 G focusing field). The beam contains approximately 2×10^{15} electrons per pulse with a mean energy of 1.4 MeV. At lower charg-

*Work supported in part by the Atomic Energy Commission.

[1] Figures in brackets indicate the literature references at the end of this paper.

[2] Certain commercial equipment is identified in this paper in order to specify adequately experimental procedure. This identification does not imply recommendation or evaluation of this equipment by the National Bureau of Standards.

ing voltages the half maximum pulse duration is somewhat longer (about 75 ns at 16 kV charging voltage) and there are fewer electrons per pulse. The electron beam has a diameter of 3–4 cm just outside the thin titanium window of the instrument. For a given diode tube, the pulse-to-pulse reproducibility is excellent with a maximum deviation from the average of about 6 percent and an average deviation of less than 3 percent [4].

The Febetron 706 has half maximum pulse duration of about 3 ns at maximum output (30 kV charging voltage). The beam contains approximately 2×10^{14} electrons per pulse with a nominal energy of 600 keV and it has a diameter of about 1.4 cm just outside the window of the tube. For a given diode tube the pulse-to-pulse fluctuations are less than 5 percent mean square deviation [5].

A few flash photolysis experiments were carried out in the course of this study using the flash apparatus constructed by W. Braun [6].

2.2. Radiation Cells

The radiation cells used in this work were cylindrical borosilicate glass vessels 10 cm long and 3.7 cm internal diameter with a volume of 106 cm^3. Aluminum windows which were 4 mil thick were attached to each end of the cell with a vacuum epoxy cement. These cells were evacuated and filled through a PTFE valve and the reactants were condensed in a small finger at the bottom of the cell with liquid nitrogen. The outside of the cell was covered with aluminum foil which was grounded when the cell was irradiated by the electron pulse. These cells were very carefully positioned as close as possible in front of the titanium window of the Febetron.

In some of the early experiments cylindrical stainless steel cells were used which were 10 cm long and 4.7 cm internal diameter with a volume of 175 cm^3. The 4 mil aluminum windows were attached with dairy clamps and viton O-rings. Essentially similar results were obtained with either the stainless steel or the borosilicate glass cells.

2.3. Materials and Analysis

Most of the chemicals used in this investigation were of research grade quality and except for degassing there was no further purification. Two different sources of neopentane were used, but there was no substantial difference in the results obtained with different samples. Neopentane-d_{12} was purified on a gas chromatograph and checked on a mass spectrometer. It contained 8 percent $C_5D_{11}H$. The CD_3I contained 9 percent CD_2HI. The nitric oxide was stored over silica gel.

After the irradiation by the electron pulse(s), an aliquot of the mixture was injected onto a squalane column of a gas chromatograph with a flame ionization detector for quantitative analysis of the products. In those experiments in which the isotopic distributions of some of the products were determined, the hydrogen and methane were distilled at either liquid nitrogen or solid nitrogen temperatures. Then the remainder of the mixture was injected onto a silica gel column and the various products were trapped at the exit of the column in borosilicate glass spiral traps maintained at liquid nitrogen temperature and were analyzed on a mass spectrometer.

2.4. Dosimetry

Nitrous oxide at 1 atm pressure was used as the dosimetric gas using $G(N_2) = 12.4$ as determined by Willis et al. [4,7]. The relative stopping power per electron of neopentane to nitrous oxide or air was calculated from the tables of Berger and Seltzer [8] as 1.05 for 600 keV electron (Febetron 706) and 1.03 for 1.4 MeV electrons (Febetron 705). The dosimetry experiments were performed in the same cells that were used to irradiate the neopentane mixtures so that there is no error due to a difference in geometry of the cells. One pulse emitted by the Febetron 706 (3 ns pulse) operated at a charging voltage of 30 kV corresponded to a dose of 3.6×10^{19} eV/g. The dose per pulse (~ 60 ns) from the Febetron 705 was 18.2 and 5.8×10^{19} eV/g at charging voltages of 30 and 16 kV respectively.

3. Results

The yields of the measured products are given as molecules, M, of product X produced per ion pair, N_+, $(M(X)/N_+)$ [9]. A W-value of 23.2 eV for neopentane was chosen to convert number of molecules per eV to the number of molecules per ion pair [10].

Table 1 gives all of the lower hydrocarbon products whose ion pair yields have been determined. In addition the ion pair yields of 2-methyl-1-butene (0.066), 2-methyl-2-butene (0.025) and 2,2-dimethylbutane (0.050) were determined. Addition of SF_6 increased the yields of 2-methyl-1-butene, 2-methyl-2-butene and 2,2-dimethylbutane to 0.09, 0.03 and 0.068 respectively. Minor products such as *n*-butane (< 0.001) and propane (~ 0.01) are not listed in table 1.

Tables 2 and 3 present isotopic analyses of hydrocarbon products produced in the pulse radiolysis of equimolar neo-C_5H_{12}—neo-C_5D_{12} mixtures. The hydrogen was also analyzed mass spectrometrically. In the pure neopentane mixture it consisted of H_2 (50.1%); HD (26.2%) and D_2 (23.7%). Addition of 1 mol percent SF_6 did not alter this distribution in any appreciable way, giving H_2 (47.1%); HD (29.5%) and D_2 (23.4%).

Table 4 contains the isotopic analyses and ion pair yields of the hydrogen, methane, and ethane produced in the pulse radiolysis of neo-$C_5H_{12} - CD_3I$ mixtures. The propylene and isobutene which were analyzed as well, contained less than 2 percent of the deuterium labeled species.

4. Discussion

The emphasis in this discussion will be mainly on the chemical consequences of the neutralization of

TABLE 1. *Pulse radiolysis of neopentane product yields*

Pulse[1] duration (ns)	Dose/ pulse eV/ gx10^{-19}	No. of pulses	Additive mol %	M/N_+ (Ion pair yield)[2]									
				H_2	CH_4	C_2H_2	C_2H_4	C_2H_6	C_3H_6	$CH_3C \equiv CH$	$CH_2=C=CH_2$	i-C_4H_{10}	i-C_4H_8
3	3.6	1		n.d.	1.09	0.052	0.115	0.304	0.205	0.041	0.030	0.007	0.837
3	3.6	2		.35	1.07	.051	.112	.307	.215	.043	.038	.009	.849
3	3.6	2	CCl_4-2.0	n.d.	.375	.039	.097	.293	.100	.022	.013	.027	.902
3	3.6	3	CD_3I-2.0	n.d.	.496	.030	.100	.811	.107	.026	.015	.069	.738
60	18.2	1		n.d.	1.11	.052	.117	.293	.218	.050	.042	.012	.842
60	5.8	1		n.d.	1.06	.041	.108	.305	.212	.044	.033	.009	.830
60	18.2	1	SF_6-0.5	.33	.591	.039	.112	.375	.126	.033	.018	.029	.947
60	5.8	2	CD_3I-1.0	n.d.	.542	.031	.100	.742	.104	.025	.013	.067	.769
60	5.8	2	CD_3I-3.0	n.d.	.501	.032	.106	.878	.101	.023	.012	.072	.764
				Relative yields[3]									
Flash photolysis			none	n.d.	.516	.009	.065	.645	.210	.032	.036	.030	1.00

[1] Full width half maximum.
[2] Pressure neopentane = 162 torr.
[3] Pressure neopentane = 5.0 torr.
n.d. = not determined.

TABLE 2. *Pulse radiolysis of neo-C_5D_{12} – neo-C_5H_{12} (1:1) isotopic compositions of ethane and methane*

Dose/pulse eV/g × 10^{-19}	Additive mole %	Ethane distribution (%)					M/N_+ ($C_2H_5^+ + C_2D_5^+$)
		C_2H_6	C_2H_5D	$C_2H_3D_3$	C_2D_5H	C_2D_6	
Pulse radiolysis:							
18.2	none	26.5	5.5	37.6	5.0	23.7	0.062
18.2	SF_6-1.0	26.5	4.4	41.3	4.0	22.1	.060
3.6	NO-3.0	27.5	18.0	13.0	16.5	25.0	.047
Low Dose Rate Radiolysis (ref. 3):							
	NO-5.0	29.5	20.5	.....	21.2	28.8	.062
		Methane distribution (%)					M/N_+ (Molecular methane)
		CH_4	CH_3D	CH_2D_2	CHD_3	CD_4	
Pulse radiolysis:							
18.2	none	30.8	16.0	2.6	27.5	23.1	~ 0.11
18.2	SF_6-1.0	35.2	13.0	2.0	22.5	27.3	.16
3.6	NO-3.0	42.6	7.3	.....	12.2	37.9	.16
Low Dose Rate Radiolysis (ref. 3):							
	NO-5.0	44.3	4.3	.....	5.2	46.2	.18

Pressure of neopentane: pulse radiolysis 160 torr, low dose rate radiolysis (ref. 3) 40 torr.

the positive ions. In order to obtain information about this, one must examine all of the free radical and ion-molecule reactions which occur during and immediately after the pulse. Only when end products resulting from these reactions are accounted for, can one proceed to derive concrete information concerning the chemical consequences of the encounters between the unreactive positive ions and the negatively charged species.

Passage of an electron beam through neopentane will lead to the production of electronically excited neutral molecules and of excited parent ions [3]. These species are expected to dissociate within 10^{-12} to 10^{-13} s [11, 12], and the following dissociative processes have been invoked to account for the products observed in the low dose rate experiments.

$$C_5H_{12}^* \rightarrow i\text{-}C_4H_8 + CH_3 + H \quad (1)$$

$$\rightarrow C_3H_6 + CH_3 + CH_3 \quad (2)$$

$$\rightarrow i\text{-}C_4H_8 + CH_4 \quad (3)$$

$$C_5H_{12}^+ \rightarrow t\text{-}C_4H_9^+ + CH_3 \quad (4)$$

$$\rightarrow i\text{-}C_4H_8^+ + CH_4 \quad (5)$$

$$\rightarrow C_3H_5^+ + CH_3 + CH_4 \quad (6)$$

$$\rightarrow C_2H_5^+ + CH_3 + C_2H_4 \quad (7)$$

$$\rightarrow C_2H_3^+ + H_2 + CH_3 + C_2H_4 \quad (8)$$

$$\rightarrow C_3H_3^+ + H_2 + CH_3 + CH_4 \quad (9)$$

TABLE 3. *Pulse radiolysis of neo-C_5D_{12}—neo-C_5H_{12} (1:1) isotopic compositions of ethylene and propylene*

Dose/pulse eV/g × 10^{-19}	Additive mole %	Ethylene distribution (%)				M/N_+ ($C_2H_3^+ + C_2D_3^+$)
		C_2H_4	C_2H_3D	C_2D_3H	C_2D_4	
Pulse radiolysis:						
18.2	none	48.1	7.3	7.0	37.9	0.032
3.6	NO-3.0	49.5	6.8	5.9	37.8	.028
Low dose rate radiolysis (ref. 3):						
	NO-5.0	45.1	6.0	6.2	42.7	.028
		Propylene distribution (%)				M/N_+ ($C_3H_5^+ + C_3D_5^+$)
		C_3H_6	C_3H_5D	C_3D_5H	C_3D_6	
Pulse radiolysis:						
18.2	none	41.6	5.4	5.2	41.7	0.044
3.6	SF_6-1.0	40.3	8.2	7.9	38.1	.041
Low dose rate radiolysis (ref. 3):						
	NO-5.0	37.1	11.1	11.2	40.0	.048

Pressure of neopentane: pulse radiolysis 160 torr, low dose rate radiolysis (ref. 3) 40 torr.

TABLE 4. *Pulse radiolysis of neo-C_5H_{12}—CD_3I mixtures*

CD_3I mol %	M/N_+ (Ion Pair Yields)							$CH_{4_{corr}}/CD_3H$ [a]	$[CH_3]/[CD_3]$ $CD_3CH_3/2C_2D_6$	$C_2H_{6_{corr}}^{1/2}/C_2D_6^{1/2}$
	H_2	HD	CD_3H	CH_4	C_2D_6	CD_3CH_3	C_2H_6			
1	.30	.006	.184	.358	.147	.330	.254	1.08	1.12	1.18
3.1			.176	.325	.225	.413	.240	0.94	0.92	0.92
6.1	.32	.013	.184	.312	.280	.472	.259	0.83	.84	.86

Dose per pulse: 5.8×10^{19} eV/g.
[a] $CH_{4_{corr}}$: measured yield of CH_4 minus contribution due to reactions 3, 5, 6, and 9.
[b] $C_2H_{6_{corr}}$: measured yield of C_2H_6 minus contribution due to reaction 19.

Propyl ions are also produced but at a neopentane pressure of 300 torr [3], $M(C_3H_7^+)/N_+ = 0.01$.

Process 4 is the major mode of fragmentation of $C_5H_{12}^+$. At a pressure of 150 torr, $M(t\text{-}C_4H_9^+)/N_+$ has been estimated [3] to be 0.75, while $M(i\text{-}C_4H_8^+)/N_+$ has been estimated at 0.03. Concrete information concerning relative importances of the neutral dissociative processes is not available. Far ultraviolet photolysis experiments indicate however that process 1 is more important than processes 2 or 3. The total number of neutral electronically excited molecules ($C_5H_{12}^*$) per positive ion, N_{ex}/N_i, in the gas phase radiolysis is not exactly known. On the basis of low dose rate experiments an estimated value of 0.2 has been assigned to N_{ex}/N_i (number of neutral excited molecules per ion pair). Later in the discussion an attempt is made to derive more definitive information concerning the role of the neutral dissociative processes.

4.1. Yields of Fragment Ions

Partially labeled hydrocarbon products such as C_2D_5H, C_2D_3H, and C_3D_5H which were also seen in low dose rate experiments carried out in the presence of NO (tables 2 and 3), can be axcribed to the exothermic hydride ion transfer reactions:

$$C_2D_5^+ + \text{neo-}C_5H_{12} \rightarrow C_2D_5H + C_5H_{11}^+ \quad (10)$$

$$C_2D_3^+ + \text{neo-}C_5H_{12} \rightarrow C_2D_3H + C_5H_{11}^+ \quad (11)$$

$$C_3D_5^+ + \text{neo-}C_5H_{12} \rightarrow C_3D_5H + C_5H_{11}^+ \quad (12)$$

Because the rate constants of these reactions are approximately 10^{-9} cm^3/molec · s[13], more than 99 percent of the $C_2D_5^+$, $C_2D_3^+$ and $C_3D_5^+$ will react with neopentane even at the highest dose rates used in this study.

If, as in the earlier low dose rate studies [3], one accepts that in fast ion-molecule reactions, isotope effects can be ignored, maximum ion pair yields of the three reactant ions can be obtained by multiplying the sums of ion pair yields of $C_2D_5H + C_2DH_5$, $C_2D_3H + C_2DH_3$, and $C_3D_5H + C_3DH_5$ by a factor of two. The values thus obtained are given in the last column of tables 2 and 3. They compare rather well with those derived from low dose rate experiments carried out at a lower pressure of neopentane in the presence of NO as a free radical interceptor. At low dose rates, low concentrations of NO or O_2 will effectively remove free radicals from the system, and thus prevent contributions of radical-radical interactions to the partially labeled hydrocarbon products. Nitric oxide or oxygen

are obviously less efficient as free radical scavengers under our pulse radiolysis conditions. At high dose rates radical-radical interactions will compete with radical-scavenger molecule ractions. Nevertheless, using a 3 ns pulse and a dose of 1.8 eV/g per pulse, the methyl radicals which, according to processes 1 through 8, are the most abundant alkyl radicals produced during the pulse, can be removed to a significant extent upon addition of 5 mol percent NO to neopentane. This is demonstrated by the pronounced drop of $M(CH_4)/N_+$ and $M(C_2H_6)/N_+$ as a function of the pressure of NO as seen in figure 1.

Furthermore the CH_3CD_3 which can be unambiguously ascribed to the radical combination reaction

$$CH_3 + CD_3 \rightarrow CH_3CD_3 \qquad (13)$$

diminishes sharply with respect to the other partially deuterium labeled ethanes when NO is added (table 2). The ion pair yield of 0.047 for the ethyl ions derived from this experiment can be considered as more reliable than the 0.060 calculated from the isotopic ethane distributions observed in the unscavenged experiments (table 2). The value obtained for M(ethyl ion)/N_+ is bracketed by the low dose rate values of 0.068 and 0.035 obtained at neopentane pressures of 30 and 300 torr respectively [3]. The drop of $M(C_2H_5^+)/N_+$ with pressure has been ascribed [3] to collisional quenching of process 7.

4.2. Yields of Molecular CH_4 and CH_3

The total yield of molecular methane formed by the fragmentation processes 3, 5, and 6 can be estimated from the isotopic analysis given in table 2 assuming one molecule of CD_4 or CH_4 is being produced for each molecule of CH_3D or CD_3H. In the pulse radiolysis of pure neo-C_5D_{12}-neo-C_5H_{12} mixtures there is considerable isotopic mixing (table 2) due to the combination reactions

$$CH_3 + D \rightarrow CH_3D \qquad (14)$$

$$CD_3 + H \rightarrow CD_3H. \qquad (15)$$

Addition of 5 mol percent NO drastically reduces the total methane yield (fig. 1), and more specifically, the relatively abundances of CD_3H and CH_3D in the methane fraction. From such an experiment, a reliable value of 0.16 is obtained for the ion pair yield of molecular methane. Because of the large relative yields of CH_3D and CD_3H the value for molecular methane derived from the isotopic distribution observed in pure neo-C_5H_{12}-neo-C_5D_{12} mixtures is obviously less reliable. In the C_5D_{12}—C_5H_{12}—SF_6 experiment, where the total methane yield (table 1) and the relative contributions of CD_3H and CH_3D, are lower, good agreement is obtained. Taking $M(i\text{-}C_4H_8^+)/N_+ = \sim 0.03$ [3] (process 5) and $M(C_3H_5^+)/N_+ = 0.044$ (process 6) more than half of the yield of molecular methane remains unaccounted for. If one tentatively accepts that as indicated by the 70 eV mass spectral pattern $C_3H_3^+$ is slightly less abundant than $C_2H_3^+$, one obtains a value approximately 0.10 for the molecular methane produced by fragmentation of $C_5H_{12}^+$.

$M(CH_3)/N_+$ can be estimated by summation of all the products which can be ascribed to combination of CH_3 with other radicals in the system

$$CH_3 + R \rightarrow CH_3R \qquad (16)$$

where $R = H, CH_3, (CH_3)_3CCH_2$. In view of the absence of $C_3H_3D_3$ in the propylene fraction a reaction such as

$$C_2H_3(C_2D_3) + CD_3(CH_3) \rightarrow C_3H_3D_3 \qquad (17)$$

does not occur and vinyl radicals are therefore not produced in the pulse radiolysis of pure neopentane. Similarly, the negligible contribution of $C_4D_5H_3$ to the isobutene fraction and the absence of 1-butene as a product indicates that allyl radicals play a very minor role. Finally, the minor yield of propane (see Results) points to a low abundance of ethyl radicals which if formed would mainly combine with CH_3.

After taking into account the contributions of molecular methane and $C_2H_5^+$ to the methane and ethane fractions respectively, a value of 1.48 ± 0.02 is obtained for $M(CH_3)/N_+$ in the pulse radiolysis of pure neopentane. A slightly higher value (1.5 ± 0.02) is obtained if one assumes that C_3H_8 and $i\text{-}C_4H_{10}$ are produced entirely by combination of CH_3 radicals with C_2H_5 and C_3H_7 respectively. A change in pulse duration, dose or dose rate has, within experimental error, no effect on the estimated yield of CH_3 radicals. The value for $M(CH_3)/N_+$ obtained here is in close agreement with the value of 1.45 reported for $M(CD_3H)/N_+$ produced in the low dose rate radiolysis of neo-C_5D_{12} carried out in the presence of H_2S as a free radical

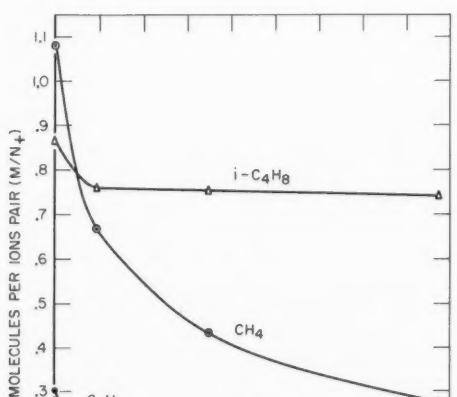

FIGURE 1. *The effect of* NO *on the major hydrocarbon products formed in the pulse radiolysis of neopentane (3ns, 3.6 eV/g* $\times 10^{19}$).

Pressure of neopentane: 162 torr.

interceptor [3]. Accepting [3] a value of 0.03 for $M(i\text{-}C_4H_8^+)/N_+$ the total ion pair of CH_3 resulting from the decomposition of the parent ion (reactions 4, 6 through 9) cannot be higher than 0.97. Since the total yield of methyl radicals derived above is ~ 1.5, it follows that CH_3 radicals are produced from other sources, such as the decomposition of electronically excited neopentane (processes 1 and 2) and of internally excited radicals produced by neutralization.

In order to verify the modes of formation of the methane and ethane products, the pulse radiolysis of neo-C_5H_{12} containing from 1 to 6.1 mol percent CD_3I (table 4) was investigated. Addition of CD_3I has the effect of introducing CD_3 radicals to the system, mainly by the dissociative electron capture step

$$CD_3I + e \rightarrow CD_3 + I^-. \qquad (18)$$

Provided the concentration of CD_3I is sufficiently low, there should be no interference with hydride ion transfer reaction,

$$C_2H_5^+ + \text{neo-}C_5H_{12} \rightarrow C_2H_6 + C_5H_{11}^+ \qquad (19)$$

and the free radicals should react in the same way as in pure neopentane. As expected on the basis of the free radical combination reaction discussed above, the methane is seen to consist exclusively of CD_3H and CH_4, while the ethane fraction contains, C_2D_6, CD_3CH_3, C_2H_6 and no other partially deuterated ethanes. If one now subtracts from $M(CH_4)/N_+$ the contribution of molecular methane, and from C_2H_6 the contribution due to the reaction 19, one obtains consistent values for CH_3/CD_3 as calculated from the product ratios given in the last three columns of table 4. It follows that the mechanism proposed for the formation of methane and ethane is well substantiated.

4.3. Formation of Hydrogen

Apparently, the majority of the H-atoms react with CH_3 to produce methane. On the basis of the results presented in tables 1 and 2, a value of 0.9 can be ascribed to the ion pair yield of H-atoms reacting in this manner. In addition, one has to consider the H_2 which is observed in all experiments. The mechanism by which this product is formed is not immediately obvious. Although the relatively low yield of HD observed in the pulse radiolysis of C_5H_{12}—C_5D_{12} mixtures, (see Results) indicates that some of the hydrogen is eliminated unimolecularly from excited intermediates, a considerable fraction must be produced via bimolecular reactions. At least some of the HD may be formed in the hydrogen abstraction reaction

$$H^* + C_5H_{12} \rightarrow H_2 + C_5H_{11} \qquad (19)$$

where H* designates a translationally excited atom. The presence of 2,2-dimethylbutane ($M/N_+ = 0.055 \pm 0.05$) can be explained by the combination of the resulting neopentyl radicals with methyl radicals. (The yield of this product is reduced in the presence of 5 percent NO, confirming the participation of a radical mechanism in its formation.)

Combination of H-atoms is excluded as a major source of HD, in view of the fact that addition of electron scavengers such as SF_6 and CD_3I reduces $M(H)/N_+$, (as indicated by the sharp drop of $M(CH_4)/N_+$ in these experiments) (table 1), but has no noticeable effect on either the yield of hydrogen or its isotopic composition.

4.4. Neutralization

The ions which under the present pulse radiolysis conditions will undergo homogeneous neutralization are: $C_4H_9^+$, $C_4H_8^+$, $C_3H_3^+$ produced in the unimolecular fragmentation steps, and $C_5H_{11}^+$ produced via the hydride ion transfer reactions involving $C_2H_5^+$, $C_2H_5^+$, and $C_3H_5^+$. The total ion pair yield of $C_5H_{11}^+$ can be estimated at 0.12 ± 0.01 and that of $t\text{-}C_4H_9^+$ at 0.80. The remaining 0.08 being accounted for by $i\text{-}C_4H_8^+$ (~ 0.03), $C_3H_7^+$ (~ 0.01), and $C_3H_3^+$ (~ 0.03). It is clear from the quantitative results presented in table 1 that the mechanism of neutralization of the $t\text{-}C_4H_9^+$ ion can be represented in the same way as recently proposed for the liquid phase radiolysis of neopentane [14]:

$$t\text{-}C_4H_9^+ + e \rightarrow t\text{-}C_4H_9^* \qquad \Delta H = -5.17 \text{ eV} \quad (20)$$

$$t\text{-}C_4H_9^* \rightarrow i\text{-}C_4H_8 + H \qquad (21)$$

$$\rightarrow C_3H_6 + CH_3. \qquad (22)$$

The $t\text{-}C_4H_9^*$ radical produced initially will possess 5.17 eV in internal energy [15] and will therefore dissociate essentially instantaneously [16]. Step 21, which on the basis of pyrolysis studies [17] requires an activation energy of 1.9 eV, is the expected mode of decomposition of internally excited $t\text{-}C_4H_9$ radicals. Decomposition step 22 which, in pyrolysis carried out at temperatures up to 857 K, plays a very minor role, is however of importance in the low intensity photolysis of neopentane at 147 and 123.6 nm [3] as well as in the flash photolysis (table 1). The internal energy content of the intermediate $t\text{-}C_4H_9^*$ radical, which in the photolysis is produced by cleavage of a C—C bond in neopentane, is comparable to that produced in the neutralization step. It is matter of conjecture if the $t\text{-}C_4H_9^*$ isomerizes first to the $i\text{-}C_4H_9^*$ structure or if a CH_3CCH_3 diradical is produced by a simple C—C cleavage of the $t\text{-}C_4H_9^*$ intermediate followed by isomerization to propylene. It is of interest, however, that isobutyl radicals have been reported in the liquid phase radiolysis [18] where some of the $C_4H_9^*$ may be collisionally stabilized. The branching ratio of steps 21 and 22 can be estimated by the decrement of $M(C_3H_6)/N_+$ noted when an electron scavenger such as SF_6, CCl_4, or CD_3I is added to neopentane (see table 1). In view of the high electron capture cross section of these molecules [19], a few mole percent should be sufficient to capture the

majority of the electrons under the pulse radiolysis conditions. This is indicated by the observation (table 4) that in the case of the least efficient electron scavenger, CD_3I, $M(CD_3)/N_+$ which is mainly produced by the dissociative electron attachment process 18 reaches values of 0.81 and 1.05 upon addition of 1 and 3 mol percent CD_3I respectively. Neutralization of a positive ion by collision with a negative ion rather than an electron will impart less energy to the neutral entity formed in the process. The electron affinity of the scavenger molecule will result in the formation of a negative ion with a greater heat of formation than the electron, so the neutralization reaction is less exothermic, and the energy content of the neutralized species will be lowered. As is indicated by the reduction of $M(H)/N_+$ in the presence of an electron scavenger, the energy may be further reduced because of the occurrence of chemical reactions such as

$$C_4H_9^+ + I^- \rightarrow HI + i\text{-}C_4H_8 \qquad (23)$$

$$C_4H_9^+ + SF_6^- \rightarrow HF + SF_5 + i\text{-}C_4H_8. \qquad (24)$$

Reduction of hydrogen atom production by electron scavengers have also been reported in numerous low dose rate radiolysis studies [20] of alkanes and cycloalkanes.

Addition of CD_3I reduces $M(C_3H_6)/N_+$ from 0.21 $\pm$0.05 to 0.10, independent of the concentration of CD_3I. CCl_4 has the same effect as CD_3I, while SF_6 seems to reduce the yield somewhat less. Accepting, on the basis of the reduction in the yield of C_3H_6 in the presence of CD_3I, a value of 0.11 for the ion pair yield of reaction 22, one can assume that the remaining $t\text{-}C_4H_9^+$ ions ($M/N_+ = 0.69$) lead to the production of $i\text{-}C_4H_8$ (reaction 21).

The $i\text{-}C_4H_8^*$ produced in the neutralization of the $i\text{-}C_4H_8^+$ ion

$$i\text{-}C_4H_8^+ + e \rightarrow i\text{-}C_4H_8^* \qquad (25)$$

will possess 9.23 eV in energy above the ground state of the $i\text{-}C_4H_8$ molecule. It may be assumed that this molecule will dissociate in a manner similar to that observed for $i\text{-}C_4H_8^*$ molecules excited by absorption of 10 eV photons, namely:

$$i\text{-}C_4H_8^* \rightarrow CH_2{=}C{=}CH_2 + H + CH_3 \qquad (26)$$

$$\rightarrow CH_3C{\equiv}CH + H + CH_3. \qquad (27)$$

Both decompositions occur via a $C_4H_7^*$ and/or $C_3H_5^*$ intermediate. Methylacetylene and allene are produced in the pulse radiolysis of neopentane (table 1), and it can be seen that addition of an electron scavenger reduced $M(C_3H_4)/N_+$ from 0.075$\pm$0.005 to 0.040$\pm$0.005. The decrement corresponds to the ion pair yield of $i\text{-}C_4H_8^+$. The residual C_3H_4 could be produced by decomposition of highly excited neutral fragments produced in the decomposition of electronically excited neopentane. Both allene and methyl-acetylene are minor products in the flash photolysis of neopentane (table 1).

The mechanism of neutralization of the $C_5H_{11}^+$ ion is rather straightforward. 2-Methyl-1-butene and 2-methyl-2-butene are products in the pulse radiolysis of neopentane (see Results). The fact that their yields are not reduced by addition of NO shows that they are not formed by a radical combination reaction. Also none of these products was observed in the flash photolysis or low intensity photolysis of neopentane. A logical interpretation involves the neutralization of $C_5H_{11}^+$ ions with the structure $(CH_3)_2CCH_2CH_3^+$

$$(CH_3)_2CCH_2CH_3^+ + e \rightarrow (CH_3)_2C{=}CHCH_3 + H \qquad (28)$$

$$\rightarrow CH_3CH_2C(CH_3){=}CH_2 + H \qquad (29)$$

process 29 occurring with a probability which is a factor of 2.5 times higher than 28. In view of the fact that in the pulse radiolysis of pure neopentane $M(C_5H_{10})/N_+ = 0.09$ it can be assumed that essentially all $C_5H_{11}^+$ ions produced in the hydride ion transfer reactions acquire the stable $t\text{-}C_5H_{11}^+$ structure prior to neutralization. Addition of SF_6 raises $M(C_5H_{10})/N_+$ to 0.12$\pm$0.01 in good agreement with the ion pair yield of the $C_5H_{11}^+$ ions (0.12). It can be surmised that in the absence of SF_6 a fraction ($M/N_+ \sim 0.03$) of the $C_5H_{11}^+$ are neutralized in the following manner:

$$(CH_3)_2CCH_2CH_3^+ + e \rightarrow (CH_3)_2CCH_2 + CH_3. \qquad (30)$$

The mechanism of neutralization involving SF_6^- is probably similar to reaction 24.

Neutralization of the remaining minor ions, $C_3H_3^+$ and sec-$C_3H_7^+$ can not be elucidated. They will probably contribute to formation of highly unsaturated products. The value of $M(C_2H_2)/N_+$, for instance, is reduced from 0.051 to $\sim$0.035 upon addition of electron scavengers.

4.5. Estimation of the Yield of Electronically Excited Neopentane Molecules

Table 5 represents a summary of the ion pair yields of free radicals and molecular products, which have been accounted for by the unimolecular dissociation of the parent ion and the major neutralization reactions

TABLE 5. *Methyl radicals and hydrocarbon molecules produced in unimolecular dissociation and neutralization reactions*

	CH_3	CH_4	C_2H_2	M/N+		C_3H_6	$i\text{-}C_4H_8$	C_5H_{10}
				C_2H_4	C_3H_4			
neo-$C_5H_{12}^+ \rightarrow$	0.97	0.10	.....	.....	.....	.....	.....	.....
$C_4H_9^+ + e \rightarrow$	.11	.....	.....	.....	.....	0.11	0.69	.....
$C_5H_{11}^+ + e \rightarrow$	.03	.....	.....	.....	.....	.....	0.03	0.09
$C_4H_8^+ + e \rightarrow$	.03	.....	.....	.....	0.03	.....	.....	.....
Total:	1.14	0.10	.....	.....	0.03	0.11	0.72	0.09
Unaccounted:	0.34	0.06	0.035	0.06	0.04	0.06	0.13	.....

proposed in the previous section. The last row of the table shows the yields of the fragments which are not yet accounted for. An ion pair yield of 0.06 must be ascribed to molecular ethylene which does not enter into any of the reactions listed so far. Even though not all of the ionic processes have been exhaustively covered, the yields given in the last row provide a reasonable balance between the C_1 products on one hand and the C_2, C_3, and C_4 products on the other hand, if one takes into account that two C_1 fragments will be formed for each C_3 fragment. If one tentatively ascribes the unaccounted for products to decomposition of electronically excited neopentane molecules produced by electron impact a value of 0.28 is obtained for N_{ex}/N_i. This estimated value may admittedly require some revision wherever the minor unexplained reaction steps can be accounted for. It falls however in the same range as the values derived from conventional low dose rate radiolysis experiments on neopentane [3] as well as other alkanes [21].

The authors thank J. H. Sparrow and R. C. Placious for their assistance in using the Febetron 705 and 706.

5. References

[1a] Cahill, R. W., Seeler, A. K., and Glass, R. A., J. Phys. Chem. **71**, 4564 (1967).
[1b] Hummel, R. W. and Hearne, J. A., J. Phys. Chem. **75**, 1164 (1971).
[2] Herzberg, G., Molecular Spectra and Molecular Structure (D. Van Nostrand, Princeton, New Jersey, 1967).
[3a] Lias, S. G. and Ausloos, P., J. Chem. Phys. **43**, 2748 (1965).
[3b] Miyazaki, T. and Shida, S., Bull. Chem. Soc. Japan **39**, 2344 (1966).
[3c] Ausloos, P. and Lias, S. G., J. Am. Chem. Soc. **92**, 5037 (1970).
[4] Willis, C., Miller, O. A., Rothwell, A. E., and Boyd, A. W., Advan. in Chem. Ser. **81**, 539 (1968).
[5] Field Emission Corporation Technical Bulletin B-21-A.
[6] Kurylo, M. J., Peterson, N. C., and Braun, W., J. Chem. Phys. **53**, 2776 (1970).
[7] Willis, C., Boyd, A. W., and Miller, O. A., Radiat. Res. **46**, 428 (1971).
[8] Berger, M. J. and Seltzer, S. M., NASA Report SP-3012 (1964).
[9] Woodward, T. W. and Back, R. A., Can. J. Chem. **41**, 1463 (1963).
[10] LeBlanc, R. M. and Herman, J. A., J. Chim. Phys. **21**, 1055 (1966).
[11] Beckey, H. D., Z. Naturforsch **160**, 505 (1961).
[12] Ausloos, P., Mol. Photochem. **4**, 39 (1972).
[13] Field, F. H. and Lampe, F. W., J. Am. Chem. Soc. **80**, 5587 (1958).
[14] Collin, G. J. and Ausloos, P., J. Am. Chem. Soc. **93**, 1336 (1971).
[15] Based on the ΔH_f (t-$C_4H_9^+$) value of 7.25 eV reported by Lossing, F. P. and Semelick, G. P., Can. J. Chem. **48**, 955 (1970).
[16] Rabinovitch, B. S. and Setser, D. W., Advan. in Photochem. Ser. **3**, 1 (1964).
[17] Benson, S. W. and O'Neal, H. E., Kinetic Data on Gas Phase Unimolecular Reactions, Nat. Stand. Ref. Data Ser., Nat. Bur. Stand. (U.S.), 21, 645 pages (Feb. 1970).
[18] Holroyd, R. A. and Klein, G. W., J. Am. Chem. Soc. **87**, 4983 (1965).
[19] Blaunstein, R. P. and Christophorou, L. G., J. Chem. Phys. **49**, 1526 (1968).
[20] See for instance:
[20a] Bansal, K. M. and Freeman, G. R., J. Am. Chem. Soc. **90**, 7183 (1968).
[20b] Johnson, G. R. A. and Redpath, J. L., Trans. Faraday Soc. **66**, 861, (1970).
[20c] Sagert, N. H., Reid, J. A., and Robinson, R. W., Can J. Chem. **47**, 2655 (1969).
[21] Ausloos, P. and Lias, S. G., Gas Phase Radiolysis of Hydrocarbons in Actions Chimiques et Biologiques des Radiations, Vol. **11**, Chapter 1, pp. 1-83, Masson et Cie Editeurs, Paris, France (1967).

(Paper 76A4-724)

JOURNAL OF RESEARCH of the National Bureau of Standards — A. Physics and Chemistry
Vol. 76A, No. 4, July–August 1972

Anatomy and Thermal History of Laser Self-Focusing Damage Tracks in Glass

Wolfgang Haller and Joseph H. Simmons

Institute for Materials Research, National Bureau of Standards, Washington, D.C. 20234

March 16, 1972

Laser induced self-focusing damage tracks in glass are analyzed. The damaged regions consist of long cylinders of altered refractive index, containing occasional bubbles and partly surrounded by arrays of small cracks. An analysis of the refractive index change in the subfracture damage tracks and the presence of bubbles leads to estimates of a minimum temperature reached by heating of the glass in the tracks. A calculation of minimum stresses developed during laser-beam heating gives a good account of the orientation of the observed cracks.

Key words: Laser damage; glass; self-focusing.

1. Introduction

Self-focusing damages caused by laser beams in glasses range from gross fractures ("starbursts" and planar cracks) to lines made up of very small bubbles ("bubble tracks") [1].[1] Less conspicuous permanent changes in the beam regions are the "filaments," variously described as bright or dark lines of 0.5 to 2.0 μm diameter [2]. These filaments appear as regions of altered refractive index and the discrepancies in their reported dimensions stem from difficulties inherent in the interpretation of microscopic refraction images.

Figure 1 shows a typical damage track produced in a piece of glass. In picture B the objective lens focuses upon the track. In pictures A and C the objective lens focuses 9 μm respectively behind and before the damage track. In the upper and lower parts of the picture, bubble tracks can be seen. These are separated by a bubble-free region in the center of the picture. A fracture in the glass appears near the lower bubble track. Pictures A and C show the refraction effect of a transparent, cylindrical region in the glass, which obviously has a different refractive index from the surrounding glass matrix. This region extends over the full length of the track and is the object of our present investigation.

2. Production of Damage

A 15 ns pulse from a nominal 10 MW ruby laser was focused into a polished cube of glass by means of a lens with a focal length of 9 cm. The glass had a composition of approximately 61 percent SiO_2; 20 percent Al_2O_3; 14 percent Na_2O; 4 percent Li_2O and 1 percent

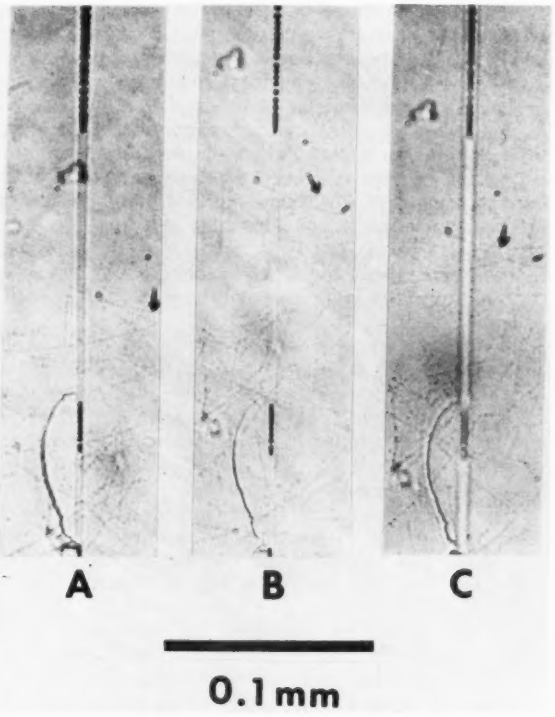

FIGURE 1. *Micrographs of a damage track illuminated in transmitted light.*

The objective lens is focused 9 μm behind (A), on (B), and 9 μm before (C) the track.

[1] Figures in brackets indicate the literature references at the end of this paper.

464-124 OL - 72 - 2

Sb_2O_3, (weight percent), and a refractive index of 1.516 at $\lambda = 0.5467$ μm. A threshold output energy of approximately 0.5 J was required to produce visible fracture damages in this glass. The laser operated in a single mode by means of a transmission sapphire etalon and had a cryptocyanine-methanol Q-switch. A ballistic thermopile-calorimeter was available to monitor the integrated energy of each pulse.

3. Refractive Index Profile

The "invisible" subfracture filamentary damage track in the glass specimen was investigated with a micro-Mach-Zehnder twin beam interferometer [3]. The glass sample containing the track was ground and polished to within optical reach of the microscope objective. the reference beam of the interferometer was directed through a simultaneously ground and polished damage-free specimen of the same thickness. Observations were made in the light of the green mercury line ($\lambda_0 = 0.546707$ μm). The correction prisms in the reference beam were adjusted until the interference fringes were perpendicular to the track. Photographs were taken on high-speed Polaroid film (3000 ASA)[2] and these were rephotographed on line film [4] to enhance contrast and eliminate background. Figure 2 shows the interference photomicrograph of the fringes across the track. Some stress birefringence was observed when the track was illuminated with polarized light. The ray polarized parallel to the track appeared to be retarded from the ray polarized perpendicular to the track by an amount corresponding to approximately 30 percent of the total index change. A corresponding difference in peak displacement was observed when parallel and perpendicularly polarized light was used in the Mach-Zehnder interferometer. Since this refractive index anisotropy is a result of the cooling history of the track and is difficult to analyze accurately, we will consider only the average index change in unpolarized light to estimate the minimum temperature which the track reached when heated by the absorption of laser energy during the self-focusing process.

The fringes show a simple displacement as would be produced by a homogeneous cylindrical inclusion of refractive index different from the surrounding matrix. The shape of the displacement gives no evidence of a tubular (hollow) inclusion as has been observed by Davit [2]. The base width of the fringe displacement measures 3 μm and it is assumed that this is the diameter of the cylindrical track. On its apex, the fringe displacement measures 0.15 fringe spacings. The direction of the fringe displacement indicates that the inclusion has a lower refractive index than the matrix. The direction of the displacement was tested by observing the movement of the fringes while blowing a gas of high refractive index (freon) through one beam of the microscope. This is in contrast to Davit's observation of an increased index region.

[2] Certain commercial materials are identified in this paper in order to specify adequately the experimental procedure. Such identification does not imply recommendation or endorsement by the National Bureau of Standards.

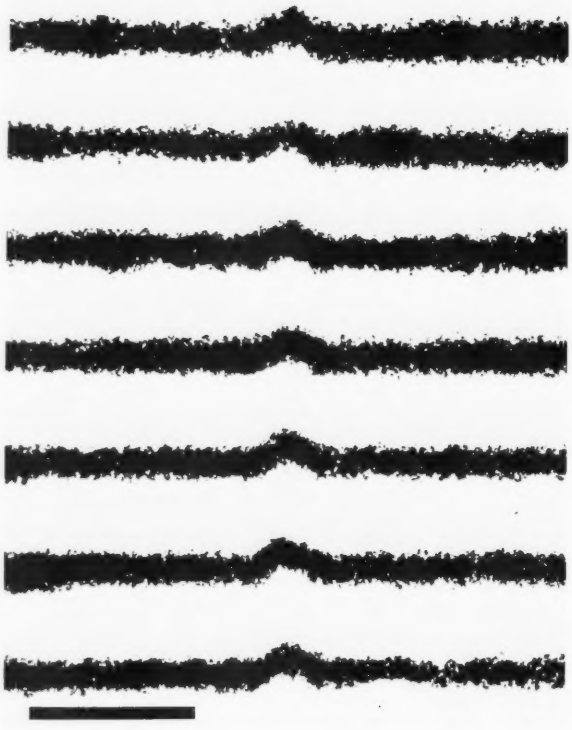

FIGURE 2. *Photomicrograph of the damage track taken with a micro-Mach-Zehnder twin beam interferometer at* $\lambda = 0.54607$ μm.

The black bar shows 10 μm.

Assuming the track to be a homogeneous cylinder of diameter $d = 3$ μm and refractive index n_2 embedded in a matrix of refractive index n_1, allows calculation of the index change in terms of the maximum fractional fringe displacement $f = 0.15$ and the wavelength of the light used (in vacuum or air):

$$n_1 - n_2 = \Delta n = \lambda_0 f/d = 2.8 \times 10^{-2}. \qquad (1)$$

The reduced refractive index indicates that the glass has been heated above its transition temperature and has been subsequently cooled rapidly. The arresting of an elevated fictive temperature structure is well known in glasses but under normal quenching conditions it has not produced such large changes. The conditions leading to the reduction in refractive index, Δn, are discussed later.

The lower refractive index, presumably corresponding to a lower density and to permanent volume expansion in the cylindrical region, has not caused a sharp radial compression in the surrounding matrix. Such a sharp compression would be visible as a counter-deflection of the fringe. The corresponding compression of the surrounding matrix occured apparently over a great distance and the associated fringe shift is therefore not observable.

4. Density of Filament

The reduced refractive index of the cylinder indicates that the glass in the cylinder has a density (ρ_2) different from that of the matrix (ρ_1). The ratio ρ_2/ρ_1 can be estimated from the Lorentz-Lorenz equation:

$$\frac{\rho_2}{\rho_1} = (n_1^2+2)(n_2^2-1)/[(n_1^2-1)(n_2^2+2)] \quad (2)$$

since n_1, the refractive index of the undamaged glass, is known ($n_1 = 1.516$) and Δn has been determined interferometrically. ρ_2/ρ_1 is calculated to be 0.95. In other words, the glass in the track has a density 5 percent below or a specific volume 5 percent above the surrounding matrix. A volume expansion of 5 percent corresponds to a linear expansion of 1.6 percent. This figure is used to calculate the heating stresses in a later part of this paper.

5. Thermal History of the Filament

The density and refractive index of an undercooled liquid such as a silicate glass are dependent on its thermal history, i.e., the rate at which the glass is cooled from its molten state. The thermal expansion coefficient is higher for a liquid than a solid. If a melt is cooled rapidly it contracts first as a liquid, but as its viscosity increases, the melt is unable to readjust its structure in pace with the changing equilibrium structure; it solidifies to a glass and then contracts as a solid. In normal technological practice, glasses are cooled at rates of approximately 2–5 °C/min. At such rates the transition from the liquid to the glassy state occurs near the equilibrium strain-point temperature which is approximately 470 °C in the glass under investigation. Since the cooling of glasses arrests a high-temperature structure, one speaks of the glass as having a certain fictive temperature. Figure 3 shows idealized curves for a fast and slow cooling treatment of a glass sample.

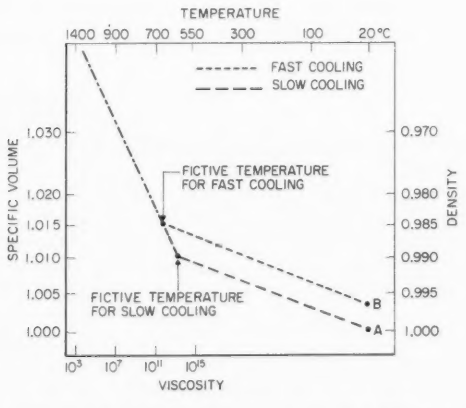

FIGURE 3. *Idealized cooling curves of a glass.*

A and B indicate room temperature densities of slowly and quickly cooled glasses respectively.

The ability of a liquid to adjust its structure with temperature changes is determined by its volume relaxation time. At high temperatures and low viscosities the relaxation times are short and a very rapid cooling rate is required to freeze-in very high temperature structures. Consequently, in order to obtain a certain fictive-temperature structure, two conditions are necessary: (a) the glass must have been heated to at least this fictive temperature and (b) it must have been cooled at a rate sufficiently fast to prevent rearrangement of the structure when cooling below this temperature.

The index change in the damage track allows us to estimate its fictive temperature from the knowledge of the thermal expansion coefficients of the glass. We also can calculate the instantaneous cooling rates of the filament as a function of temperature, compare this rate with the relaxation times at these temperatures, and estimate the temperature (T_f) at which structural rearrangements are arrested. Thus, we have two independent means of estimating the fictive temperature. The only information to be gained by this, however, is the estimate of a minimum temperature (fictive temperature) which the track reached. Much higher temperatures may have been reached during the self-focusing process, but, for the reasons given above, we only have a record of the fictive temperature.

Details of the calculation of T_f are shown in Parts 1 and 2 of the Appendix. We find from the fossil refractive index n_2 and the corresponding density ratio, ρ_2/ρ_1, that the track has at least experienced a temperature of 1450 to 2800 °C. (The range is caused by uncertainty in estimating a value for the high temperature expansion coefficient.) In all probability the temperature reached was much higher. Since, however, the cooling rate of the filament is 10^{10} °C/s (see Part 2a of Appendix) a fictive temperature not higher than 1600 to 1800 °C can be frozen in. At this temperature the relaxation time becomes so long (see Part 2b of the Appendix) that this high-temperature structure becomes arrested.

An additional clue is provided by the observation of microscopic bubbles in the track which indicates a minimum estimate of 1500 °C. The manufacture of silicate glasses requires that the melt be maintained at approximately 1500 °C for many hours in order to facilitate the expulsion of dispersed and dissolved gases (N_2, O_2, CO_2, SO_2). At the elevated temperature, the melt still contains dissolved residual gases in concentrations which correspond to the solution equilibrium at the melting temperature and atmospheric pressure. When such melts are cooled into the glassy state, uptake of more gases is minimal because of the slow diffusion. In order to produce gas bubbles in glass, it is therefore generally necessary to heat it above the temperature at which the melt was equilibrated with the atmosphere. Under the volume-restraining condition of laser track formation, the temperature of bubble formation would, however, be considerably higher than at atmospheric pressure.

All the facts discussed above support the assumption of considerable heating during track formation—at

least to temperatures at which the glass has a viscosity below 10^2 P, i.e., the viscosity at which bubble formation is expected. This assumption is also supported by evidence from other workers. Harper [5] observed the extrusion of glass fibers from laser fractures. Hercher [1] observed that black body continuum radiation was emitted during the damage and estimated a maximum temperature of 5000 K.

6. Thermal Stresses

Using the model of an expanding infinitely long cylinder with a diameter of 3 μm embedded in an infinite solid of the same mechanical properties, we have attempted to calculate the stresses in and around the damage filament. In the equations, we assumed that the cylinder expanded by 5 percent of its volume or 1.6 percent of its length isotropically. This is the total expansion indicated by our observation of the cold, fossil track. The expansion of the hot cylinder during the actual laser damage was undoubtedly much higher. We calculate (see Appendix Part 3) the minimum stresses in and around the cylinder produced during heating of the damage area to be as follows:

A. Outside the cylinder at the surface of the track, $r=1.5\,\mu$m, following the convention that tensile stresses are positive, and compressive ones negative, the radial, σ_{rr}; tangential, $\sigma_{\theta\theta}$; and longitudinal, σ_{zz}, stresses are listed below:

$$\sigma_{rr}=-6.5\times10^8\ \text{N/m}^2=[-95{,}000\ \text{psi}]$$

$$\sigma_{\theta\theta}=+6.9\times10^8\ \text{N/m}^2=[+100{,}000\ \text{psi}]$$

$$\sigma_{zz}=+0.46\times10^8\ \text{N/m}^2=[+6{,}800\ \text{psi}].$$

B. Inside the cylinder, also at the surface, $r=1.5\,\mu$m:

$$\sigma'_{rr}=-6.5\times10^8\ \text{N/m}^2=[-95{,}000\ \text{psi}]$$

$$\sigma'_{\theta\theta}=-6.5\times10^8\ \text{N/m}^2=[-95{,}000\ \text{psi}]$$

$$\sigma'_{zz}=-12.8\times10^8\ \text{N/m}^2=[-190{,}000\ \text{psi}].$$

The tangential stress in the matrix is tensile, and has the highest magnitude. Thus, it would preferentially lead to a fracture. Its actual numerical value, even considering the minimum volume change, is more than $\frac{1}{3}$ of the stress considered to be the inherent, internal strength of glass in absence of defects [6]. In the presence of the usual defects and considering the higher hot stresses around the track, the tangential stresses would be sufficient to initiate cracks. Such cracks would be expected to occur in planes perpendicular to the tangential stress direction, and thus would be in half-planes parallel to and containing the axis of the track, randomly distributed around the circumference.

The microscopic study of the numerous tracks produced in the glass, as described earlier, reveals two types of fractures: (a) gross starburst, usually not more than one or two per track and (b) very numerous, small planar circular fractures along all tracks, associated both with bubble regions of the track, and with the transparent track region between the bubbles.

All the planar fractures are almost circular, rest with one edge against the track and are in planes containing the axis of the track. Figure 4 is a sketch of the described fractures. We did not find any fractures perpendicular to the track as had been described for laser damage in polymethyl-methacrylate [7]. We believe that the gross starburst cracks were caused by foreign inclusions, while the small ubiquitous planar fractures are associated with an intrinsic self-focusing damage process.

The morphology of the observed planar fractures is in agreement with the findings of the stress calculation which predict the dominance of tangential stresses.

7. Summary

(1) Laser induced self-focusing damage tracks in glass were produced by passive irradiation.

(2) The refractive index distribution in the damaged glass was investigated by double-beam interferometry.

(3) Filamentary damages were found which consist of homogeneous cylindrical regions, 3 μm in diameter, having a refractive index of $\Delta n=2.8\times10^{-2}$ below the surrounding glass.

(4) The reduced refractive index in the damaged region is calculated to correspond to a reduction in density by a factor of $\rho_2/\rho_1=0.95$.

(5) It is calculated that the glass in the filament has a structure corresponding to a fictive temperature of 1450 to 2800 °C, the range being caused by uncertainty in the value of the high temperature expansion coefficient.

(6) It is calculated from heat flow conditions and a typical relaxation spectrum of glass that it is not possible to freeze-in a high-temperature structure corresponding to a higher fictive temperature than 1600 to 1800 °C, even though the actual temperature during laser beam exposure may have considerably exceeded this temperature.

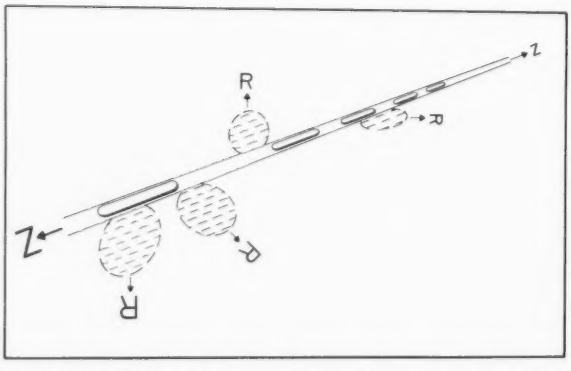

FIGURE 4. *Sketch of the small planar fractures observed along all tracks.*

The fractures are in half-planes containing the track axis (z) and a random radial vector **R**.

(7) Bubble formation in damage tracks is evidence that the laser beam heated the glass at least to 1500 °C.

(8) Equations for the axial, radial and tangential stresses in and around a heated cylindrical region in glass are derived. It is shown that for heating the cylinder to its fictive temperature only, corresponding to a volume change of 5 percent, the tensile tangential stress reaches as much as 100,000 psi which is $\frac{1}{5}$ of the inherent, internal strength of glass in absence of defects.

(9) A microscopic investigation of the laser tracks shows large numbers of small planar fractures originating from one side of the track and oriented parallel to the track. Such fractures have the proper orientation to be caused by the predicted dominant tangential stresses arising from laser-beam heating.

(10) It is concluded that thermal expansion of the glass is a sufficient mechanism to produce fractures within the glass. This conclusion is supported by the fact that glasses with low thermal expansion (fused silica, borosilicate glasses) show a higher damage threshold to passive laser beam exposure than glasses with high thermal expansion [8].

8. Appendix

Parts I and II of this appendix show detailed calculations of the estimated ranges within which the fictive temperature of the damage track occurs. These calculations rest upon assumptions and equations which are well followed, in general, by silicate glasses, and are only proposed to give an estimate of the minimum temperature reached by the damage track. Each part presents totally independent analyses which rest on different assumptions and available data.

Part III is a rigorous analysis of the stresses involved in the heating process and does not depend upon the results of Parts I and II. Since we are calculating stresses developed in heating, and the heating process was very fast, we may neglect the effect of plastic deformations, or volume relaxations and compaction effects. Therefore, Part III is only concerned with the elastic problem of heating a cylindrical filament within a cold matrix.

Part I. Calculation of Fictive Temperature from Index Change

The estimate of a fictive temperature from a change in index depends upon the variation of index with specific volume, and of specific volume with temperature. From the Lorentz-Lorenz equation, we can easily estimate Δv and Δn, but the dependence of specific volume on temperature up to high temperatures is only known in general terms. We know the expansion coefficient of this glass up to 300 °C and may apply it as high as the transformation range (550 °C). We also have measured the temperature dependence of index in the transformation region from 550 to 580 °C. From these data, we may calculate an upper and a lower temperature estimate for T_f, as shown in figure 5. The relative size is plotted versus temperature

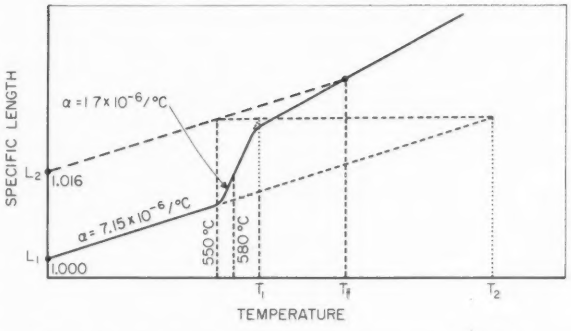

FIGURE 5. *Extrapolation procedure for estimating the high temperature specific volume of the glass.*

T_1 and T_2 are the upper and lower estimates of the fictive temperature. The measured solid expansion coefficient is shown. The expansion coefficient quoted for the transformation range (550–580 °C) has been calculated from the index data by using the Lorentz-Lorenz equation, and is only shown here for illustration.

and follows the general behavior expected of silicate glasses. The estimate, T_1, is an extrapolation of the index dependence on temperature. It uses the expansion coefficient characteristic of the transformation region, and will underestimate T_f. The estimate T_2 uses the solid expansion coefficient and will overestimate T_f.

Measurements of index change as a function of temperature in the transformation range from 550 to 580 °C are shown below:

TABLE 1

$n(\lambda = 0.58959\ \mu m)$	Temperature
1.51337	584 °C
1.51363	575 °C
1.51406	562 °C
1.51436	552 °C

These points plot as a straight line whose slope yields the temperature dependence of index:

$$\left[\frac{\Delta n}{\Delta T}\right] = -3.16 \times 10^{-5}/\,°C$$

The observed change of $\Delta n = -0.028$ gives a temperature change of 900 °C. The base glass is assumed to have a fictive temperature of 550 °C, therefore we estimate $T_1 \simeq 1450$ °C.

In the calculation of T_2, we now invoke the Lorentz-Lorenz equation to calculate the difference in volume between the track and matrix. If n_1 is the index of the matrix at 1.516, corresponding to a matrix fictive temperature of 550 °C, and Δn is -0.028 we may calculate n_2 to be 1.488 and calculate the size ratio L_2/L_1 to be 1.016. The solid expansion coefficient is $7.15 \times 10^{-6}/\,°C$, therefore, the corresponding temperature change is calculated to be 2240 °C. Adding the fictive temperature of the matrix leads to an estimate for $T_2 \simeq 2800$ °C. The fictive temperature estimate is therefore seen to be between 1450 and 2800 °C by this method.

Part II. A. Calculation of Cooling Rate of Filament

The hot filament may cool by thermal conduction and/or radiation. Due to the good thermal contact assumed between the hot zone and its surroundings, the heat flow by conduction is much larger than by radiation, and the latter may be totally neglected.

The problem of a hot cylinder embedded in a matrix has been solved by Carslaw and Jaeger [9] for the change in temperature of the matrix as a function of time and distance from the hot zone. Due to the good thermal contact between the cylinder and matrix, we expect a very high cooling rate, therefore, we are only interested in the short-time solutions. The cooling rate may be calculated from the heat flow between the hot cylinder and a larger concentric cold sink surface. We shall, therefore, use the solutions of Carslaw and Jaeger to estimate the distance of this cold sink from the hot zone. An analysis of their calculations [fig. 41, p. 337, ref. 9] leads to table 2 below, assuming a heat conductivity, $K = 0.0121$ J cm^{-1} s^{-1} °C^{-1}; a specific heat, $C = 1.34$ J g^{-1} °C^{-1}; a density, $\rho = 2.1$ g/cm^3, and a filament radius $a = 1.5$ μm.

TABLE 2

Distance from filament r_0/a	Temperature at r_0: T_0/T(filament)	Time taken to increase the temperature of r_0 to the value T_0
10	0.4	8×10^{-2} s
10	.2	8×10^{-3}
1.4	.4	3.2×10^{-5}
1.17	.4	2.4×10^{-6}
1.17	.2	8×10^{-7}
1.09 extrapolate	.4	8×10^{-7}
1.04 extrapolate	.4	2.4×10^{-7}

Since we are interested in finding the cooling rate applicable for the first 200 °C drop in temperature, and the cooling rates we expect to obtain are of the order 10^9 to 10^{10} °C/s, let us consider a cold sink at $r_0 = 1.17a$ for a slow rate, and $r_0 = 1.04a$ for a fast cooling rate estimate. The cooling rate can be calculated as follows:

$$\frac{dT}{dt} = \frac{1}{\rho V C}\frac{dq}{dt} = \frac{2\pi a L K (T_{\text{fil}} - T_0)}{C\,\pi\rho a^2 L (r_0 - a)} = \frac{2K(T_{\text{fil}} - T_0)}{C\,\rho a\,(r_0 - a)}$$

where K is the thermal conductivity, dq/dt is the rate of heat flow, C is the specific heat, V is the filament volume, L is a unit length and T_0 is the matrix temperature at r_0. The low and high rates ($r_0 = 1.17a$ and $r_0 = 1.04a$) are calculated respectively to be:

$$\left(\frac{dT}{dt}\right)_l = 2.3\times10^6\,[T_{\text{fil}} - T_0]\,(°\text{C/s})$$

$$\left(\frac{dT}{dt}\right)_h = 9.5\times10^6\,[T_{\text{fil}} - T_0]\,(°\text{C/s}).$$

The resulting heat conduction cooling rates are listed in table 3 below and it is seen that the filament cools fast enough to undergo a temperature change of approximately 100 °C in less than 4×10^{-8} s, and therefore our assumed cold sinks remain so during that period. In the calculation of cooling rates, it is, therefore, suitable to assume that T_0 represents room temperature, 20 °C, and thus ignore it.

TABLE 3

Filament temperature	$\left(\frac{dT}{dt}\right)_h$	$\left(\frac{dT}{dt}\right)_l$
1000 °C	1.0×10^{10} °C/s	2.4×10^9 °C/s
1200 °C	1.2	2.8
1400 °C	1.4	3.3
1600 °C	1.6	3.8
1800 °C	1.8	4.2
2000 °C	2.0	4.7
2200 °C	2.2	5.2

Part II. B. Calculation of Volume Relaxation Time for the Filament

The volume relaxation time at high temperatures may be estimated by comparing this glass to a sodium-borosilicate for which high-temperature data have been reported [10]. At temperatures above 1400 °C most oxide glasses are found to have a single or narrow distribution of relaxation times, therefore, characterizing the most probable relaxation time will suffice to analyze the relaxation processes. Results from the soda-borosilicate study [10] also show that at high temperatures the volume relaxation time is approximately 3 times the shear relaxation time. The latter may then be found by considering the shear viscosity data, and comparing it with the soda-borosilicate (SBS) glass [10]:

$$\tau = \frac{\eta}{\eta_{\text{SBS}}}\,\tau_{\text{SBS}}.$$

This equation rests upon the likely assumption that the moduli of the two glasses are equal. This falls well within the order of magnitude estimate which we are seeking. The volume relaxation time is thus found as:

$$\tau_v = 3\,\frac{\eta}{\eta_{\text{SBS}}}\,\tau_{\text{SBS}}.$$

Once τ_v is calculated, we have the rate at which the structure rearranges itself. The minimum cooling rate necessary for freezing a given structure is found by requiring τ_v to be the time necessary for the relaxation time to increase by a factor of 2. This factor approximates the width of what is usually assumed to be a single relaxation process. Thus, by the time τ_v has elapsed, it would require the structure $2\,\tau_v$ to rearrange and so on until room temperature is reached. Once the cooling rate necessary to freeze a structure equals the heat conduction cooling rate, then the latter is a likely mechanism for arresting structural changes at the tem-

perature of coincidence. The volume relaxation time and minimum cooling rates are given in table 4 below:

TABLE 4

Temperature	Minimum cooling rate	Volume relaxation time τ_v
1000	2.5×10^{6} °C/min	10^{-5} s
1200	10^{8}	5×10^{-7}
1400	10^{9}	3×10^{-8}
1600	8×10^{9}	6×10^{-9}
1800	4×10^{10}	2×10^{-9}
2000	1.5×10^{11}	5×10^{-10}
2200	4×10^{11}	2×10^{-10}

Referring to table 3 we may now compare the two aforementioned cooling rates, and find the point of coincidence. An upper and a lower estimate of the conduction cooling rate were calculated, therefore, we have two temperature estimates. The temperatures obtained from these calculations give us an estimate of fictive temperature from 1600 to 1800 °C.

Part III. Solution of Stresses Developed by Heating of the Laser Track

In this section, we are interested in calculating the stresses developed both inside and outside the cylinder representing the laser track when its temperature reaches a value corresponding to the measured change in index. By the Lorentz-Lorenz equation, we can calculate the change in volume associated with the index change without having to speculate about the temperature dependence of the index of this glass. The stresses can then be directly calculated from the volume change.

After a somewhat detailed look through the literature, for a general solution of the problem, we unfortunately found that the most common solutions involve the "plane-strain" approximation. This approach assumes that there is no strain in the longitudinal direction and that the necessary stress is provided externally to the system. The solution does not represent the problem at hand, since a large longitudinal stress is expected to develop in the cold matrix. The need to determine all stresses in the matrix (outside the hot cylinder) requires a more general solution which is given below.

Some solutions of the generalized plane-strain problem may be found in the literature [13], where, in this case, the longitudinal stress is assumed to be a constant. We have not found one which proceeded beyond the first motions of solving the problem, therefore, we have chosen to solve the problem from the general stress-strain relations.

The problem is best expressed in cylindrical coordinates, since the angular symmetry eliminates the θ-dependence of the solutions. The general stress-strain relations used here are taken from Love [11], and particularly from Boley and Weiner [12].

The solutions derived below are based upon the assumption that the positive volume change of the cylinder in the longitudinal (z) direction occuring during the heating process, induces stresses outside the cylinder which occur throughout the cold matrix and reach a maximum at the interface. Outside the cylinder, the longitudinal extension (U_z) is therefore proportional to the length [or distance away from the origin which we locate in the middle of the cylinder], and the longitudinal strain is uniform. The latter, ϵ_{zz}, is only a function of the radial distance:

$$U_z = f(r)z; \qquad \epsilon_{zz} = f(r)$$

This allows solution of the equilibrium equation in the axial direction:

$$\frac{\partial \sigma_{rz}}{\partial r} + \frac{\partial \sigma_{zz}}{\partial z} + \frac{\sigma_{rz}}{r} = 0$$

where

$$\sigma_{rz} = \mu \left[\frac{\partial U_r}{\partial z} + \frac{\partial U_z}{\partial r} \right]$$

and

$$\sigma_{zz} = (\lambda + 2\mu)\, \epsilon_{zz} + \lambda \epsilon_{rr} + \lambda \epsilon_{\theta\theta}$$

λ and μ are the Lamé elastic constants for the material, and the strains, $\epsilon_{ij} \equiv \frac{1}{2}\left[\frac{\partial U_i}{\partial X_j} + \frac{\partial U_j}{\partial X_i}\right]$ and the stresses σ_{ij} are defined in Love [11], and Boley and Weiner [12]. The cylinder is considered infinite to avoid end effects, therefore, the radial displacement, U_r, has no z-dependence. Since neither ϵ_{zz}, nor ϵ_{rr}, nor $\epsilon_{\theta\theta}$ depend on the z-variable, the differential equation is easily solvable for $f(r)$:

$$\frac{d^2 f(r)}{dr^2} + \frac{1}{r}\frac{df(r)}{dr} = 0$$

and leads to the following solution with B_0 and r_0 as integration constants.

$$f(r) = B_0 \ln (r_0/r)$$

$$U_z = B_0 z \ln (r_0/r)$$

$$\epsilon_{zz} = B_0 \ln (r_0/r).$$

The equilibrium equation in the radial direction may now be written for the region outside the cylinder:

$$\frac{\partial \sigma_{rr}}{\partial r} + \frac{\partial \sigma_{rz}}{\partial z} + \frac{\sigma_{rr} - \sigma_{\theta\theta}}{r} = 0$$

with:

$$\sigma_{rr} = (\lambda + 2\mu)\frac{\partial U_r}{\partial r} + \lambda \frac{U_r}{r} + \lambda \frac{\partial U_z}{\partial z}$$

$$\sigma_{\theta\theta} = (\lambda + 2\mu)\frac{U_r}{r} + \lambda \frac{\partial U_r}{\partial r} + \lambda \frac{\partial U_z}{\partial z}$$

$$\sigma_{rz} = -\mu B_0 z/r.$$

The resulting differential equation is again easily solvable:

$$\frac{d}{dr}\left[\frac{dU_r}{dr}+\frac{U_r}{r}\right]=\left(\frac{\lambda+\mu}{\lambda+2\mu}\right)B_0/r$$

with the following solution:

$$U_r(r)=-\frac{B_0}{2}\left[\frac{\lambda+\mu}{\lambda+2\mu}\right]r\ln(r_0/r)+Q/r.$$

The characteristic length of the logarithmic term r_0, is taken to be the same as for U_z. While this assumption is made for simplicity in solving the problem, it is reasonable, as r_0 characterizes the penetration of the effect of the longitudinal stress into the matrix. Q is a constant whose value will be determined by the boundary conditions. The logarithmic term in both solutions is only valid up to $r=r_0$. The following expressions are then obtained for the stresses outside the cylinder:

$$\sigma_{rr}=(\lambda+\mu)\,B_0/2+\left[\lambda-\frac{(\lambda+\mu)^2}{(\lambda+2\mu)}\right]B_0\ln(r_0/r)-2\mu\,Q/r^2$$

$$\sigma_{\theta\theta}=\left[\lambda\left(\frac{\lambda+\mu}{\lambda+2\mu}\right)\right]B_0/2+\left[\lambda-\frac{(\lambda+\mu)^2}{(\lambda+2\mu)}\right]B_0\ln(r_0/r)+2\mu\,Q/r^2$$

$$\sigma_{zz}=\mu\left[\frac{3\lambda+4\mu}{\lambda+2\mu}\right]B_0\ln(r_0/r)+\lambda\left[\frac{\lambda+\mu}{\lambda+2\mu}\right]B_0/2.$$

Inside the cylinder, the solutions resemble the "plane-strain" approximation with the exception of an allowed expansion of the cylinder in the longitudinal direction [see ref. [12], pp. 288–291].

$$U'_r(r)=\frac{1}{2}\left[\frac{3\lambda+2\mu}{\lambda+2\mu}\right]\left[\frac{\Delta L}{L}\right]r$$

$$U'_z=Az$$

$\frac{\Delta L}{L}$ is the total fractional expansion of the material in heating to the temperature of the track, and A is a constant to be determined by the boundary conditions. Since the cylinder is small, we have not allowed a variation of U_z with radial distance. This approximation proposes that the rod expands uniformly in the longitudinal direction, and greatly simplifies the problem without much effect on the final conclusions. The resulting stresses may be written as follows:

$$\sigma'_{rr}=\lambda A-\left[\frac{\mu(3\lambda+2\mu)}{(\lambda+2\mu)}\right]\frac{\Delta L}{L}$$

$$\sigma'_{\theta\theta}=\lambda A-\left[\frac{\mu(3\lambda+2\mu)}{(\lambda+2\mu)}\right]\frac{\Delta L}{L}$$

$$\sigma'_{zz}=(\lambda+2\mu)A-\left[\frac{2\mu(3\lambda+2\mu)}{(\lambda+2\mu)}\right]\frac{\Delta L}{L}$$

$$\epsilon'_{zz}=A.$$

We now turn to boundary conditions to solve for the four unknown constants: A, B_0, r_0, and Q, assuming the following typical values for the Lamé constants and the calculated elongation, $\frac{\Delta L}{L}$:

$$\lambda=2.1\times10^{10}\ \mathrm{N/m^2}$$

$$\mu=2.66\times10^{10}\ \mathrm{N/m^2}$$

$$\Delta L/L=0.016.$$

The boundary conditions are as follows:

(i) the radial stress is continuous across the boundary:

$$\sigma_{rr}(a)=\sigma'_{rr}(a)\qquad\text{B.C.–1}$$

(ii) the tangential strain and the radial displacement are continuous across the boundary:

$$U_r(a)=U'_r(a)\qquad\text{B.C.–2}$$

(iii) the longitudinal strain is continuous across the boundary:

$$\epsilon_{zz}(a)=\epsilon'_{zz}(a)\qquad\text{B.C.–3}$$

(iv) there are no external longitudinal forces on the sample:

$$\int_{S_0}\sigma_{zz}\cdot ds+\int_{S_0}\sigma'_{zz}\cdot ds=0$$

where S_0 is the cross-sectional area. This becomes:

$$\int_a^{r_0}\sigma_{zz}rdr+\int_0^a\sigma'_{zz}rdr=0\qquad\text{B.C.–4}$$

Starting with B.C.–2 and B.C.–3 we calculate Q from an estimate of A:

$$Q=2.82\times10^{-14}+7.23\times10^{-13}A.$$

Then, B_0 and r_0 are calculated in turn from B.C.–1 and B.C.–3 as follows:

$$B_0=1.29\mathrm{A}+9.95\times10^{11}\,\mathrm{Q}-2.8\times10^{-2}$$

$$r_0=\mathrm{EXP}\left[\frac{A-13.41\,B_0}{B_0}\right].$$

Finally, a new value of A is computed from B.C.–4 and reinserted into B.C.–2. The integrations of B.C.–4 for the region outside the cylinder are limited to r_0

since the solutions are only valid in this range. They lead to:

$$A = 10^{-2} + 2.78 \times 10^{-5} B_0 - 1.23 \times 10^{12} B_0 r_0^2.$$

The iteration converges quickly and the following values are obtained for the constants, after we reached a variation smaller than 0.5 percent of each term:

$$A = 6.22 \times 10^{-4}$$

$$Q = 2.86 \times 10^{-14} \text{ m}^2$$

$$B_0 = 1.31 \times 10^{-3}$$

$$r_0 = 2.46 \times 10^{-6} \text{ m}.$$

The stresses at the surface are then computed for $r = a = 1.5\ \mu$m.

OUTSIDE[3]

$$\sigma_{rr} = -6.5 \times 10^8 \text{ N/m}^2 = -\ 95{,}000 \text{ psi}$$

$$\sigma_{\theta\theta} = +6.9 \times 10^8 \text{ N/m}^2 = +100{,}000 \text{ psi}$$

$$\sigma_{zz} = +4.6 \times 10^7 \text{ N/m}^2 = +\ 6{,}800 \text{ psi}$$

INSIDE

$$\sigma'_{zz} = -6.5 \times 10^8 \text{ N/m}^2 = -\ 95{,}000 \text{ psi}$$

$$\sigma'_{\theta\theta} = -6.5 \times 10^8 \text{ N/m}^8 = -\ 95{,}000 \text{ psi}$$

$$\sigma'_{zz} = -12.8 \times 10^8 \text{ N/m}^2 = -190{,}000 \text{ psi}$$

Tensile stresses are positive while compressive ones are negative. Inside, the radial and tangential stresses are equal as in the plane strain problem, but their magnitude is slightly reduced due to the allowed longitudinal strain through the shear modulus. The longitudinal stress is seen to be very large, and all 3 stresses are compressive, as expected. Outside, the tangential and longitudinal stresses are tensile, with the former equaling three times the latter. The low value of the external longitudinal stress at the interface stems from the elastic distribution of the total force far into the matrix.

[3] A shear stress, σ_{rz} is also present outside. It reaches a large value near the ends of the tracks (2×10^9 N/m^2 for a track 0.2 mm long). However, since the tracks are finite, the glass matrix around the ends acts to dissipate the forces, and the model of an infinite track cannot apply.

The authors wish to acknowledge the help of H. Dardy in producing the damage tracks and A. Napolitano and R. M. Waxler for measuring the high temperature refractive index and the thermal expansion of the undamaged base glass.

9. References

[1] Hercher, M., Laser-Induced Damage in Transparent Media, J. Opt. Soc. of America **54**, 563 (1964).
[2] Davit, J., Filamentary damage in glasses (Proc. Symp. on Damage in Laser Materials, Boulder, Colorado, June 24–25, 1970), Nat. Bur. Stand. (U.S.), Spec. Publ. 341, 126 pages (Dec. 1970).
[3] Leitz Interference Microscope, Type SII, 50X-objective lens, 0.85 aperture.
[4] "Codalith," Kodak.
[5] Harper, D. W., Laser Damage in Glass, Brit. J. Appl. Phys. **16**, 751–752 (1965).
[6] Ernsberger, F. M., Tensile and Compressive Strength of Pristine Glasses by an Oblate Bubble Technique, Physics and Chemistry of Glasses **10**, 240–245 (1969).
[7] Ashkinadze, B. M., Valdimirov, V. I., Likhachev, V. A., Ryvkin, S. M., Salmanov, V. M., and Yardshetsyii, I. D., Damage Produced by Laser Beam in Transparent Dielectric, Soviet Physics—Doklady **11**, No. 8, pp. 703–705 (Feb. 1967).
[8] Haller, W., and Dardy, H., Effect of microdomains formed by liquid/liquid immiscibility upon the damage threshold of glass, Nat. Bur. Stand. (U.S.), Tech. Note 574, p. 22 (May 1971).
[9] Carslaw, H. S., and Jaeger, J. C., Conduction of Heat in Solids, second edition (Clarendon Press, Oxford 1959).
[10] Simmons, J. H., and Macedo, P. B., Shear and Volume Structural Relaxation in Immiscible Oxide Melts, Amorphous Materials, R. W. Douglas and B. Ellis, Eds., Chapter 7 (John Wiley & Sons, London 1971).
[11] Love, A. E. H., A Treatise on the Mathematical Theory of Elasticity, Fourth Edition (Dover, New York 1944).
[12] Boley, B. A., and Weiner, J. H., Theory of Thermal Stresses, Chapter 4 (John Wiley & Sons, New York 1960).
[13] Wang, C. T., Applied Elasticity, Chapter 4 (McGraw-Hill, New York 1953).

(Paper 76A4–725)

JOURNAL OF RESEARCH of the National Bureau of Standards—A. Physics and Chemistry
Vol. 76A, No. 4, July–August 1972

Normal Emissivity of an Isothermal, Diffusely Reflecting Cylindrical Cavity (With Top) as a Function of Inside Radius

W. B. Fussell

Institute for Basic Standards, National Bureau of Standards, Washington, D.C. 20234

(March 16, 1972)

The normal emissivity of an isothermal cylindrical cavity (with top), with a diffusely reflecting interior of reflectivity much less than 1, is calculated approximately as a function of the inside radius of the cylinder by the DeVos method. The calculation is analytical, and considers the singly and doubly reflected radiation escaping from the cavity aperture. The results of the analysis indicate that, for cylinders whose length-to-lid aperture ratio is much larger than 1: (a), for a given cylinder length and lid aperture, the configuration with the inside diameter approximately 0.64 the length has the *smallest* normal emissivity; (b), as the inside diameter increases or decreases from the configuration of smallest normal emissivity, the normal emissivity *increases* monotonically.

Key words: Cavity; cylindrical cavity; diffusely reflecting; emissivity; normal emissivity; radiation; reflectance.

1. Introduction

It is often important to establish design criteria for cavity radiators. A frequently used configuration is the cylindrical cavity with top (fig. 1). If the interior of the cavity is *isothermal*, the normal emissivity of the cylinder may be defined as the ratio of the normal radiance of the cylinder aperture to the normal radiance of a blackbody at the temperature of the interior. If the bidirectional reflectance characteristics of the cylinder interior are known, the DeVos method [1][1] theoretically enables the normal emissivity of an isothermal cylinder to be computed from the sum of: (a), the radiation emitted parallel to the cylinder axis by the area of the base defined by the projection of the aperture (parallel to the axis) onto the base; (b), the radiation emitted by the interior of the cylinder which is incident upon the projection of the aperture onto the base, and then reflected out the cavity aperture parallel to the axis; (c), multiply reflected radiation which escapes from the cavity aperture in a direction parallel to the axis. That is, a DeVos analysis is a series expansion of the normal emissivity of a cavity in terms involving successively greater numbers of interreflections within the cavity. This series converges rapidly if the reflectance, r, of the cavity interior is much less than 1; therefore, the reflectance of the cylinder interior is assumed to satisfy this condition. To simplify the analysis further, it is also assumed that the interior of the cylinder reflects and emits diffusely.[2] (Many cavity radiator materials are approximately diffuse in their reflecting and emitting characteristics.)

Let e_{CN} be the normal emissivity of the cylinder and e the diffuse emissivity of the cylinder interior. Then e_{CN} may be written,

$$e_{CN}=e[1+rA_1+r^2A_2+\ \ldots], \tag{1}$$

where A_1, A_2, etc., are coefficients which depend only on the cylinder configuration. From Kirchhoff's law [2] and the assumption that the cylinder walls are opaque, it is clear that

$$r_{CN}=1-e_{CN}, \tag{2}$$

and that

$$r_{CN}=rB_1+r^2B_2+\ldots, \tag{3}$$

where

$$B_1=1-A_1,$$

$$B_2=A_1-A_2,$$

etc.

Quinn has shown [4] that, for the cylindrical cavity of figure 1 with length L, aperture radius R_1, and inside radius R_2,

$$B_1=2[\overline{L}^2+2+\overline{L}(\overline{L}^2+4)^{0.5}]^{-1}, \tag{4}$$

where

$$\overline{L}=L/R_1. \tag{5}$$

Quinn also shows that

$$B_2=16\overline{R}_2^3\int_0^{\overline{M}}d\overline{Y}(\overline{M}^2-\overline{Y}^2)$$

[1] Figures in square brackets indicate the literature references at the end of this paper.
[2] In this paper, the terms "diffuse" and "diffusely" refer to reflection or emission that follows Lambert's cosine law [3].

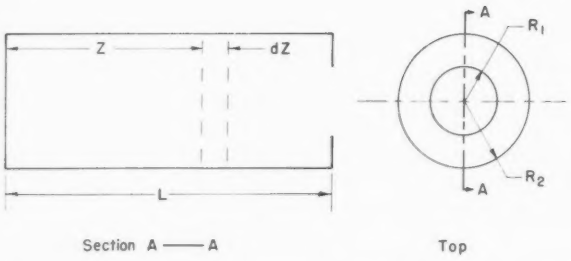

FIGURE 1. *Cross section and top view of cylindrical cavity:* L, *length of cylinder;* R_1, *radius of aperture;* R_2, *inside radius of cylinder;* Z, *height of differential element above base of cylinder.*

$$X[(\bar{M}+\bar{Y})^2+\bar{R}_2^2+1+([(\bar{M}+\bar{Y})^2+\bar{R}_2^2+1]^2 - 4\bar{R}_2^2)^{0.5}]^{-1}$$

$$X[(\bar{M}-\bar{Y})^2+\bar{R}_2^2+1+([(\bar{M}-\bar{Y})^2+\bar{R}_2^2+1]^2 - 4\bar{R}_2^2)^{0.5}]^{-1}$$

$$X[([(\bar{M}+\bar{Y})^2+\bar{R}_2^2+1]^2-4\bar{R}_2^2)^{0.5}]^{-1}$$

$$X[([(\bar{M}-\bar{Y})^2+\bar{R}_2^2+1]^2-4\bar{R}_2^2)^{0.5}]^{-1}, \quad (6)$$

where

$$\bar{R}_2 = R_2/R_1, \quad (7)$$

$$\bar{M} = \bar{L}/2, \quad (8)$$

$$\bar{Y} = \bar{Z} - \bar{M} \qquad \text{(see fig. 1).} \quad (9)$$

2. Analysis

It is now assumed that $\bar{M}$ is much greater than 1; that is, the cylinder length $\bar{L}$ is much greater than the lid aperture, $2\bar{R}_1$. It is desired to compute B_2 for the two cases: (a), R_2 equals R_1; (b), R_2 much greater than R_1.

2.1. Calculation of B_2 for R_2 Equals R_1

Since $\bar{M}$ is much greater than 1, it is convenient to expand B_2 as a series in powers of $(\bar{M})^{-1}$. For R_2 equal to R_1, it is found that

$$B_2 = 4^{-1}(\bar{M})^{-3} + 2^{-1}(\bar{M})^{-4} + \ . \ . \ ., \quad (10)$$

to order $(\bar{M})^{-4}$; that is, terms of order $(\bar{M})^{-5}$ or higher are discarded.

2.2. Calculation of B_2 for R_2 Much Greater Than R_1

If R_2 is much greater than R_1, Quinn shows [4] that B_2 may be approximated with fractional error roughly $2(\bar{M}\bar{R}_2^3)^{-1}$ by

$$B_2' = 4\bar{S}_2^3(\bar{M})^{-2}\int_0^1 d\bar{V}(1-\bar{V}^2)$$

$$X[(1+\bar{V})^2+\bar{S}_2^2]^{-2}[(1-\bar{V})^2+\bar{S}_2^2]^{-2}, \quad (11)$$

where

$$\bar{S}_2 = \bar{R}_2/\bar{M}, \quad (12)$$

$$\bar{V} = \bar{Z}/\bar{M} - 1 \qquad \text{(see fig. 1).} \quad (13)$$

B_2' has the closed form solution,

$$B_2' = \bar{S}_2[16\bar{M}^2(\bar{S}_2^2+1)^3]^{-1}$$

$$X[4(1-\bar{S}_2^4) + \bar{S}_2^2(\bar{S}_2^4+3\bar{S}_2^2+6)\ \ln\ (1+4/\bar{S}_2^2) + 2\bar{S}_2^2(3-\bar{S}_2^2)\ \cot^{-1}\ (\bar{S}_2/2)]. \quad (14)$$

It is useful to define the function

$$F = B_2'\bar{M}^2, \quad (15)$$

which is *independent* of $\bar{M}$.

It is seen from eq (15) that

$$\lim_{\bar{S}_2\to 0} B_2' = 4^{-1}\bar{S}_2(\bar{M})^{-2} = 4^{-1}\bar{R}_2(\bar{M})^{-3}, \quad (16)$$

and that

$$\lim_{\bar{S}_2\to\infty} B_2' = (2/3)(\bar{S}_2^5\bar{M}^2)^{-1}. \quad (17)$$

Thus B_2' approaches 0 as $\bar{S}_2$ approaches 0 and as $\bar{S}_2$ becomes infinite; hence B_2' must have *at least one maximum* as $\bar{S}_2$ varies from 0 to infinity. Direct computation of B_2' (see table 1) establishes a maximum at

$$\bar{S}_{2\text{MAX}} = 0.644. \quad (18)$$

The physical symmetry of the problem suggests that there is only 1 maximum of B_2' as $\bar{S}_2$ varies from 0 to infinity; however, this has *not* been proved mathematically.

TABLE 1. *The normalized, approximate second order DeVos reflection coefficient,* $F(\bar{S}_2)$, *for a diffusely reflecting cylindrical cavity with length much greater than the aperture (see fig. 1): for values of the ratio of the aperture to the length,* $\bar{S}_2$, *between 0.1 and 1.0*

$\bar{S}_2$	$F(\bar{S}_2)$	
0.1	0.034350	
.2	.070853	
.4	.166720	
.6	.208828	
.644	.210088	(Maximum)
.8	.197426	
1.0	.160336	

3. Conclusions

From eq (3) for r_{CN}, eq (4) for B_1, and the preceding analysis of B_2, it is seen that:

a. B_1 is independent of R_2.
b. Since $\bar{M}$ is much greater than 1, to order $(\bar{M})^{-3}$,

$$B_2 \approx B_2' \approx 4^{-1}\bar{R}_2(\bar{M})^{-3}.$$

c. As R_2 varies from R_1 to $0.64R_1\overline{M}$ (for $\overline{M} \gg 1$), B_2 increases monotonically to its maximum value,

$$B_{2MAX} \approx B'_{2MAX} = 0.210(\bar{M})^{-2}.$$

d. As R_2 varies from $0.64R_1\overline{M}$ to infinity (for $\overline{M} \gg 1$), B_2 decreases monotonically to 0.

e. Since r is much less than 1 and $\overline{M}$ is much greater than 1, r_{CN} is approximately,

$$r_{CN} \approx 4^{-1}r(\bar{M})^{-2}(1 + 4rB'_2\bar{M}^2).$$

f. As R_2 varies from R_1 to $0.64R_1\overline{M}$ (for $M \gg 1$, $r \ll 1$), r_{CN} increases monotonically to its maximum value,

$$r_{CN(MAX)} \approx 4^{-1}r(\bar{M})^{-2}(1 + 0.840r).$$

g. As R_2 varies from $0.64R_1\overline{M}$ to infinity (for $\overline{M} \gg 1$, $r \ll 1$), r_{CN} decreases monotonically to its minimum value.

$$r_{CN(MIN)} \approx 4^{-1}r(\bar{M})^{-2}.$$

4. References

[1] DeVos, J. C., Evaluation of the quality of a blackbody, Physica **20**, 669 (1954).

[2] Jenkins, F. A., and White, H. E., Fundamentals of Optics, 2nd ed., p. 430 (McGraw-Hill Book Co., Inc., New York, N.Y., 1950).

[3] Walsh, J. W. T., Photometry, 3rd. ed., p. 137 (Dover Publications, Inc., New York, N.Y., 1958).

[4] Quinn, T. J., The calculation of the emissivity of cylindrical cavities giving near blackbody radiation, Brit. J. Appl. Phys. **18**, 1105 (1967).

(Paper 76A4–726)

JOURNAL OF RESEARCH of the National Bureau of Standards—A. Physics and Chemistry
Vol. 76A, No. 4, July–August 1972

Lattice Vibrations of Antiparallel Chain Sheet Structures

Bruno M. Fanconi

Institute for Materials Research, National Bureau of Standards, Washington, D.C. 20234

(January 21, 1972)

Methods are developed for calculating the normal coordinate vibrations of isolated helical homopolymers and of the antiparallel sheet structures formed by some helical polymers in the solid state. The dynamical equations are expressed in Cartesian displacement coordinates starting from an internal coordinate harmonic force field. As an example of the method the dynamical equations of the honeycomb lattice are derived.

Key words: Antiparallel chain sheet structures; honeycomb lattice; lattice vibrations.

1. Introduction

An essential feature of many polymeric crystals is layered structures which are held together primarily by interchain hydrogen bonding. Examples of polymeric materials which form this type of structure include some nylons, synthetic polypeptides, and fibrous proteins. Interchain bonding is expected to influence vibrational properties especially in the low frequency region and thereby affect the infrared and Raman spectra, the inelastic neutron scattering, and thermodynamic properties such as the low temperature specific heat.

With the availability of commercial Fourier transform infrared spectrophotometers and low light scattering Raman spectrometers low frequency vibrational studies on polymeric systems are now practical and several such studies have recently appeared in the literature [1–3]. The assignment of vibrational spectra obtained from solid state samples has been based mainly on normal coordinate calculations of isolated chain models [4–7]. Interchain effects have been either totally ignored or treated in part by perturbation methods [4, 8, 9] because the vibrational secular equation may become quite large. For example, the normal mode frequencies of polyglycine, $(CH_2NHCO)_n$, in the fully extended conformation, polyglycine I, may by calculated from an isolated chain model with C_{2v} symmetry by solving a secular equation of dimensionality twenty-one. For the more realistic two-dimensional pleated sheet model the dimensionality of the secular equation is 84 since four glycine residues comprise the two-dimensional unit cell. To calculate the vibrational frequency as a function of the phase differences (phonon dispersion curves) requires the solution of a secular equation which is twice as large because the matrix elements are, in general, complex. The phonon dispersion curves are useful for comparisons with the inelastic neutron scattering data [7, 10] and with the low temperature specific heat [7].

In this paper a method is introduced for calculating the normal coordinates in terms of the Cartesian displacement coordinates of isolated helical homopolymers. This method is extended to antiparallel sheet structures with four chemical repeat units comprising the two-dimensional unit cell. The method is demonstrated for the honeycomb lattice shown in figure 1.

2. Method for Calculating the Normal Coordinates of an Isolated Chain

The adaption of the Wilson GF method [11] to the calculation of the normal coordinates of helical infinite polymers was first described by Higgs [12] who utilized symmetry adapted internal coordinates. Miyazawa and coworkers [13] extended Higgs' method by defining the

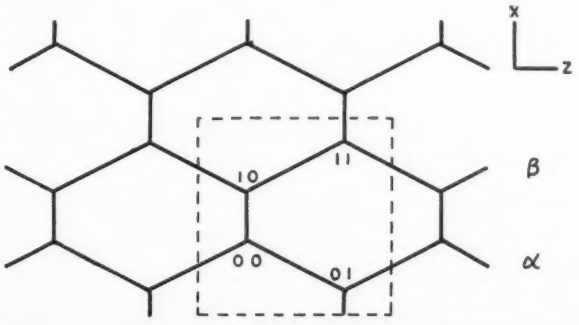

FIGURE 1. *Honeycomb lattice unit cell is indicated by dotted lines.*
The polymer chains lie along the z axis. The interchain bonds are parallel to the x axis.

internal coordinates in terms of the helical parameters. This method is rather cumbersome especially for complicated chemical repeat units. Small, et al. [6] have developed a method by which the vibrational secular equation may be set up from the internal coordinates of one chemical repeat unit defined in the Cartesian coordinate system. The dynamical matrix in terms of the internal coordinates in nonhermitian so as to require two separate matrix diagonalizations. Furthermore, there are usually redundant internal coordinates introduced so that the dimensionality of the secular matrix is larger than $3M$ where M is the number of atoms in the chemical repeat unit. Both of these disadvantages are removed by expressing the vibrational problem in Cartesian displacement coordinates. An expression for the vibrational secular equation for helical polymers in the symmetrized Cartesian displacement coordinate basis set will now be developed following the method devised by Small, et al. [6], for the internal coordinates.

The kinetic energy in terms of the Cartesian displacements is

$$2T = \sum_{r=-N/2+1}^{N/2} \sum_{j=1}^{3M} \dot{X}_j^r m_j \dot{X}_j^r \tag{1}$$

where X_j^r is the jth displacement coordinate of the rth chemical repeat unit for a polymer of N total repeat units with reentrant boundary conditions and m_j is the mass of the atom undergoing the X_j^r displacement.

The potential energy assuming harmonic forces is

$$2V = \sum_{r,p} \sum_{j,l} X_j^r f_{j,l}^{r,p} X_l^p \tag{2}$$

where

$$f_{j,l}^{r,p} = \partial^2 V / \partial X_j^r \partial X_l^p$$

are force constants in terms of Cartesian displacement coordinates.

In matrix notation eqs (1) and (2) become

$$2T = \sum_r \tilde{\underline{\mathbf{X}}}^r \underline{\underline{\mathbf{M}}} \dot{\underline{\mathbf{X}}}^r \tag{3}$$

and

$$2V = \sum_{r,p} \tilde{\underline{\mathbf{X}}}^r \underline{\underline{\mathbf{f}}}^{r,p} \underline{\mathbf{X}}^p \tag{4a}$$

where the tilde means the transpose vector. The potential energy, eq (4a), may be rewritten as

$$2V = \sum_r \sum_{s=-k}^{k} \tilde{\underline{\mathbf{X}}}^r \underline{\underline{\mathbf{f}}}^{r,r+s} \underline{\mathbf{X}}^{r+s} \tag{4b}$$

where the index s labels the neighboring units of the rth unit and $\underline{\underline{\mathbf{f}}}^{r+s} = 0$ for $|s| > k$.

The symmetry coordinates, $\underline{\mathbf{X}}(\theta)$, are linear combinations of equivalent coordinates. Unlike the internal coordinates which are invariant of unit location and equivalent, the Cartesian coordinates depend on unit location but may be made to form an equivalent set through the rotational operator $\underline{\underline{\mathbf{H}}}^r(\psi)$. The matrix $\underline{\underline{\mathbf{H}}}^r(\psi)$ is comprised of M 3×3 blocks along the diagonal where each block is of the form

$$\begin{pmatrix} \cos(r\psi) & -\sin(r\psi) & 0 \\ \sin(r\psi) & \cos(r\psi) & 0 \\ 0 & 0 & 1 \end{pmatrix} \tag{5}$$

and ψ is the helical angle.

The matrix $\underline{\underline{\mathbf{H}}}^r(\psi)$ rotates the x,y coordinates of the 0th unit into those of the rth unit. The form of transformation given in eq (5) assumes a right-handed helix with helical axis Z and with $r > 0$ labeling units reached by clockwise rotations plus translations.

The normalized symmetry coordinates $\underline{\mathbf{X}}(\theta)$ are defined as

$$\underline{\mathbf{X}}(\theta) = 1/\sqrt{N} \sum_r \exp(-ir\theta) \underline{\underline{\mathbf{H}}}^{-r}(\psi) \underline{\mathbf{X}}^r. \tag{6}$$

Solving eq (6) for $\underline{\mathbf{X}}^r$ and substituting into eq (4b) yields

$$2V = \sum_{r,s} \sum_{\theta,\theta'} \exp[\mathrm{ir}(\theta' - \theta)]$$

$$\tilde{\underline{\mathbf{X}}}(\theta) \underline{\underline{\mathbf{H}}}^{-r}(\psi) \underline{\underline{\mathbf{f}}}^{r,r+s} \underline{\underline{\mathbf{H}}}^r(\psi) \underline{\underline{\mathbf{H}}}^s(\psi) \underline{\mathbf{X}}(\theta') \exp(is\theta') \tag{7}$$

From the definition of the transformation matrix $\underline{\underline{\mathbf{H}}}^r(\psi)$ and the covariance of $\underline{\underline{\mathbf{f}}}^{r,r+s}$ it follows that

$$\underline{\underline{\mathbf{H}}}^{-r}(\psi) \underline{\underline{\mathbf{f}}}^{r,r+s} \underline{\underline{\mathbf{H}}}^r(\psi) = \underline{\underline{\mathbf{f}}}^{0,s}.$$

With this result eq (7) becomes

$$2V = \sum_{s,\theta} \tilde{\underline{\mathbf{X}}}(\theta) \underline{\underline{\mathbf{f}}}^{0,s} \underline{\underline{\mathbf{H}}}^s(\psi) \underline{\mathbf{X}}(\theta) \exp(is\theta). \tag{8}$$

The potential energy may also be expressed in the internal coordinate basis set as

$$2V = \sum_{t,q} \tilde{\underline{\mathbf{R}}}^t \underline{\underline{\mathbf{F}}}^{t,q} \underline{\mathbf{R}}^q \tag{9}$$

where $\underline{\mathbf{R}}^q$ is the column vector of internal coordinates in the qth chemical repeat unit and

$$F_{i,j}^{t,q} = \partial^2 V / \partial R_i^t \partial R_j^q$$

are the internal coordinate force constants.

The internal coordinates are defined through the **B** matrices [6],

$$\underline{\mathbf{R}}^q = \sum_p \underline{\underline{\mathbf{B}}}^{q,p} \underline{\mathbf{X}}^p$$

so that eq (9) becomes

$$2V = \sum_{t,q} \sum_{p,r} \tilde{\underline{\mathbf{X}}}^r \tilde{\underline{\underline{\mathbf{B}}}}^{t,r} \underline{\underline{\mathbf{F}}}^{t,q} \underline{\underline{\mathbf{B}}}^{q,p} \underline{\mathbf{X}}^p$$

which yields upon comparison with eq (4a)

$$\underline{\underline{\mathbf{f}}}^{r,p} = \sum_{t,q} \tilde{\underline{\underline{\mathbf{B}}}}^{t,r} \underline{\underline{\mathbf{F}}}^{t,q} \underline{\underline{\mathbf{B}}}^{q,p}.$$

Utilizing the expression [6]

$$\underline{\underline{\mathbf{B}}}^{q,p} = \underline{\underline{\mathbf{B}}}^{0,p-q}\underline{\underline{\mathbf{H}}}^{-q}(\psi)$$

and the fact that $\underline{\underline{\mathbf{F}}}^{t,q} = \underline{\underline{\mathbf{F}}}^{0,q-t}$ we have

$$\underline{\underline{\mathbf{f}}}^{0,s} = \sum_{t,r} \underline{\underline{\mathbf{H}}}^{t}(\psi)\underline{\underline{\tilde{\mathbf{B}}}}^{0,-t}\underline{\underline{\mathbf{F}}}^{0,r}\underline{\underline{\mathbf{B}}}^{0,s-t-r}\underline{\underline{\mathbf{H}}}(\psi)^{-(t+r)} \quad (10)$$

where the summations are over positive and negative values. We find by substitution of eq (10) into eq (8) the potential energy in terms of the Cartesian displacement symmetry coordinates and the internal coordinate force matrix:

$$2V = \sum_{\theta} \sum_{r,s,t} \underline{\tilde{\mathbf{X}}}(\theta)\underline{\underline{\mathbf{H}}}^{-t}(\psi)\underline{\underline{\tilde{\mathbf{B}}}}^{0,t} \exp(-it\theta)\underline{\underline{\mathbf{F}}}^{0,r} \exp(ir\theta)\underline{\underline{\mathbf{B}}}^{0,s}\underline{\underline{\mathbf{H}}}^{s}(\psi) \exp(is\theta)\underline{\mathbf{X}}(\theta). \quad (11)$$

Defining

$$\underline{\underline{\mathbf{B}}}(\theta) = \sum_{s} \exp(is\theta)\underline{\underline{\mathbf{B}}}^{0,s}\underline{\underline{\mathbf{H}}}^{s}(\psi) \quad (12)$$

and

$$\underline{\underline{\mathbf{F}}}(\theta) = \sum_{r} \exp(ir\theta)\underline{\underline{\mathbf{F}}}^{0,r}. \quad (13)$$

Equation (11) becomes

$$2V = \sum_{\theta} \underline{\tilde{\mathbf{X}}}(\theta)\underline{\underline{\tilde{\mathbf{B}}}}(\theta)\underline{\underline{\mathbf{F}}}(\theta)\underline{\underline{\mathbf{B}}}(\theta)\underline{\mathbf{X}}(\theta). \quad (14)$$

The kinetic energy, eq (3), becomes in the Cartesian symmetry coordinates

$$2T = \sum_{\theta} \dot{\underline{\tilde{\mathbf{X}}}}(\theta)\,\underline{\underline{\mathbf{M}}}\,\dot{\underline{\mathbf{X}}}(\theta)$$

or in the conjugate momenta

$$2T = \sum_{\theta} \underline{\tilde{\mathbf{P}}}(\theta)\underline{\underline{\mathbf{M}}}^{-1}\underline{\mathbf{P}}(\theta). \quad (15)$$

From eqs (14 and 15), we find through Hamilton's equations the eigenvalue equation

$$\underline{\underline{\mathbf{M}}}^{-1}\underline{\underline{\tilde{\mathbf{B}}}}(\theta)\underline{\underline{\mathbf{F}}}(\theta)\underline{\underline{\mathbf{B}}}(\theta)\underline{\mathbf{L}}_X(\theta) = \underline{\mathbf{L}}_X(\theta)\underline{\Delta}(\theta) \quad (16)$$

where $\Lambda(\theta)$ is the diagonal matrix of the squares of the eigenfrequencies and L_X is the matrix of eigenvectors. Equation (16) may be symmetrized in the form

$$\underline{\underline{\mathbf{M}}}^{-1/2}\underline{\underline{\tilde{\mathbf{B}}}}(\theta)\underline{\underline{\mathbf{F}}}(\theta)\underline{\underline{\mathbf{B}}}(\theta)\underline{\underline{\mathbf{M}}}^{-1/2}\underline{\mathbf{L}}'_X(\theta) = \underline{\mathbf{L}}'_X(\theta)\underline{\Delta}(\theta) \quad (17)$$

where $\underline{\mathbf{L}}'_X(\theta) = \underline{\underline{\mathbf{M}}}^{1/2}\underline{\mathbf{L}}_X$ is the matrix of eigenvectors in the mass-reduced symmetry coordinates.

The form of eq (17) is identical to that given previously [14] for translational symmetry (i.e. $\underline{\underline{\mathbf{H}}}^{r}(\psi)$ is the unit matrix). The essential feature in this derivation is that the dimensionality of $\underline{\underline{\mathbf{B}}}(\theta)$ equals the number of independent coordinates in the chemical repeat unit and that only the internal coordinates of one chemical repeat unit in terms of Cartesian displacement coordinates need be specified.

3. Two-Dimensional Lattice of Antiparallel Chains

Consider a two dimensional lattice, figure 1, in the X, Z plane with two chains passing through the unit cell and helical axes parallel to Z. The helical angle, ψ, is 180° and there is a two-fold screw rotation axis along X. The latter symmetry operation reverses the sense of the two chains to produce the antiparallel structure. The translational unit cell contains four chemical repeat units numbered (0, 0), (0, 1) in the α chain and (1, 0), (1, 1) in the β chain.

The four units are related by the two-fold screw axes along Z and X. For the two-dimensional lattice we have [14]

$$\underline{\underline{\mathbf{f}}}(\phi, \theta) = \underline{\underline{\tilde{\mathbf{B}}}}(\phi, \theta)\underline{\underline{\mathbf{F}}}(\phi, \theta)\underline{\underline{\mathbf{B}}}(\phi, \theta) \quad (18)$$

where

$$\underline{\underline{\mathbf{B}}}(\phi, \theta) = \sum_{r,s} \underline{\underline{\mathbf{B}}}^{r,s} \exp[i(r\phi + s\theta)]$$

$$\underline{\underline{\mathbf{F}}}(\phi, \theta) = \sum_{r,s} \underline{\underline{\mathbf{F}}}^{r,s} \exp[i(r\phi + s\theta)]$$

with

$$\phi = \underline{\mathbf{k}}_X \cdot \underline{\mathbf{t}}_X$$

$$\theta = \underline{\mathbf{k}}_Z \cdot \underline{\mathbf{t}}_Z.$$

The quantities $\mathbf{t}_X$, $\mathbf{t}_Z$ are the lattice vectors directed along the X and Z axes and $\mathbf{k}_X$, $\mathbf{k}_Z$ are the wavevectors. The quantities ϕ and θ are the phase differences between identical displacements in neighboring unit cells. The dimensionality of the matrix $\underline{\underline{\mathbf{f}}}(\phi, \theta)$ is $3m \times 3m$ where m is the number of atoms in the two-dimensional unit cell whereas the dimensionality of $\underline{\underline{\mathbf{F}}}(\phi, \theta)$ equals the number of internal coordinates which is usually greater than $3m$ since redundant coordinates are included.

The basis set used to express the quantities in eq (18) are linear combinations of equivalent chemical repeat units:

$$\underline{\mathbf{X}}_{j,l}(\phi, \theta) = 1/\sqrt{N_X N_Z} \sum_{r=0}^{N_X-1} \sum_{t=0}^{N_Z-1} \exp[-i(r\phi + t\theta)]\,\mathbf{X}^{r,t}_{j,l} \quad (19)$$

where j, $l = 0$, 1 label the chemical repeat unit and r, t the unit cell. The symmetry coordinates, eq (19), may be related to those of eq (6) as follows. The chemical repeat units are renumbered so that $\mathbf{X}^{p,q}$ equals $\underline{\mathbf{X}}^{(p-j)/2,\,(q-l)/2}_{j,l}$ with j, $l = 0$ or 1 for p, q even or odd. A generalization of eq (6) yields the symmetry coordinates

$$\underline{\mathbf{X}}(\phi', \theta') = 1/2\sqrt{N_X N_Z} \sum_{p=0}^{2N_X-1} \sum_{q=0}^{2N_Z-1} \exp[-i(p\phi' + q\theta')]\underline{\underline{\mathbf{H}}}^{-p,-q}\mathbf{X}^{p,q} \quad (20)$$

464-124 OL -72 - 3

where $\underline{\underline{\mathbf{H}}}^{p,q}$ is the transformation matrix representing p 2-fold rotations about X and q 2-fold rotations about Z. The matrix $\underline{\underline{\mathbf{H}}}^{p,q}$ is comprised of m 3×3 blocks with each block given by

$$\begin{pmatrix} (-1)^q & 0 & 0 \\ 0 & (-1)^{q+p} & 0 \\ 0 & 0 & (-1)^p \end{pmatrix}.$$

Using the relationship between $\underline{\mathbf{X}}^{p,q}$ and $\underline{\mathbf{X}}^{r,t}_{j,l}$, eq (20) may be rewritten as

$$\begin{aligned}\underline{\mathbf{X}}(\phi',\theta') = 1/2\sqrt{N_X N_Z}\ \Bigg\{ & \sum_{p,\text{ even}}\sum_{q,\text{ even}} \exp\left[-i\,(p\phi'+q\theta')\right]\underline{\mathbf{X}}^{p/2,\,q/2}_{0,0} \\ & + \sum_{p,\text{ even}}\sum_{q,\text{ odd}} \exp\left[-i\,(p\phi'+q\theta')\right]\underline{\underline{\mathbf{H}}}^{0,1}\underline{\mathbf{X}}^{p/2,\,(q-1)/2}_{0,1} \\ & + \sum_{p,\text{ odd}}\sum_{q,\text{ even}} \exp\left[-i\,(p\phi'+q\theta')\right]\underline{\underline{\mathbf{H}}}^{1,0}\underline{\mathbf{X}}^{(p-1)/2,\,q/2}_{1,0} \\ & + \sum_{p,\text{ odd}}\sum_{q,\text{ odd}} \exp\left[-i\,(p\phi'+q\theta')\right]\underline{\underline{\mathbf{H}}}^{1,1}\underline{\mathbf{X}}^{(p-1)/2,\,(q-1)/2}_{1,1}\Bigg\}\end{aligned} \tag{21}$$

$$\begin{aligned}\mathbf{X}(\phi',\theta') = 1/2\,[&\mathbf{X}_{0,0}(2\phi',2\theta') + \underline{\underline{\mathbf{H}}}^{0,1}\underline{\mathbf{X}}_{0,1}(2\phi',2\theta')\exp(-i\theta') \\ &+ \underline{\underline{\mathbf{H}}}^{1,0}\underline{\mathbf{X}}_{1,0}(2\phi',2\theta')\exp(-i\phi') + \underline{\underline{\mathbf{H}}}^{1,1}\underline{\mathbf{X}}_{1,1}(2\phi',2\theta')\exp(-i(\theta'+\phi'))].\end{aligned}$$

Functions orthogonal to $\underline{\mathbf{X}}(\phi,\ \theta)$ are $\underline{\mathbf{X}}(\phi,\ \theta+\pi)$, $\underline{\mathbf{X}}(\phi+\pi,\ \theta)$, and $\underline{\mathbf{X}}(\phi+\pi,\ \theta+\pi)$ which are related to those of eq (19)

$$\begin{bmatrix} \mathbf{X}(\phi,\theta) \\ \mathbf{X}(\phi,\theta+\pi) \\ \mathbf{X}(\phi+\pi,\theta) \\ \mathbf{X}(\phi+\pi,\theta+\pi) \end{bmatrix} = \frac{1}{2}\begin{bmatrix} \mathbf{I} & e^{-i\theta}\underline{\underline{\mathbf{H}}}^{0,1} & e^{-i\phi}\underline{\underline{\mathbf{H}}}^{1,0} & e^{-i(\phi+\theta)}\underline{\underline{\mathbf{H}}}^{1,1} \\ \mathbf{I} & -e^{-i\theta}\underline{\underline{\mathbf{H}}}^{0,1} & e^{-i\phi}\underline{\underline{\mathbf{H}}}^{1,0} & -e^{-i(\phi+\theta)}\underline{\underline{\mathbf{H}}}^{1,1} \\ \mathbf{I} & e^{-i\theta}\underline{\underline{\mathbf{H}}}^{0,1} & -e^{-i\phi}\underline{\underline{\mathbf{H}}}^{1,0} & -e^{-i(\phi+\theta)}\underline{\underline{\mathbf{H}}}^{1,1} \\ \mathbf{I} & -e^{-i\theta}\underline{\underline{\mathbf{H}}}^{0,1} & -e^{-i\phi}\underline{\underline{\mathbf{H}}}^{1,0} & e^{-i(\phi+\theta)}\underline{\underline{\mathbf{H}}}^{1,1} \end{bmatrix}\begin{bmatrix} \underline{\mathbf{X}}_{0,0}(2\phi,2\theta) \\ \underline{\mathbf{X}}_{0,1}(2\phi,2\theta) \\ \underline{\mathbf{X}}_{1,0}(2\phi,2\theta) \\ \underline{\mathbf{X}}_{1,1}(2\phi,2\theta) \end{bmatrix} \tag{22}$$

or

$$\begin{bmatrix} \underline{\mathbf{X}}(\phi,\theta) \\ \underline{\mathbf{X}}(\phi,\theta+\pi) \\ \\ \underline{\mathbf{X}}(\phi+\pi,\theta) \\ \underline{\mathbf{X}}(\phi+\pi,\theta+\pi) \end{bmatrix} = \underline{\underline{\mathbf{U}}}(\phi,\theta)\begin{bmatrix} \underline{\mathbf{X}}_{0,0}(2\phi,2\theta) \\ \underline{\mathbf{X}}_{0,1}(2\phi,2\theta) \\ \\ \underline{\mathbf{X}}_{1,0}(2\phi,2\theta) \\ \underline{\mathbf{X}}_{1,1}(2\phi,2\theta) \end{bmatrix} \tag{23}$$

where $\mathbf{I}$ is the identity matrix.

We now derive an expression similar to eq (22) for the internal coordinates so that $\underline{\mathbf{f}}(\phi,\ \theta)$, eq (18), may be transformed to the new symmetry coordinates. It is convenient to list the internal symmetry coordinates of the lattice as $[\underline{\mathbf{R}}_{0,0}(\phi,\ \theta),\ \underline{\mathbf{R}}_{0,1}(\phi,\ \theta),\ \underline{\mathbf{r}}_{\alpha}(\phi,\ \theta),\ \underline{\mathbf{R}}_{1,0}(\phi,\ \theta),\ \underline{\mathbf{R}}_{1,1}(\phi,\ \theta),\ \underline{\mathbf{r}}_{\beta}(\phi,\ \theta)]$ where $\underline{\mathbf{R}}_{j,l}(\phi,\theta)$ are intrachain coordinates of the $j,\ l$ repeat unit, $\underline{\mathbf{r}}_{\alpha}(\phi,\ \theta)$ and $\underline{\mathbf{r}}_{\beta}(\phi,\ \theta)$ are interchain coordinates associated with the α and β chain respectively. In a manner analogous to that which lead to eq (22) we find

$$\begin{bmatrix} \underline{\mathbf{R}}(\phi,\theta) \\ \underline{\mathbf{R}}(\phi,\theta+\pi) \\ \underline{\mathbf{r}}(\phi,\theta) \\ \\ \\ \underline{\mathbf{R}}(\phi+\pi,\theta) \\ \underline{\mathbf{R}}(\phi+\pi,\theta+\pi) \\ \underline{\mathbf{r}}(\phi+\pi,\theta) \end{bmatrix} = \frac{1}{2} \begin{bmatrix} 1 & e^{-i\theta} & 0 & e^{-i\phi} & e^{-i(\phi+\theta)} & 0 \\ 1 & -e^{i\theta} & 0 & e^{-i\phi} & e^{-i(\phi+\theta)} & 0 \\ 0 & 0 & \sqrt{2} & 0 & 0 & \sqrt{2}\,e^{-i\theta} \\ & & & & & \\ & & & & & \\ 1 & e^{-i\theta} & 0 & -e^{-i\phi} & -e^{-i(\phi+\theta)} & 0 \\ 1 & -e^{i\theta} & 0 & -e^{-i\phi} & e^{-i(\phi+\theta)} & 0 \\ 0 & 0 & \sqrt{2} & 0 & 0 & -\sqrt{2}\,e^{-i\theta} \end{bmatrix} \begin{bmatrix} \underline{\mathbf{R}}_{0,0}(2\phi,2\theta) \\ \underline{\mathbf{R}}_{0,1}(2\phi,2\theta) \\ \underline{\mathbf{r}}_{\alpha}(2\phi,\theta) \\ \\ \\ \underline{\mathbf{R}}_{1,0}(2\phi,2\theta) \\ \underline{\mathbf{R}}_{1,1}(2\phi,2\theta) \\ \underline{\mathbf{r}}_{\beta}(2\phi,\theta) \end{bmatrix} \tag{24}$$

$$= \underline{\underline{\mathbf{W}}}(\phi,\theta) \begin{bmatrix} \underline{\mathbf{R}}_{0,0}(2\phi,2\theta) \\ \underline{\mathbf{R}}_{0,1}(2\phi,2\theta) \\ \underline{\mathbf{r}}_{\alpha}(2\phi,\theta) \\ \\ \\ \underline{\mathbf{R}}_{1,0}(2\phi,2\theta) \\ \underline{\mathbf{R}}_{1,1}(2\phi,2\theta) \\ \underline{\mathbf{r}}_{\beta}(2\phi,\theta) \end{bmatrix} \tag{25}$$

The $\underline{\underline{\mathbf{H}}}^{p,q}$ matrices do not enter into $\underline{\underline{\mathbf{W}}}(\phi,\theta)$ since the internal coordinates are invariant to position within the unit cell. Using eqs (23), (25), $\underline{\mathbf{f}}(\phi,\theta)$ is transformed to

$$\underline{\mathbf{f}}'(\phi,\theta) = \underline{\tilde{\mathbf{B}}}'(\phi,\theta)\underline{\mathbf{F}}'(\phi,\theta)\underline{\mathbf{B}}'(\phi,\theta)$$

where

$$\underline{\mathbf{B}}'(\phi,\theta) = \underline{\underline{\mathbf{W}}}(\phi,\theta)\underline{\underline{\mathbf{B}}}(2\phi,2\theta)\underline{\tilde{\mathbf{U}}}(\phi,\theta) \tag{26}$$

and

$$\underline{\mathbf{F}}'(\phi,\theta) = \underline{\underline{\mathbf{W}}}(\phi,\theta)\underline{\underline{\mathbf{F}}}(2\phi,2\theta)\underline{\tilde{\mathbf{U}}}(\phi,\theta).$$

In the absence of interchain interactions $\underline{\mathbf{f}}'(\phi,\theta)$ consists of four noninteracting blocks, two of which correspond to intrachain phase difference θ and the other two to $\theta+\pi$. It will be shown that with certain types of interchain interactions $\underline{\mathbf{f}}'(\phi,\theta)$ contains nonzero elements only between the blocks (ϕ,θ) and $(\phi+\pi,\theta+\pi)$ and between $(\phi,\theta+\pi)$, $(\phi+\pi,\theta)$ so that the dimensionality of the dynamical matrix has been reduced by a factor of two.

Let

$$\underline{\underline{\mathbf{B}}}_i'(\phi,\theta) = 1/\sqrt{2} \begin{bmatrix} 1 & e^{-i\phi} \\ \\ 1 & -e^{-i\phi} \end{bmatrix} \begin{bmatrix} \underline{\underline{\mathbf{B}}}_i^{\alpha}(2\phi,2\theta) \\ \\ \underline{\underline{\mathbf{B}}}_i^{\beta}(2\phi,2\theta) \end{bmatrix} \underline{\tilde{\mathbf{U}}}(\phi,\theta) \tag{27}$$

where $\underline{\underline{\mathbf{B}}}_i^{\alpha}(2\phi,2\theta)$, $B_i^{\beta}(2\phi,2\theta)$ are the B matrices associated with coordinates $\underline{\mathbf{r}}_{\alpha}$, $\underline{\mathbf{r}}_{\beta}$ respectively. These B matrices may be expanded in terms of contributions from each of the four residues in the unit cell.

$$\begin{bmatrix} \underline{\underline{\mathbf{B}}}_i^{\alpha}(2\phi, 2\theta) \\ \underline{\underline{\mathbf{B}}}_i^{\beta}(2\phi, 2\theta) \end{bmatrix} = \begin{bmatrix} \underline{\underline{\mathbf{B}}}_{0,0}^{\alpha} & \underline{\underline{\mathbf{B}}}_{0,1}^{\alpha} & \underline{\underline{\mathbf{B}}}_{1,0}^{\alpha} & \underline{\underline{\mathbf{B}}}_{1,1}^{\alpha} \\ \underline{\underline{\mathbf{B}}}_{0,0}^{\beta} & \underline{\underline{\mathbf{B}}}_{0,1}^{\beta} & \underline{\underline{\mathbf{B}}}_{1,0}^{\beta} & \underline{\underline{\mathbf{B}}}_{1,1}^{\beta} \end{bmatrix}. \tag{28}$$

Letting,

$$\underline{\underline{\mathbf{B}}}^{\alpha}(\phi, \theta) = \underline{\underline{\mathbf{B}}}_i^{\alpha}(2\phi, 2\theta)\, \underline{\underline{\tilde{\mathbf{U}}}}(\phi, \theta)$$

we find upon substitution of eq (28)

$$\underline{\underline{\mathbf{B}}}^{\alpha}(\phi, \theta) = \frac{1}{2} \sum_{j,k=0}^{1} \exp\left[i(j\phi + k\theta)\right] \underline{\underline{\mathbf{B}}}_{j,k}^{\alpha}\, \underline{\underline{\mathbf{H}}}^{-j,-k} \tag{29a}$$

and

$$\underline{\underline{\mathbf{B}}}^{\beta}(\phi, \theta) = \frac{1}{2} \sum_{j,k=0}^{1} \exp\left[i(j\phi + k\theta)\right] \underline{\underline{\mathbf{B}}}_{j,k}^{\beta}\, \underline{\underline{\mathbf{H}}}^{-j,-k}. \tag{29b}$$

Substitution of the expression for $\underline{\underline{\mathbf{B}}}_i^{\alpha}(2\phi, 2\theta)\underline{\underline{\tilde{\mathbf{U}}}}(\phi, \theta)$ into eq (27) yields

$$\underline{\underline{\mathbf{B}}}_i'(\phi, \theta) = \begin{bmatrix} \underline{\underline{\mathbf{B}}}^{+}(\phi, \theta) & \underline{\underline{\mathbf{B}}}^{+}(\phi, \bar{\theta}) & \underline{\underline{\mathbf{B}}}^{+}(\bar{\phi}, \theta) & \underline{\underline{\mathbf{B}}}^{+}(\bar{\phi}, \bar{\theta}) \\ \underline{\underline{\mathbf{B}}}^{-}(\phi, \theta) & \underline{\underline{\mathbf{B}}}^{-}(\phi, \bar{\theta}) & \underline{\underline{\mathbf{B}}}^{-}(\bar{\phi}, \theta) & \underline{\underline{\mathbf{B}}}^{-}(\bar{\phi}, \bar{\theta}) \end{bmatrix} \tag{30}$$

where

$$\underline{\underline{\mathbf{B}}}^{\pm}(\phi, \theta) = 1/\sqrt{2}\, [\underline{\underline{\mathbf{B}}}^{\alpha}(\phi, \theta) \pm \exp(-i\phi)\underline{\underline{\mathbf{B}}}^{\beta}(\phi, \theta)] \tag{31}$$

and

$$\bar{\theta} = \theta + \pi, \bar{\phi} = \phi + \pi.$$

If a diagonal valence force field is assumed for the interchain interactions

$$\underline{\underline{\mathbf{F}}}'(\phi, \theta) = \begin{pmatrix} \underline{\underline{\mathbf{F}}}(\theta) & 0 & 0 & 0 & 0 & 0 \\ 0 & \underline{\underline{\mathbf{F}}}(\bar{\theta}) & 0 & 0 & 0 & 0 \\ 0 & 0 & \underline{\underline{\mathbf{F}}}^{\circ} & 0 & 0 & 0 \\ 0 & 0 & 0 & \underline{\underline{\mathbf{F}}}(\theta) & 0 & 0 \\ 0 & 0 & 0 & 0 & \underline{\underline{\mathbf{F}}}(\bar{\theta}) & 0 \\ 0 & 0 & 0 & 0 & 0 & \underline{\underline{\mathbf{F}}}^{\circ} \end{pmatrix} \tag{32}$$

where $\underline{\underline{\mathbf{F}}}(\theta)$ is the isolated chain force matrix. eq (13), and $\underline{\underline{\mathbf{F}}}^{\circ}$ is the valence field force matrix for interchain interactions. From eqs (30–32) we have

$$\underline{\mathbf{f}}'(\phi, \theta) = \begin{bmatrix} f_r(\theta) + f_i(\phi + \theta) & f_i(\phi, \theta; \phi, \bar{\theta}) & f_i(\phi, \theta; \bar{\phi}, \theta) & f_i(\phi, \theta; \bar{\phi}, \bar{\theta}) \\ & f_r(\bar{\theta}) + f_i(\phi, \bar{\theta}) & f_i(\phi, \bar{\theta}; \bar{\phi}, \theta) & f_i(\phi, \bar{\theta}; \bar{\phi}, \bar{\theta}) \\ & c.c. & f_r(\theta) + f_i(\bar{\phi}, \theta) & f_i(\bar{\phi}, \theta; \bar{\phi}, \bar{\theta}) \\ & & & f_r(\bar{\theta}) + f_i(\bar{\phi}, \bar{\theta}) \end{bmatrix} \tag{33}$$

where $f_r(\theta)$ is the symmetrized force matrix for the isolated chain [from eq (16), $f_r(\theta) = \underline{\underline{\tilde{\mathbf{B}}}}(\theta)\underline{\underline{\mathbf{F}}}(\theta)\underline{\underline{\mathbf{B}}}(\theta)$],

$$f_i(\phi, \theta; \phi, \bar{\theta}) = \underline{\underline{\tilde{\mathbf{B}}}}^{+}(\phi, \theta)\, \underline{\underline{\mathbf{F}}}^{\circ}\underline{\underline{\mathbf{B}}}^{+}(\phi, \bar{\theta}) + \underline{\underline{\mathbf{B}}}^{-}(\phi, \theta)\, \underline{\underline{\mathbf{F}}}^{\circ}\underline{\underline{\mathbf{B}}}^{-}(\phi, \bar{\theta}) \tag{33b}$$

and

$$f_i(\phi, \theta) \equiv f_i(\phi, \theta; \phi, \theta)$$

The vibrational secular equation for the two-dimensional lattice is

$$| \underline{\underline{\mathbf{M}}}^{-1/2} \underline{\underline{\mathbf{f}}}' (\phi, \theta) \underline{\underline{\mathbf{M}}}^{-1/2} - \omega^2 \mathbf{I} | = 0. \tag{34}$$

A relationship exists between $\underline{\underline{\mathbf{B}}}^{\alpha}(\phi, \theta)$ and $\underline{\underline{\mathbf{B}}}^{\beta}(\phi, \theta)$ which is helpful in the further simplification of $f'(\phi, \theta)$. The quantities $\underline{\underline{\mathbf{B}}}^{\alpha}_{j,k}(\phi, \theta)$, $B^{\beta}_{j,k}(\phi, \theta)$ which appear in eqs (29 a, b) are sums of B matrices multiplied by phase factors.

$$\underline{\underline{\mathbf{B}}}^{\alpha}_{j,k}(2\phi, 2\theta) = \sum_{l,n} \exp [2i(l\phi + n\theta)] \underline{\underline{\mathbf{B}}}^{\alpha, l, n}_{j,k} \tag{35a}$$

and

$$\underline{\underline{\mathbf{B}}}^{\beta}_{j,k}(2\phi, 2\theta) = \sum_{l,n} \exp [2i(l\phi + n\theta)] \underline{\underline{\mathbf{B}}}^{\beta, l, n}_{j,k} \tag{35b}$$

where the superscripts l, n label the unit cell. As the internal coordinates given by $\underline{\underline{\mathbf{B}}}^{\beta}_{j,k}(\phi, \theta)$ and $\underline{\underline{\mathbf{B}}}^{\alpha}_{j,k}(\phi, \theta)$ are equivalent it follows that

$$\underline{\underline{\mathbf{B}}}^{\beta, l, n}_{j,k} = \underline{\underline{\mathbf{B}}}^{\alpha,\ l+j-1,\ -n}_{1-j,\ 1-k} \underline{\underline{\mathbf{H}}}^{-1, 0}$$

and from eq (35b)

$$\underline{\underline{\mathbf{B}}}^{\beta}_{j,k}(2\phi, 2\theta) = \exp [-2i(j-1)\phi] \underline{\underline{\mathbf{B}}}^{\alpha}_{1-j,\ 1-k}(2\phi, -2\theta) \underline{\underline{\mathbf{H}}}^{-1, 0}.$$

Substituting the above expression into eq (29b) yields

$$\underline{\underline{\mathbf{B}}}^{\beta}(\phi, \theta) = \exp [i(\phi + \theta)] \underline{\underline{\mathbf{B}}}^{\alpha}(\phi, -\theta) \underline{\underline{\mathbf{H}}}^{0, 1}$$

and from eqs (31) and (33b)

$$f(\phi, \theta; \phi', \theta') = \underline{\underline{\tilde{\mathbf{B}}}}^{\alpha}(\phi, \theta) \underline{\underline{\mathbf{F}}}^{0} \underline{\underline{\mathbf{B}}}^{\alpha}(\phi', \theta') + \exp [-i(\phi - \phi' + \theta - \theta')] \underline{\underline{\mathbf{H}}}^{0, -1} \underline{\underline{\tilde{\mathbf{B}}}}^{\alpha}(\phi, -\theta) \underline{\underline{\mathbf{F}}}^{0} \underline{\underline{\mathbf{B}}}^{\alpha}(\phi', -\theta') \underline{\underline{\mathbf{H}}}^{0, 1}. \tag{36}$$

The secular equation may be constructed from the B and F matrices for the isolated chain and the interactions between the two chains in the unit cell. Under certain conditions as shall now be shown $\underline{\underline{\mathbf{f}}}'(\phi, \theta)$ reduces to block form.

We assume the polymer possesses a plane of symmetry and that the two chains in the unit cell are coplanar. If the internal coordinate connecting the two chains is a bond stretch directed along the x axis as in figure 1 $\underline{\underline{\mathbf{B}}}^{\alpha}(\phi, -\theta)$ is independent of θ and

$$\underline{\underline{\mathbf{f}}}_{ij}(\phi, \theta; \phi', \theta') = [1 + \exp [-i(\phi - \phi' + \theta - \theta')]] \underline{\underline{\tilde{\mathbf{B}}}}^{\alpha}(\phi, \theta) \underline{\underline{\mathbf{F}}}^{0} \underline{\underline{\mathbf{B}}}^{\alpha}(\phi', \theta'). \tag{37}$$

The quantity $\underline{\underline{\mathbf{f}}}_{ij}(\phi, \theta; \phi', \theta') = 0$ *if* $(\phi', \theta') = (\phi + \pi, \theta)$ or $(\phi', \theta') = (\phi, \theta + \pi)$ and $\underline{\underline{\mathbf{f}}}'(\phi, \theta)$, eq (33a) becomes upon rearrangement

$$\underline{\underline{\mathbf{f}}}'(\phi, \theta) = \begin{bmatrix} f_r(\theta) + f_i(\phi, \theta) & f_i(\phi, \theta; \bar{\phi}, \bar{\theta}) & 0 & 0 \\ & f_r(\bar{\theta}) + f_i(\bar{\phi}, \bar{\theta}) & 0 & 0 \\ c.c. & & f_r(\bar{\theta}) + f_i(\phi, \bar{\theta}) & f_i(\phi, \bar{\theta}; \bar{\phi}, \theta) \\ & & & f_r(\theta) + f_i(\bar{\phi}, \theta) \end{bmatrix} \tag{38}$$

Hence, for interchain interactions directed along the x axis (perpendicular to the chain axis) the chain modes given by ϕ, θ interact with those of the other chain in the unit cell given by $\phi+\pi$, $\theta+\pi$ with the interaction given by $2\underline{\underline{\mathbf{B}}}_1^{\alpha}(\phi, \theta)\underline{\underline{\mathbf{F}}}^{0}\underline{\underline{\mathbf{B}}}_1^{\alpha}(\phi+\pi, \theta+\pi)$.

A dynamical matrix of the form of eq (38) is retained for interchain interactions which couple x and z motions if the chain possesses local C_2 symmetry about the interchain bond as in the case of the honeycomb lattice, figure 1. Consider the internal coordinates which are deformations of the angles formed by the interchain bond in figure 1. The two angles with common apex atom are equivalent because of the local C_2 symmetry. Under the two-fold screw rotation about x these internal coordinates are carried into an equivalent pair in the second chain. These four internal coordinates are therefore equivalent and if the equivalent ones in $\underline{\underline{\mathbf{B}}}_1^{\beta}$ are renumbered it follows that

$$\underline{\underline{\mathbf{B}}}_{j,k}^{\beta,\,l,\,n}=\underline{\underline{\mathbf{B}}}_{1-j,\,1-k}^{\alpha,\,j+l-1,\,n+k}$$

from which it can be shown that

$$\underline{\underline{\mathbf{B}}}^{\beta}(\phi, \theta)=\exp\,[i\,(\phi-\theta)]\,\underline{\underline{\mathbf{B}}}^{\alpha}(\phi, \theta)\,\underline{\underline{\mathbf{H}}}^{-1,\,-1}.$$

For in-plane internal coordinates

$$\underline{\underline{\mathbf{B}}}^{\beta}(\phi, \theta)=-\exp\,[i\,(\phi-\theta)]\,\underline{\underline{\mathbf{B}}}^{\alpha}(\phi, \theta)$$

and eq (38) follows.

4. Example: Honeycomb Lattice

The preceding method will now be applied to the honeycomb lattice shown in figure 1. The in-plane intrachain internal coordinates of the honeycomb lattice are R_1^0, bond stretch and R_2^0, angle bend; one of the set of two equivalent interchain coordinates consists of r_α^0, bond stretch and r_α^{2-5}, angle deformations. Let 2ϵ be the intrachain angle, $s=\sin\,\epsilon$, $c=\cos\,\epsilon$ and r, R the intrachain and interchain bond distances respectively. The intrachain coordinates are

$$\begin{pmatrix}R_1^0\\R_2^0\end{pmatrix}=\begin{pmatrix}0&0\\s/r-c/r\end{pmatrix}\underline{\mathbf{X}}_1^{-1}\begin{pmatrix}c&-s\\-2s/r\;0\end{pmatrix}\underline{\mathbf{X}}_1^{0}+\begin{pmatrix}-c&s\\s/r\;c/r\end{pmatrix}\underline{\mathbf{X}}_1^{1}$$

and the interchain coordinates

$$\begin{pmatrix}r_\alpha^0\\r_\alpha^1\\r_\alpha^2\\r_\alpha^3\\r_\alpha^4\end{pmatrix}=\begin{pmatrix}0&0\\s/r&c/r\\0&0\\0&0\\0&0\end{pmatrix}\underline{\mathbf{X}}_{1,\,1}^{0,\,-1,\,1}+\begin{pmatrix}0&0\\0&0\\0&0\\s/r&c/r\\0&0\end{pmatrix}\underline{\mathbf{X}}_{1,\,1}^{0,\,-1,\,-1}+\begin{pmatrix}-1&0\\s/r&-(c/r+1/R)\\s/r&c/r+1/R\\0&1/R\\0&-1/R\end{pmatrix}\underline{\mathbf{X}}_{0,0}^{0,\,0}$$

$$+\begin{pmatrix}0&0\\0&0\\-s/r&-c/r\\0&0\\0&0\end{pmatrix}\underline{\mathbf{X}}_{0,\,1}^{0,\,0,\,1}+\begin{pmatrix}1&0\\0&1/R\\0&-1/R\\-s/r&-(c/r+1/R)\\-s/r&(c/r+1/R)\end{pmatrix}\underline{\mathbf{X}}_{1,\,0}^{0,\,0,\,1}+\begin{pmatrix}0&0\\0&0\\0&0\\0&0\\s/r&-c/r\end{pmatrix}\underline{\mathbf{X}}_{1,\,1}^{0,\,0,\,-1}$$

From eqs (12 and 13) the dynamical matrix for the isolated chain is, assuming a valence force field,

$$\underline{\underline{\mathbf{F}}}(\theta)=\begin{bmatrix}4\cos^2\theta/2(f_rc^2+4s^2f_\epsilon/r^2\cos^2\theta/2) & 2isc\sin\theta(f_r-4f_\epsilon/r^2\cos^2\theta/2)\\-2isc\sin\theta(f_r-4f_\epsilon/r^2\cos^2\theta/2) & 4f_rs^2\sin^2\theta/2+4f_\epsilon/r^2c^2\sin^2\theta\end{bmatrix}$$

where f_r, f_ϵ are the bond stretch and angle deformation force constants respectively. The interaction matrices are found through eqs (28), (29a), and (37) to be

$$f(\phi,\theta;\phi,\theta)=\begin{bmatrix} 2f_R \sin^2(\phi/2)+8f_\delta s^2/r^2\cos^2\theta/2 & -4if_\delta s/r\sin(\theta)[c/r+\cos^2(\phi/2)/R] \\ 4if_\delta s/r\sin(\theta)[c/r+\cos^2(\phi/2)/R] & 8f_\delta(c^2/r^2\sin^2(\theta/2)+1/R_1^2\cos^2(\phi/2)+2c/rR \\ & \cos^2(\phi/2)\sin^2(\theta/2)) \end{bmatrix}$$

$$f(\phi,\theta;\bar{\phi},\bar{\theta})=\begin{bmatrix} if_R\sin\phi & -2f_\delta s/rR\sin\phi\sin\theta \\ -2f_\delta s/rR\sin\phi\sin\theta & -4if_\delta/R\sin(\phi)(1/R+c/r) \end{bmatrix}$$

where f_R, f_δ are the interchain force constants for bond stretch and angle bend respectively. From $f(\phi,\theta;\phi,\theta)$ and $f(\phi,\theta;\bar{\phi},\bar{\theta})$ the first block of $\underline{\underline{\mathbf{f}}}'(\phi,\theta)$, eq (38), may be constructed. The resultant secular equation may be solved for values of $0\leq\phi\leq\pi/2$ and $0\leq\theta\leq\pi$ to obtain the phonon dispersion curves over the z-extended zone. The variation of phonon energies with $\underline{\mathbf{k}}_z$ for a particular value of $\underline{\mathbf{k}}_x$ are found by folding the phonon dispersion curves about $\theta=90°$.

5. Summary

Utilizing the unit cell symmetry, the dynamical matrix (eq (33a)) of the antiparallel chain lattice has been derived. The elements of this matrix are expressed in terms of the dynamical matrix for the isolated chain and the B and F matrices for the interchain coordinates. The dynamical matrix of the isolated chain and hence that of the lattice may be determined by specifying the internal coordinates of one chemical repeat unit. It was found that with certain types of interchain forces the dynamical matrix of the antiparallel chain lattice may be reduced to block form for arbitrary values of the intrachain and interchain phases. All normal modes may be determined by solving one of the two blocks of resulting secular equation for $0\leq\phi\leq\pi/2$ and $0\leq\theta\leq\pi$. The reduction in the dimensionality of the secular equation with certain types of interchain forces can lead to a significant reduction in computation time especially for more complicated homopolymers such as polyglycine.

The methods used to derive the dynamical matrix of the antiparallel chain lattice may also be applied to other polymeric crystal structures.

6. References

[1] Peticolas, W. L., Hibler, G. W., Lippert, J. L., Peterlin, A., and Olf, H., Appl. Phys. Let. **18**, 87 (1971).
[2] Itoh, K., Nakahara, T., and Shimanouchi, T., Biopolymers **6**, 1759 (1968).
[3] Fanconi, B., and Peticolas, W. L., Biopolymers (in press).
[4] Fukushima, K., Ideguchi, Y., and Miyazawa, T., Bull. Chem. Soc. Japan **36**, 1301 (1963).
[5] Gupta, V. D., Trevino, S., and Boutin, H., J. Chem. Phys. **48**, 3008 (1968).
[6] Small, E. W., Fanconi, B., and Peticolas, W. L., J. Chem. Phys. **52**, 4369 (1970).
[7] Fanconi, B., Small, E. W., and Peticolas, W. L., Biopolymers **10**, 1277 (1971).
[8] Miyazawa, T., J. Chem. Phys. **32**, 1647 (1960).
[9] Gribov, L. A., Opt. Spectrosc. **29**, 465 (1970).
[10] Gupta, V. D., Gupta, A. K., and Krishnan, M. V., Chem. Phys. Letters **6**, 317 (1970).
[11] Wilson, E. B., Jr., J. Chem. Phys. **7**, 1047 (1939).
[12] Higgs, P. W., Proc. Roy. Soc. (London) **A220**, 472 (1953).
[13] Miyazawa, T., J. Chem. Phys. **35**, 693 (1961); **38**, 2709 (1963).
[14] Piseri, L., and Zerbi, G., J. Mol. Spectry. **26**, 254 (1968).
[15] Dean, P., and Bacon, M. D., Proc. Roy. Soc. (London), Ser. **A283**, 64 (1964).

(Paper 76A4–727)

JOURNAL OF RESEARCH of the National Bureau of Standards—A. Physics and Chemistry
Vol. 76A, No. 4, July–August 1962

Publications of the National Bureau of Standards*

Selected Abstracts

Baker, M. A., **Three-year inspection of nature-tone porcelain enamels on steel,** *Nat. Bur. Stand. (U.S.), Tech. Note 707, 16 pages (Dec. 1971) 30 cents, SD Catalog No. C13.46:707.*

Key words: Acid resistance; color; continuity of coating; porcelain enamel; weather resistance.

A weather exposure test on nature-tone porcelain enamels on steel was initiated by the National Bureau of Standards and the Porcelain Enamel Institute in 1966. Laboratory measurements for changes in gloss and color were made after the enamels had been exposed for 0.5, 1 and 3 years at Kure Beach, North Carolina, Miami, Florida and Gaithersburg, Maryland. The average gloss and color retained for all 450 specimens exposed at 3 sites for 3 years were 90.5 and 99.1 respectively. There was a tendency for the enamels exposed at the marine sites to rust around pinhole-type defects. Scanning electron microscope studies of these defects showed a layer of readily corrodible enamel on the bottom of the defects. A high-voltage test for continuity of coating was effective in detecting specimens that were apt to rust during the first year's exposure.

Bechtoldt, C. J., **An x-ray diffraction method for determining the amount of austenite in an austenite-ferrite mixture,** *Nat. Bur. Stand. (U.S.), Tech. Note 709, 15 pages (Feb. 1972) 30 cents, SD Catalog No. C13.46:709.*

Key words: Austenite; computer; ferrite; phase measurement; quantitative analysis; retained austenite; x-ray diffraction.

A method for determining the relative phase volume of austenite in an austenite-ferrite mixture is described in detail. Results obtained by applying this method to an austenite-ferrite stainless steel composite material are presented. The method can be extended to other multi-phase materials.

Bennett, L. H., Editor, **Electronic density of states,** *Nat. Bur. Stand. (U.S.), Spec. Publ. 323, 834 pages (Dec. 1971) $7.75, SD Catalog No. C13.10:323.*

Key words: Band structure; disordered systems; electronic density of states; ion neutralization; Knight shift; magnetic susceptibility; many-body effects; optical properties; photoemission; soft x-ray; specific heat; superconductivity; transport properties; tunneling.

This volume is based on materials presented at the Third Materials Research Symposium of the National Bureau of Standards, held November 3–6, 1969. It provides a review of various experimental and theoretical techniques applied to the study of the electronic density of states in solids and liquids. The topics covered in a series of invited and contributed papers include theory of and experiments to obtain the one-electron density-of-states; many-body effects; optical properties; spectroscopic methods such as photoemission (x-ray and UV), ion neutralization, and soft x-ray; obtaining the density-of-states at the Fermi level by specific heat, magnetic susceptibility, and the Knight shift; the disordered systems of alloys, liquids, dirty semiconductors, and amorphous systems; and superconducting tunneling and the application of density of states to properties such as phase stability. An edited discussion follows many of the papers.

Berry, R. J., Riddle, J. L., **Intercomparison of oxygen boiling point realizations in standards laboratories,** *Metrologia* **7,** *No. 2, 56–58 (1971).*

Key words: IPTS–68; oxygen point.

The experimental realization of the normal boiling point of oxygen maintained in several national standards laboratories are compared.

Block, S., **The user's viewpoint on x-ray diffraction safety standards,** *Proc. Conf. Radiation Safety in X-ray Diffraction and Spectroscopy, University of Pennsylvania, Philadelphia, Pa., Jan. 6–7, 1970 pp. 211–221 (Sept. 1971).*

Key words: Diffraction; fluorescence analysis; radiation safety; x-rays.

The user's point of view on safety standards for x-ray diffraction and fluorescence analysis equipment is presented as part of a panel discussion.

Bloss, R. L., Orloski, M. J., Editors, **Precision measurement and calibration—Mechanics,** *Nat. Bur. Stand. (U.S.), Spec. Publ. 300, Vol.* **8,** *590 pages (Jan. 1972) $6.25, SD Catalog No. C13.10:300/v.8.*

Key words: Acoustics; fluid mechanics; force; gravity; humidity; pressure; strain; vacuum; vibration; viscosity.

This volume is one of an extended series which brings together the previously published papers, monographs, abstracts, and bibliographies by NBS authors dealing with the precision measurement of specific physical quantities and the calibration of the related metrology equipment. The contents have been selected as being useful to the standards laboratories of the United States in tracing to NBS standards the accuracies of measurement needed for research work, factory production, or field evaluation.
Volume 8 consists primarily of published works of the staff of the Mechanics Division of NBS. It includes papers in the fields of acoustics, fluid mechanics, force, gravity, humidity, pressure, strain, vacuum, vibration, and viscosity. Although most of the papers had been previously published, original papers in the fields of "gravity" and "viscosity" are included.

Brady, G. W., Gravatt, C. C., Jr., **Determination of the radial distribution function and the direct correlation function of spheres by x-ray small-angle scattering,** *J. Chem. Phys.* **55,** *No. 10, 5095–5101 (Nov. 15, 1971).*

Key words: Hard sphere fluid; liquids; radial distribution function; small angle x-ray scattering.

An experimental determination of the pair correlation function of polystyrene latex spheres in the high density limit has been made. From this the direct correlation function and the pair potential for hard spheres has been calculated. The significance of these quantities as they bear on the Percus-Yevick and the hypernetted chain approximation are discussed.

Braun, W., Carlone, C., Carrington, T., Van Volkenburgh, G., Young, R. A., **Collisional deactivation of H(2^2P) fluorescence,** *J. Chem. Phys.* **53,** *No. 11, 4244–4248 (Dec. 1, 1970).*

Key words: Deactivation; fluorescence; hydrogen atoms; quenching.

Collision cross sections for deactivation of $H^*(n=2)$ at 300 K have been measured by observations of the quenching of Lyman-α fluorescence in a discharge flow system. The quenchers (with cross section in Å^2) are $H_2(84\pm8)$, $D_2(84\pm8)$, $N_2(62\pm6)$, He(<3). For H^*+H_2, less than 1% of the total quenching produces ions. Care has been taken to work with systems optically thin in Lyman α so

that the rate of escape of radiation, which is the reference to which the quenching rate is compared, is not reduced by resonance trapping.

Carter, G. C., Swartz, J. C., **Nuclear magnetic resonance Knight shifts and quadrupole effects in transition metal diborides,** *J. Phys. Chem. Solids* **32,** *2415–2421 (Jan. 1971).*

Key words: Electric quadrupole coupling constant; Knight shift; NMR; ScB_2; transition metal diborides.

Nuclear magnetic resonance data for ScB_2, YB_2 and MnB_2 are presented. These data together with earlier NMR data provide a complete picture of the 3*d* and 4*d* transition metal diborides: ScB_2 through MnB_2 and YB_2 through MoB_2. The Knight shifts, electric quadrupole coupling constants, and linewidths of the central resonance of the ^{45}Sc and ^{11}B nuclei in ScB_2 are essentially temperature independent in the range 4–300 K. The boron Knight shifts $\kappa(B)$ are 0.00(1)%, −0.004(10)% and −0.05(2)% in ScB_2, YB_2 and MnB_2, respectively. $\kappa(Sc) = 0.07(1)\%$ and $\kappa(Y) = 0.20(3)\%$ in the respective diborides. The difference between these values and the higher values for metallic Sc and Y is attributed primarily to reduced orbital and Pauli contributions. For the 3*d* series ScB_2 to MnB_2, the Knight shifts, electronic specific heats, magnetic susceptibilities and transport properties indicate increasing *d*-electron character with increasing group number. The quadrupole coupling constant of ^{11}B across both 3*d* and 4*d* series does not correlate with the *c*/*a* ratio or unit cell volume. This may indicate deviation of the boron atoms from a planar configuration.

Cashion, J. K., Mees, J. L., Eastman, D. E., Simpson, J. A., Kuyatt, C. E., **Windowless photoelectron spectrometer for high resolution studies of solids and surfaces,** *Rev. Sci. Instr.* **42,** *No. 11, 1670–1674 (Nov. 1971).*

Key words: High resolution electron energy analyzer; photoelectron spectroscopy; photoemission from solids and chemisorbed gases; ultra high vacuum; ultra violet source.

An ultra high vacuum photoelectron spectrometer capable of measuring electron energy distributions for solids and chemisorbed gases at photon energies of 16.8, 21.2, 26.9, and 40.8 eV is described.

Cezairliyan, A., **Recent developments in thermophysical properties research,** *Proc. Committee Thermophysical Properties, Washington, D.C., Dec. 1, 1971, HTD–3, 12–13 (American Society of Mechanical Engineers, New York, N. Y., 1971).*

Key words: High-speed measurements; high temperature; thermophysical properties; thermodynamics.

Recent developments in high-speed measurement of thermophysical properties at high temperatures are summarized. Emphasis is placed on methods that allow the performance of measurements in subsecond duration on electrically conducting substances in the solid phase. High-speed measurements of properties, such as specific heat, electrical resistivity, hemispherical total emittance, normal spectral emittance, and temperatures and energies of phase transitions and transformations are described.

Chang, S. S., Bestul, A. B., **Heat capacity and thermodynamic properties of *o*-terphenyl crystal, glass, and liquid,** *J. Chem. Phys.* **56,** *No. 1, 503–516 (Jan. 1, 1972).*

Key words: Calorimetry; configurational entropy; glass; heat capacity; o-terphenyl; residual entropy; viscosity; vitreous state.

The heat capacity of *o*-terphenyl has been measured with an adiabatic calorimeter for the crystal from 2K to T_m (329.35 K), for the glasses from 2K to T_g (around 240 K) and for the liquid from T_g to 360 K, on a sample with less than 0.005 mol percent impurity. The heat of fusion and the entropy of fusion are 17191 J mol and 52.20 J K^{-1} mol^{-1}, respectively. The residual entropy of the glasses at 0 K is about 15 J K^{-1} mol^{-1}. Above 170 K, heat capacity of the *o*-terphenyl crystal is nearly proportional to the temperature to within 1%. Configurational entropy of the supercooled liquid, estimated from the result of this investigation, is used to relate the relaxation properties of glass-forming liquids according to the theory of Adam and Gibbs. Good agreement is found for both viscosity and NMR correlation frequency data.

Clark, S. K., Editor, **Mechanics of pneumatic tires,** *Nat. Bur. Stand. (U.S.), Monogr. 122, 853 pages, Nov. 1971)* ***$4.75, SD Catalog No. C13.44:122.***

Key words: Friction; rubber; skid; tires; tire cord; tire contact; tire stress; tire structure; vehicles.

The pneumatic tire has been an integral part of automotive transportation almost since its inception, yet it remains a product whose characteristics are not easily predictable or comprehensible by conventional engineering techniques. This treatise is an attempt to provide a rational descriptive and analytical basis for tire mechanics. Chapters of this book are contributed by active research workers in the fields of rubber and textile properties, friction, material properties, tire stress problems, tire design and construction, vehicle skid and handling, and tire mechanical properties.

Cooper, J. W., Kolbenstvedt, H., **Differential energy and angular cross sections for ionization by several-hundred-keV electrons: Theory and comparison and experiment,** *Phys. Rev.* **A 5,** *No. 2, 677–687 (Feb. 1972).*

Key words: Bremsstrahlung; differential cross section; electron ionization; energy losses.

A procedure for calculating cross sections for ionization of electrons in various shells of an atomic differential in both angle and final electron energy is developed. Calculations for ionization of carbon, copper, and gold for incident energies in the range 100–400 keV are presented and compared with recent experimental results.

Cooper, M. J., **Various expansions in thermodynamic scaling,** *Phys. Rev.* **A. 5,** *No. 1, 318–320 (Jan. 1972).*

Key words: Critical region; equation of state; scaling laws; thermodynamic scaling.

Several recently proposed general extensions of thermodynamic scaling are compared and a single comprehensive form suggested.

Dalke, J. L., **International standards for magnetic materials and components,** *IEEE Trans. Magnetics* **MAG–7,** *No. 3, 545–548 (Sept. 1971).*

Key words: IEC; international standards; magnetic components; magnetic materials; magnetic measurements; magnetic standards.

In practically all of the industrially developed countries of the world there are strong national standards organizations. The International Electrotechnical Commission (IEC) coordinates and unifies electrical and electronic standards by drafting international recommendations from which member countries may draw for national standards. The benefits derived from this work include better understanding among electrical and electronic engineers and scientists, and a means for initiating and expanding international trade. The upsurge in development and application of ferrites led the IEC to establish, some fifteen years ago, a committee on ferromagnetic oxide parts which rapidly expanded into a full Technical Committee on Magnetic Materials and Components (TC 51). The magnetic activities include recommendations for: terms and definitions; dimensional standardization; measurement methods; inductors and transformers; data storage devices; strip-wound cores; and laminations; variability (temperature and time); gyromagnetic applications (microwave); and antenna rods. Some eleven TC 51 IEC Publications are now available. Numerous others are in process.

Daney, D. E., **Thermal conductivity of solid argon, deuterium, and methane from one-dimensional freezing rates,** *Cryogenics* **11,** *No. 4, 290–297 (August 1971).*

Key words: Instrument; solid argon; solid deuterium; solidified gases; solid methane; thermal conductivity.

The thermal conductivities of solid argon, deuterium, and methane have been determined near their triple points from measurements

of one-dimensional freezing rates. In this new technique, a cylinder of liquid is frozen axially from one end, and the thermal conductivity of the freezing solid is evaluated from the freezing rate and the cylindrical cell end temperatures. A plastic cell wall offers the advantages of visual observation of the freezing solid and negligible cell wall conduction. The estimated random and systematic errors for the apparatus are 5% and 3% respectively. Improved instrumentation may reduce these errors by one-half.

Dean, J. A., Rains, T. C., **Standard solutions for flame spectrometry,** *Chapter 13 in Flame Emission and Atomic Absorption Spectrometry II, 327–339 (Marcel Dekker, Inc., New York, N.Y., July 1971).*

Key words: Atomic absorption spectrometry; flame emission spectrometry; standard solutions; stock solutions.

The availability of Standard samples and high-purity materials for preparing reference and standard solutions is an important criterion for the solution of an analytical method. For application in the fields of atomic absorption and flame emission spectrometry various types, as well as the source, of standard samples and high purity materials are listed. Procedures for preparing standard stock solutions for 74 elements and special solutions for a variety of matrices are described.

de Graaf, L. A., Mozer, B., **Structure study of liquid neon by neutron diffraction,** *J. Chem. Phys.* **55,** *No. 10, 4967–4973 (Nov. 15, 1971).*

Key words: Correlation function; interatomic potential; neon; neutron diffraction; structure factor.

Neutron-diffraction measurements with high statistical accuracy were performed on liquid neon at 35.05 K and at three different densities. The structure factors $S(\kappa)$, measured to momentum transfers κ of 13.2 Å^{-1}. The data have been used to calculate the radial distribution functions $g(r)$, the direct correlation functions $c(r)$, and effective interatomic potentials.

De Simone, D. V., **Moving to metric makes dollars and sense,** *Harvard Bus. Rev., pp. 100–111 (Jan.–Feb. 1972).*

Key words: Business and industry; economy; education; international relations; international standards; international trade; metric; technology assessment.

The article will be a summary of the report, "A Metric America," which evaluates and distills the findings of the U.S. Metric Study in which thousands of individuals, firms and organized groups, representative of our society, participated. On the basis of all the evidence marshalled in the Study, the report concludes that the United States should change to the metric system through a coordinated national program.

Diller, D. E., **The specific heats (C_v) of dense simple fluids,** *Cryogenics* **11,** *No. 3, 186–191 (June 1971).*

Key words: Density dependence; molecular dynamics; simple fluids; specific heats; temperature dependence.

Most of our knowledge of the thermodynamic properties of dense fluids has previously been derived from high precision *PVT* measurements. However, we wish to demonstrate that direct wide-range specific heat measurements on dense simple fluids give further valuable information on the temperature derivatives of the thermodynamic properties, and that they can also provide a very sensitive test of molecular theories of thermodynamic property behavior. A few publications reporting direct wide-range specific measurements on dense monatomic and diatomic fluids have appeared recently. Among them are publications by Hill and Lounasmaa on Helium-4, by Gladun et al. on neon and krypton, and from this laboratory on parahydrogen, oxygen, and fluorine. The purpose of this paper is to use these direct specific heat measurements to examine further the dependences of the specific heats on temperature and on density, to compare the behavior of the internal specific heats of the classical monatomic fluids with that of several diatomic fluids and quantum fluids, and to compare the behavior of measured specific heats with internal specific heats derived from molecular dynamics calculations.

Dise, J. R., **Recent developments in cement testing,** *Proc. General Technical Committee, Portland Cement Association, San Francisco, Calif., Sept. 22, 1971, Mill Session Papers M–197, 34–42 (1971).*

Key words: Hydraulic cement; testing of cement.

Recent and prospective changes in the physical and chemical tests for hydraulic cements are enumerated; and relevant background information obtained from the records of Committee C–1 on Cement of the American Society for Testing and Materials, and the Cement and Concrete Reference Laboratory at the National Bureau of Standards, is provided.

Domalski, E. S., **Evaluating experimental data on heats of combustion,** *J. Chem. Soc.* **11,** *No. 4, 234–237 (1971).*

Key words: Corrections; data evaluation; heats of combustion; recommendations; selection of best values.

The approach used by data evaluators at the Chemical Thermodynamic Data Center of the National Bureau of Standards for the interpretation of published articles reporting values of the heats of combustion is discussed. An appropriate set of corrections is applied to the values when required to bring all data under study to a common base. Corrections which must be considered are: changes in calibration, reduction of the sample mass to vacuum, changes in atomic mass, reduction to standard states, expression of the data in proper energy units, and bringing the reference temperature for the combustion process to 298.15 K. Some corrections must be estimated because insufficient information is given in certain articles for a standard reanalysis. Guidelines are offered to authors of papers which will provide a maximum amount of data for the re-examination of experimental results, but yet maintain conciseness in the over-all presentation.

Escalante, E., Kruger, J., **Stress corrosion cracking of pure copper,** *J. Electrochem. Soc.* **118,** *No. 7, 1062–1066 (July 1971).*

Key words: Copper; cupric acetate; kinetics; oxidation; stress corrosion; tarnish film.

It is known that the rate of tarnish film formation is an important factor in the stress corrosion cracking (SCC) of brass. Because copper immersed in cupric acetate and sulfate solutions has tarnish film growth rates comparable to those found for brasses susceptible to SCC, it should undergo cracking in such solutions if kinetics play a role. It was found that pure copper is susceptible to cracking in cupric acetate solution but not in cupric sulfate. Light, which retards film formation on copper, but not corrosion, prevents stress cracking in the cupric acetate solution. In the absence of stress, oxide forms all over the copper surface, while stress concentrates oxide formation at the grain boundaries. These experiments point to a brittle-film rupture mechanism of stress cracking.

Evenson, K. M., Day, G. W., Wells, J. S., Mullen, L. O., **Extension of absolute frequency measurements to the cw He-Ne laser at 88 THz (3.39 μ),** *Appl. Phys. Letters* **20,** *No. 3, 133–134 (Feb. 1, 1972).*

Key words: CO_2 laser; helium neon laser; laser frequency measurement; MOM diode; 3.39 μm laser.

The highest absolute frequency measurement yet reported is described. The frequency of the 3.39 μm line from a He-Ne laser oscillating at the methane absorption frequency was found to be 88.376 245 (55) THz. The frequency was measured by beating the 88 THz radiation with the R(30) line from a cw CO_2 laser and a 48 GHz klystron in a tungsten-on-nickel point contact diode. The speed of light calculated from this frequency and previous wavelength measurements is in agreement with the accepted value and of comparable accuracy.

Fatiadi, A. J., Schaffer, R., **Periodic acid as a new oxidant for the degradation of bile pigments. Isolation of a biliverdine**

type of reaction intermediate on oxidation of bilirubin with periodic acid, *Experientia* **27,** *No. 10, 1139–1141 (Oct. 15, 1971).*

Key words: Acid; bile; bilirubin; buliverdine; charge-transfer; complex; degradation; iodine; methyl-sulfoxide; periodic; pigment; structure.

Degradation of porphyrins and bile pigments can be performed with aqueous periodic acid by use of methyl sulfoxide, acetic acid, or tetrahydrofuran as the co-solvent. By the use of methyl sulfoxide as the co-solvent in the oxidation of bilirubin with periodic acid, it was possible to isolate a biliverdine-iodine complex to which a charge-transfer structure has been assigned.

Fickett, F. R., **Aluminum 1. A review of resistive mechanisms in aluminum,** *Cryogenics* **11,** *No. 5, 349–367 (Oct. 1971).*

Key words: Aluminum; electron scattering; magnetoresistivity; resistivity; superconductivity.

Various mechanisms affecting the electrical resistivity of aluminum are reviewed. Brief treatments are given of the theory, experimental techniques, and the results of experiments to measure the effect of phonons, electron-electron interactions, boundaries, vacancies and interstitials, chemical impurities, dislocations, and stacking faults on the resistivity of aluminum at room temperature and below. Also reviewed are experimental data on superconductivity, magnetoresistivity, and the effects of interactions between the various mechanisms. Where appropriate, suggested values are given for the resistivity contribution of a particular mechanism.

Fraker, A. C., Ruff, A. W., Jr., **Studies of oxide film formation on titanium alloys in saline water,** *Corrosion Sci.* **11,** *763–765 (Dec. 1971).*

Key words: Electron microscopy; hot saline water corrosion; oxide films; titanium; titanium alloy corrosion.

Oxide films formed on five titanium alloys were characterized after corrosion in 3.5 wt. percent NaCl solutions over the temperature range of 100 °C–200 °C. Electron transmission microscopy and electron diffraction of corroded thin foils showed the oxide film to be TiO and Ti_2O_3 in the early corrosion stages and to change in the 150 °C–200 °C temperature range to a final surface oxide, TiO_2 (anatase).

Giarratano, P. J., Arp, V. D., Smith, R. V., **Forced convection heat transfer to supercritical helium,** *Cryogenics* **11,** *No. 5, 385–393 (Oct. 1971).*

Key words: Correlations; cryogenics; forced convection; heat transfer; helium; supercritical.

Heat transfer coefficients have been measured for supercritical helium, circulated around a closed flow loop by a miniature centrifugal pump. Reynolds numbers in the 0.208 cm i.d. by 10 cm long stainless steel test section ranged from 1×10^4 to 3.8×10^5 with pressures 3 to 20 atm (0.3 to 2 MNm^{-2}) and fluid temperatures 4.4 to 30 K. Wal-to-bulk temperature ratios varied from approximately 1.3 to 3.0. Results indicate an enhancement in heat transfer as the bulk temperature of the fluid approaches the transposed critical temperatures. This improvement is qualitatively predicted by classical correlations due to the increase of thermal conductivity and specific heat in the region. Over the range of variables included in the measurements it was found that a modification of the Dittus-Boelter heat transfer correlation can be used to predict the heat transfer coefficient satisfactorily for most engineering calculations.

Glass, A. J., Guenther, A. H., **Damage in laser materials: 1971,** *Nat. Bur. Stand. (U.S.), Spec. Publ. 356, 174 pages (Nov. 1971) $1.50, SD Catalog No. C13.10:356.*

Key words: Laser damage; laser materials; self-focusing.

The third ASTM Symposium on Damage in Laser Materials was held at the National Bureau of Standards in Boulder, Colorado, on May 19–20 of this year. The symposium is held as part of the activity of Subcommittee II on Lasers and Laser Materials, of the ASTM. Subcommittee II is charged with the responsibility of formulating standards for laser materials, components, and devices. The chairman of Subcommittee II is John D. Myers, of Owens-Illinois, Inc. Co-chairmen for the damage symposia are Dr. Arthur H. Guenther, of the Air Force Weapons Laboratory, and Professor Alexander J. Glass, Chairman of the Department of Electrical Engineering at Wayne State University.

Approximately 50 attendees at the symposium heard 17 papers on topics relating to laser-induced damage in glass, crystalline materials, nonlinear optical materials, thin film dielectric coatings, and mirrors. Particular attention was given to the processes of plasma formation at dielectric surfaces, and to the role played by self-focusing in bulk damage in solids. The principal recommendations for future investigations are summarized below.

The proceedings of these Symposia represent the major source of information in the field of damage in laser materials. The Symposia themselves, along with the periodic meetings of Subcommittee II, provide a unique forum for the exchange of information regarding laser materials specifications among the manufacturers and users of laser devices, components and systems. The Symposium also serves as a mechanism of information gathering, to enable the Subcommittee to write informed and realistic specifications.

Goldstein, J. I., Yakowitz, H., **Metallic inclusions and metal particles in the Apollo 12 lunar soil,** *Chapter in Proceedings 2nd Lunar Science Conference, Houston, Texas, Jan. 1971, 1, 177–191 (MIT Press, Cambridge, Mass., March 1971).*

Key words: Electron probe microanalyzer; lunar age; lunar materials; meteorites; Scanning Electron Microscopy.

Almost all the reduced metal in the Apollo 12 lunar soil was found as inclusions in the individual soil particles. The inclusions contain $< 0.1 ->$ 20.0 weight % Ni and < 0.1–2.5 weight % Co. These Ni and Co contents are similar to those measured for metal grains in Apollo 12 igneous rocks. Curves of Ni vs. Co contents for meteoritic metal were used to differentiate the meteoritic metal component from the lunar component. On this basis over 80% of the metal areas examined had Ni and Co contents outside of the known meteoritic composition range and were derived from the lunar igneous rocks. The presence of the meteoritic inclusions in the soil particles can be explained by low velocity impacts in the lunar soil during major meteoritic bombardment on the moon.

Six individual metal particles > 125 μm in size, separated from 50 grams of Apollo 12 soil, were studied. Four of the six particles are meteoritic. Two of the meteoritic particles exhibit deformation bands produced by peak shock pressures < 150 kb. The other two meteoritic particles $\sim 1/2$ mm in phosphide-kamacite eutectic structure is present in the other. The structures and compositions of the phases present in these particles indicate either slow cooling or a reheating of these particles on the moon's surface in the 500–600 °C temperature range for a year or more. Most of the meteoritic particles studied were probably originally pieces of chondrites.

Guttman, C. M., **Low-temperature heat-capacity differences between glasses and their crystals,** *J. Chem. Phys.* **56,** *No. 1, 627–630 (Jan. 1, 1972).*

Key words: Crystals; disordered crystal; glasses; heat capacity; low temperature.

It is suggested that the low temperature heat capacity difference between glasses and their crystal may be computed by considering the simple process

$$C_x(V_x) \underset{(a)}{\rightarrow} C_x(V_g) \underset{(b)}{\rightarrow} C_g(V_g)$$

where $C_x(V_x)$ is the constant volume heat capacity of the crystal at its equilibrium volume at normal pressures, V_x, $C_x(V_g)$ is the heat capacity of the substance of identical structure as the crystal but of a volume, V_g, equivalent to that of the glass, and $C_g(V_g)$ is the constant volume heat capacity of the glass. Estimates are made of the change in heat capacity due to step (a) (the change in heat capacity at constant crystal structure due to a volume change) and to step (b) (the change in heat capacity due to disordering at constant volume) for a one dimensional model of a glass and crystal. These suggest that step (a) contributes more to the heat capacity difference

than does step (b). Contributions to step (a) from a three dimensional Debye model show reasonable agreement with experiment.

Hamilton, W. F., Jespersen, J. L., **Application of VLF theory to time dissemination,** *Nat. Bur. Stand. (U.S.), Tech. Note 610, 170 pages (Nov. 1971) $1.50, SD Catalog No. C13.46:610.*

Key words: Diurnal phase; Omega; time; time dissemination; VLF propagation; zonal harmonics.

The characteristics of time dissemination systems are discussed. Particular emphasis is placed on the advantages and problems of very low frequency (VLF) timing systems. The parameters affecting VLF propagation along with causes of variations in these parameters, are discussed. Three methods of computing VLF propagation delays—mode theory, geometric-optics, and zonal harmonics—are compared. The method of zonal harmonics, used for the calculations in this paper, is discussed in more detail. A method of calculating reflection coefficients for a continuously varying ionosphere is described. The theoretical values are compared with experimental measurements. Graphical results of the calculations are included.

Hastie, J. W., Plante, E. R., **Entropy in isotopic systems,** *High Temp. Sci.* **3,** *No. 5, 412–414 (Sept. 1971).*

Key words: Entropy; isotopes; symmetry number; third law.

Many current textbooks and even the research literature appear inadequate in recognizing or discussing certain entropy conventions. The present article elaborates on this question with particular reference given to a recent research article that amply demonstrates the errors that can result from the misunderstanding of entropy conventions in isotopic systems.

Heinrich, K. F. J., **Errors in theoretical correction systems in quantitative electron probe microanalysis—a synopsis,** *Anal. Chem.* **44,** *No. 2, 350–354 (Feb. 1972).*

Key words: Electron probe microanalysis; errors; fluorescence; iteration; x-ray absorption; x-ray emission.

Accurate electron probe microanalysis with simple reference materials requires the use of theoretical models describing the emission of direct and indirect characteristic x-radiation, and of an iterative calculation procedure. The presently accepted theoretical equations for the calculation of intensities are presented, with discussion of the main sources of error. An efficient iteration procedure which uses a hyperbolic approximation to the analytical calibration curve is discussed in detail.

Hellwig, H., Barnes, J. A., Glaze, D. J., Kartaschoff, P., **Frequency shifts due to Ramsey type interrogation in atomic beam tubes,** *Nat. Bur. Stand. (U.S.), Tech. Note 612, 25 pages (Feb. 1972) 35 cents, SD Catalog No. C13.46:612.*

Key words: Cavity phase shift; cesium beam tube; frequency accuracy; frequency standard; power shift; resonance line shape.

Part I: A phase difference between the two interaction regions of a Ramsey excitation resonance structure results in a frequency bias in the measured beam resonance. A simple mathematical model is discussed which describes the dependence of this bias on the phase difference, the microwave power level, the modulation amplitude, and the resonance linewidth. This dependence results from the interaction of the modulated microwave excitation frequency with the asymmetric shape of the slightly shifted resonance line. In a first order approximation, no dependency on the frequency modulation amplitude is expected. Near-linear dependencies on the linewidth and microwave power level which are quite pronounced even at relatively small cavity phase differences are predicted. The theoretical results are compared with one set of experimental data on the microwave power dependence as measured in 1969 with the primary cesium beam standard NBS-III. After a correction is applied to remove the power dependence due to spectral impurity of the microwave excitation, the remaining measured power dependence agrees quantitatively with that calculated using a cavity phase difference of about 3 milliradians.
Part II: One of the most serious effects limiting the accuracy of atomic beam resonators is the uncertainty of phase shifts between the oscillating fields in a Ramsey excitation cavity. A technique using the linewidth dependence on the excitation power to measure the phase-shift induced bias has recently been proposed. The conditions under which this method is valid and their implications on the design of beam optics will be discussed with consideration of available experimental results.

Heydemann, P., **Ultrasonic measurements at very high pressures,** *Phys Acoust.* **8,** *203–236 (1971).*

Key words: Equation of state; high pressure; liquids; solids; ultrasonic measurements.

Ultrasonic measurements are used to determine equations of state for solids and liquids at very high pressures. These measurements are made in piston and cylinder, piston and die, belt or girdle and anvil apparatus. A particularly useful apparatus is the piston and die system with fluid container which is described in greater detail. Often ultrasonic measurements can be combined with isothermal compression measurements to give additional information on c_p/c_v, γ_G and α. Examples of results and estimates of the attainable accuracy are given.

Hockey, B. J., **Plastic deformation of aluminum oxide by indentation and abrasion,** *J. Am. Ceram. Soc.* **54,** *No. 5, 223–231 (May 1971).*

Key words: Abrasion; alumina; annealing; dislocations; electron microscopy; indentation; plastic deformation; surface regions; transmission electron microscopy; twinning.

Transmission electron microscopy provided direct evidence that plastic deformation occurs during the room-temperature indentation and abrasion of Al_2O_3. Examination of single-crystal and polycrystalline specimens showed that high densities of dislocations are produced within the near-surface regions by mechanical polishing with a fine diamond compound (0.25 μm) and that plastic deformation by both slip and mechanical twinning occurs during the placement of Vickers microhardness indentations. The occurrence of plastic deformation in this normally brittle material is considered to be a consequence of the nature and magnitude of the local stresses developed under pointed indenters and irregularly shaped abrasive particles. Preliminary results on the effect of annealing on the retained substructure are also presented. Annealing at 900 °C and higher resulted in the reduction of residual stresses through the motion of dislocations and their rearrangement into lower-energy configurations.

Huie, R. E., Herron, J. T., Davis, D. D., **Absolute rate constants for the reaction of atomic oxygen with 1-butene over the temperature range of 259–493 °K,** *J. Phys. Chem.* **75,** *No. 25, 3902–3903 (1971).*

Key words: Atomic oxygen; flash photolysis; 1-butene; kinetics.

Rate constants for the reaction of atomic oxygen with 1-butene have been measured over a temperature range of 259 to 493 K using the flash photolysis-resonance fluorescence technique. No dependence of rate constance on pressure or reactant concentration was observed. The rate constant for the reaction of atomic oxygen with 1-butene was found to be:

$$k = 1.46 \pm 0.15 \times 10^{-11} \exp\left(\frac{-762 \pm 60 \text{ cal. mol.}^{-1}}{RT}\right).$$

Hust, J. G., Clark, A. F., **The Lorenz ratio as a tool for predicting the thermal conductivity of metals and alloys,** *Mater. Res. Stand.* **11,** *No. 8, 22–24 (Aug. 1971).*

Key words: Alloys; cryogenics; electrical resistivity; electron conductivity; low temperature research; metals; thermal conductivity; thermal resistance.

From a knowledge of the Lorenz ratio of a given class of alloys and a simple electrical resistivity measurement, one can calculate the thermal conductivity of a specimen with reasonable accuracy. A discussion contrasts the characteristic temperature dependence of the

Lorenz ratios, $\rho\lambda/T$ (ρ = electrical resistivity, λ = thermal conductivity, T = temperature) of metals and alloys with high conductivity with that of metals and alloys with low conductivity. An additional classification of alloys in terms of Lorenz ratio further enhances the predictive capabilities of the method. The advantages as well as the limitations of the method are discussed.

Jennings, D. A., Varga, A. J., **Efficient second harmonic generation in ADP with two new fluorescein dye lasers,** *J. Appl. Phys.* **42,** *No. 12, 5171–5172 (Nov. 1971).*

Key words: ADP crystals; dye laser; fluorescein dye; second harmonic generation; tunable UV source.

This paper reports two new solutions of fluorescein dyes for flashlamp-pumped dye lasers. Lasers using these dyes have peak powers on the order of kilowatts and are tunable in the 550–580-nm range. Efficient 90° phase-matched second harmonic generation demonstrated with these and other dyes provides a flash-excited μv source tunable from 250 to 290 nm with peak powers on the order of 10W.

Johns, J. W. C., Olson, W. B., **The infrared spectrum of thioformaldehyde,** *J. Mol. Spectry.* **39,** *No. 3, 479–505 (Sept. 1971).*

Key words: High resolution; infrared; rotational constants; short lived molecule; spectrum; thioformaldehyde.

The infrared spectrum of thioformaldehyde (H_2CS) has been observed in the C–H stretching region. The spectrum was obtained under conditions of high resolution and rotational analyses have been carried out on the three observed bands. The main results (in cm^{-1}) for the excited states are given below.

Band	ν_0	A	B	C
ν_4	3024.61	9.676	0.5893	0.5554
ν_1	2971.03	9.647	0.5906	0.5543
$2\nu_6$(?)	2877.12	9.821	0.5935	0.5533

Several local perturbations have been observed in the two fundamentals ν_4 and ν_1. These are presumably caused by overtones and combinations of the lower lying fundamentals but it has not been possible to make specific assignments of the perturbing levels.

Johnson, D. R., Lovas, F., **A new look at the laboratory microwave spectrum of cyanoacetylene,** *Astrophys. J.* **169,** *617–619 (Nov. 1, 1971).*

Key words: Cyanoacetylene; hyperfine structure; interstellar microwave emission; laboratory microwave spectrum; radio astronomy; rotational transitions.

Laboratory measurements have been made on several rotational transitions in cyanoacetylene with potential application to radio astronomy. Observations of $J=1\leftarrow 0$ and $J=2\leftarrow 1$ rotational transitions are reported for the isotopic species $H^{12}C^{12}C^{12}C^{14}N$, $H^{13}C^{12}C^{12}C^{14}N$, and $H^{12}C^{12}C^{12}C^{15}N$. Measurement errors and resolution of hyperfine structure are discussed in some detail.

Julienne, P. S., Krauss, M., Wahl, A. C., **Hartree-Fock energy curves for $X^2\Pi$ and $^2\Sigma^+$ states of HF^+,** *Chem. Phys. Letters* **11,** *No. 1, 16–20 (Sept. 15, 1971).*

Key words: $D_0^\circ(HF)$; dissociation energy; $De(HF)^+$; Hartree-Fock; photoelectron spectra; vibrational energy levels.

Hartree-Fock energy curves have been calculated for the $X^2\Pi$ and $^2\Sigma^+$ states of HF^+ and applied to an analysis of the photoelectron spectra of HF. The $^2\Sigma^+$ energy curve is found to have a barrier about 0.07 eV high due primarily to a repulsive ion-quadrupole interaction, and a depth of 0.37 eV. This curve will support two bound states and one shape resonance with a half-width of 0.015 eV. The energy curves are probably accurate to 0.1 eV but the analysis shows that results accurate to within 0.03 eV are required to resolve the experimental questions on the dissociation energy for the ground state of HF. The most recent experimental photoelectron results of Berkowitz (following article) encouraged a model calculation of the vibrational states of the $^2\Sigma^+$ state. Assuming a dissociation energy of 0.45 eV and retaining the barrier three bound and one shape resonance vibrational levels are calculated for HF^+ in agreement with the results reported by Berkowitz.

Kestin, J., Paykoc, E., Sengers, J. V., **On the density expansion for viscosity in gases,** *Physics* **54,** *1–19 (1971).*

Key words: Chapman-Enskog theory; correlated collision; density expansion; molecular interaction; thermal conductivity; viscosity.

The paper presents the results of new, precise measurements of the viscosity of nitrogen, argon, and helium at 25 °C. The measurements were performed over a nominal range of pressures 1–100 atm and at very closely spaced density intervals. The data were subjected to a stringent statistical analysis in order to determine whether the density expansion consists of a pure polynomial or whether a term of the form $\rho^2 \ln \rho$ must be included in it. The existence of such a term was discovered theoretically by several investigators. The analysis indicates that if such a term exists, its factor must be very small. Moreover, the statistically significant interval of values which this factor can assume includes zero in it.
This result is interpreted as indicating that correlations which extend over distances of the order of a mean free path are negligible when compared with correlations which extend over distances of the order of the range of molecular interactions.

Kirby, R. K., Rothrock, B. D., **Thermal expansion of platinum to 1900 K and reference materials for thermophysical properties,** *Proc. European Conf. Thermophysical Properties of Solid Materials at High Temperatures, Baden-Baden, Germany, Nov. 11–13, 1968, pp. 600–620 (Feb. 1970).*

Key words: Platinum; standard reference materials; thermal expansion.

The thermal expansion of two specimens of platinum has been measured with a precision optical comparator. A controlled-gradient vacuum furnace was used to heat each specimen to temperatures between 1000 and 1900 K. Within this temperature range the linear thermal expansion of the two specimens is given by

$$\frac{L_T - L_{293}}{L_{293}} \times 10^6 = -2685 + 8.972\,T + 2.505\times 10^{-4} T^2 + 4.641\times 10^{-7} T^3.$$

The National Bureau of Standards is actively engaged in certifying several standard reference materials for thermophysical properties. These include expansivity standards of vitreous silica, borosilicate glass, single-crystal sapphire, copper and tungsten and a calorimetric standard of single-crystal sapphire.

Koonce, C. S., Mangum, B. W., Thornton, D. D., **Magnetic properties of the antiferromagnet $DyPO_4$ in applied fields,** *Phys. Rev. B* **4,** *No. 11, 4054–4069 (Dec. 1, 1971).*

Key words: Antiferromagnet; Bethe-Peierls-Weiss approximation; $DyPO_4$; heat capacity; intermediate state; Ising model; magnetization; molecular field; phase transitions; susceptibility.

The magnetization and susceptibility of the Ising antiferromagnet $DyPO_4$ have been measured as a function of temperature and applied field for samples having demagnetization factors $D \approx 0.02$ and $D \approx 1.0$. Also, the temperature at which peaks in the heat capacity at constant applied field occurred were measured for a number of applied fields. These results have been compared with predictions of the molecular-field approximation and the Bethe-Peierls approximation including long-range dipolar interactions. The temperature below which the antiferromagnetic-paramagnetic transition is first order has been obtained within the molecular-field approximation. In addition, expressions are obtained for the magnitude of the discontinuity in the heat capacity at the transition between the intermediate (or mixed) state and the antiferromagnetic or paramagnetic states for samples having nonzero demagnetization factors. These expressions do not depend on the molecular-field or Bethe-Peierls approximations.

Kuriyama, M., **X-ray Compton-Raman scattering,** *Acta Cryst.* **A27,** *Part 6, 634–647 (Nov. 1971).*

Key words: Absorption; charge correlation; Compton effect; core electrons; current correlation; inelastic scattering; solid; theory; valence electrons; x-ray Raman effect.

The x-ray Compton-Raman scattering is examined from an original point of view. The differential cross section for x-ray inelastic scattering from crystals is derived from first principles to explain the coexisting Compton and Raman scattering in solids. This derivation makes it possible to express the cross section in terms of the current correlation of electrons in a crystal. All the electrons, including the core electrons are treated on an equal basis in this formulation. The relationship between the x-ray absorption spectrum and the inelastic scattering spectrum is discussed in detail. This formulation provides a theoretical justification to the importance of x-ray inelastic scattering experiments in connection with an experimental determination of the two particle Green's function. In the Appendices the theoretical formulations are given in detail, which can apply not only to the ordinary inelastic scattering process, but to the processes involving Bragg diffraction.

Kusuda, T., Editor, **Use of computers for environmental engineering related to buildings,** *Nat. Bur. Stand. (U.S.), Bldg. Sci. Ser. 39, 826 pages (Sept. 1971) $7.75, SD Catalog No. C13.29/2:39.*

Key words: Building heat transfer analysis; energy usage; environmental engineering; heating and air conditioning; use of computers.

This proceedings of the First Symposium on the Use of Computers for Environmental Engineering Related to Buildings contains all of the technical papers and invited addresses presented at the symposium, which was held November 30–December 2, 1970, at the National Bureau of Standards.
The fifty-nine papers deal with the application of the computer to such environmental engineering problems as building heat transfer calculations, heating and cooling load calculations, system simulations, energy usage analyses, computer graphics, air and smoke movement inside buildings, and weather data analyses for load and energy usage calculations.

Lew, H. S., Leyendecker, E. V., Dikkers, D. R., **Engineering aspects of the 1971 San Fernando earthquake,** *Nat. Bur. Stand. (U.S.), Bldg. Sci. Ser. 40, 419 pages (Dec. 1971) $3, SD Catalog No. C13.29/40.*

Key words: Bridge; building; codes; dams; earthquake; earthquake damage; foundation geology; highways; housing; hospital; mobile home; seismic; standards; structural engineering.

Immediately following the San Fernando, California earthquake (Feb. 9, 1971), a four-man team from the Building Research Division of the National Bureau of Standards' Institute for Applied Technology, surveyed the damage to buildings and other structures. This report is based primarily on the data gathered during the survey but includes some data provided by other agencies and individuals. Based on study of these data and observations made during the survey, recommendations are made pertaining to the improvement of building and other structural design and construction practices.

McAlister, A. J., Williams, M. L., Cuthill, J. R., Dobbyn, R. C., **Relation between the 5*d* band structure and soft x-ray $N_{6,7}$ emission spectrum of Au,** *Solid State Commun.* **9,** *1775–1777 (July 1971).*

Key words: Band structure; emission spectrum; gold; N spectrum; soft x-rays.

The $N_{6,7}$ soft x-ray emission spectrum of Au (5*d* to 4*f* transition) has been measured. Distinct structural features are observed. The absolute positions in photon energy of these features are derivable from x-ray and UV induced photoemission spectra. In turn, these experiments agree well with recent band calculations for Au and thus offer further support to the single particle description of the occupied band structure of metals.

McNesby, J. R., Byerly, R., Jr., **Measures for air quality, Annual Report FY 1971,** *Nat. Bur. Stand. (U.S.), Tech. Note 711, 77 pages (Jan. 1972) 70 cents, SD Catalog No. C13.46:711.*

Key words: Air pollution; carbon monoxide; hydrocarbons; nitrogen oxide; ozone; particulates; standard reference materials; sulfur dioxide.

A compilation of reports covering the air pollution related projects at NBS during FY 1971. There are 23 projects in all, and they cover many areas of air pollution measurement. A table of contents lists descriptive project titles.

Maki, A. G., **A high resolution study of *l*-type resonance in cyclopropane,** *J. Mol. Spectrosc.* **41,** *No. 1, 177–181 (Jan. 1972).*

Key words: Cyclopropane; energy levels; infrared; *l*-type resonance; molecular structure; spectroscopy.

The $\nu_5+\nu_{10}$ band of cyclopropane (C_3H_6) centered at 2089.52 cm^{-1} has been measured and analyzed taking into account the *l*-type resonance effect described by Cartwright and Mills. A least squares fit of more than 300 well resolved transitions gave a set of band constants which reproduced the measurements with a standard deviation of 0.003 cm^{-1}. The analysis confirms the *l*-type resonance treatment given by Cartwright and Mills and shows that their band contour fit gave remarkably accurate constants for this band.

Mann, D. B., **Cryogenic flow-metering research at NBS,** *Cryogenics* **11,** *No. 3, 179–185 (June 1971).*

Key words: Cryogenic; flowmetering; liquefied natural gas; liquid hydrogen; liquid nitrogen; measurement.

One very pressing cryogenic problem is that of cryogenic fluid flow measurement. An NBS programme, which focuses attention on the problem, has as its objectives to (1) establish present state-of-the-art by evaluating existing measurement methods, (2) establish methodology to maintain precision and accuracy of field-measurement devices, and (3) establish a comprehensive programme to develop new cryogenic fluid-measurement systems. The scope of this programme includes a precision measurement capability for measuring the flow of liquid nitrogen and liquid argon, a transfer of technology from the traditional cryogenic fluids to measuring the flow of liquefied natural gas and methane, and a concerted effort to develop new mass-flow measurements for cryogenic fluids such as slush or liquid hydrogen. Cryogenic flow-metering history is given as well as a description of three flow facilities that establish experimental confirmation of the cryogenic flow-measurement system under investigation.

Mason, H. L., Peiser, H. S., Editors, **Metrology and standardization in less-developed countries: The role of a national capability for industrializing economics,** *Nat. Bur. Stand. (U.S.), Spec. Publ. 359 390 pages (Dec. 1971) $5.00, SD Catalog No. C13.10:359.*

Key words: Africa; Asia; engineering standards; industrialization; Latin America; less developed countries; measurement standards; NBS; quality control; U.S. AID.

The National Bureau of Standards held a 4-day Seminar in an effort to learn how its experience in metrology and standardization for the science and technology of U.S.A. might be used most effectively for less developed countries. With financial support of the Agency for International Development, participants came from Argentina, Brazil, Ethiopia, Ghana, Guatemala, India, Israel, League of Arab States, New Zealand, Peru, and Vietnam; from several international agencies; and from industries, professional societies, and government in U.S.A. The papers presented and the informal discussions were organized around the session titles:

Perspective
The Sociological, Economic, and Managerial Environment in Industrializing Countries
Making Scientific and Technological Measurement Meaningful
The Dissemination of Information
Promoting More Effective Use of Science and Technology

Additional Case Histories
Promoting Economic Strength and Commercial Equity
Guidance for NBS Technological Assistance Effort

It was concluded that industrializing economies would benefit from NBS activities in these fields, and specific suggestions were offered to that end.

Mentall, J. E., Gentieu, E. P., Krauss, M., Neumann, D., **Photoionization and absorption spectrum of formaldehyde in the vacuum ultraviolet,** *J. Chem. Phys.* **55,** *No. 12, 5471–5479 (Dec. 15, 1971).*

Key words: Formaldehyde; integrated oscillator strength; photoionization coefficient; Rydberg spectrum; SCF calculations; vacuum UV spectrum.

Absorption and photoionization coefficients have been measured for H_2CO in the 600–2000 Å region. Integrated oscillator strengths were determined for a number of strong Rydberg transitions above 1200 Å. From the photoionization curve the first adiabatic ionization potential was found to be 10.87 ± 0.01 eV. As an aid in interpreting the absorption spectrum, theoretical calculations were made using a single-configuration self-consistent field procedure for the Rydberg states and a model which included mixing between the Rydberg and valence states. On this basis weak absorption features between 1340 and 1430 Å have been assigned to the $^1B_1(\sigma \rightarrow \pi^*)$ valence state. The $^1A_1(\pi \rightarrow \pi^*)$ valence state is deduced to be strongly autoionized just above the $^2B_2$ ionization limit.

Mielczarek, S. R., Miller, K. J., **Dependence of generalized oscillator strength of H_2O on momentum transfer,** *Chem. Phys. Letters* **10,** *No. 4, 369–370 (Aug. 15, 1971).*

Key words: Electronic excitation; generalized oscillator strength; H_2O; inelastic electron scattering; momentum transfer.

Experimental results on the dependence of generalized oscillator strengths of water on momentum transfer, showing the appearance of extreme and characteristic features in the electron scattering spectra are reported and discussed.

Mighell, A. D., Santoro, A., **The crystal and molecular structures of hexakis(imidazole)cadmium(II) nitrate, $[Cd(C_3H_4N_2)_6](NO_3)_2$, and hexakis(imidazole)cadmium(II) hydroxide nitrate tetrahydrate, $[Cd(C_3H_4N_2)_6](OH)(NO_3) \cdot 4H_2O$,** *Acta Cryst.* **B27,** *Part 11, 2085–2097 (Nov. 1971).*

Key words: Cadmium complex; $[Cd(C_3H_4N_2)_6](NO_3)_2$; $[Cd(C_3H_4N_2)_6](OH)(NO_3) \cdot 4H_2O$; crystal structure; x-ray.

The crystal and molecular structures of hexakis(imidazole)cadmium (II) nitrate, $[Cd(C_3H_4N_2)_6](NO_3)_2$, and hexakis(imidazole)cadmium (II) hydroxide nitrate tetrahydrate, $[Cd(C_3H_4N_2)_6](OH)(NO_3) \cdot 4H_2O$, have been determined by single-crystal x-ray diffraction techniques. $[Cd(C_3H_4N_2)_6](NO_3)_2$ crystallizes in the trigonal system space group R3. The lattice parameters (hexagonal axes) are $a = 12.633$ (2), $c = 15.049$ (2) Å, $Z = 3$, $\rho_o = 1.54$ g.cm^{-3}, $\rho_c = 1.54$ g.cm^{-3}. The final three-dimensional full-matrix least-squares refinement resulted in an R value of 3.6% based on 1343 observed reflections. $[Cd(C_3H_4N_2)_6](OH)(NO_3) \cdot 4H_2O$ crystallizes in the hexagonal system, space group $P6_3/m$. The lattice parameters are $a = 9.0376$ (8), $c = 21.729$ (3)Å, $Z = 2$, $\rho_c = 1.45$ g.cm^{-3}, $\rho_o = 1.44$ g.cm^{-3}. The final three-dimensional full-matrix least-squares refinement resulted in an R value of 5.4% based on 996 observed reflections. Both structures consist of discrete $Cd(C_3H_4N_2)_6^{2+}$ cations and NO_3^- anions but as a result of the presence of water molecules and OH^- ions in the hydroxide complex, the packing of the cations in the two structures is considerably different. The ligand imidazole molecules are coordinated through the pyridine type nitrogen atoms (N) to the Cd^{2+} ions with an average bond distance Cd . . . N of 2.363 Å and they are hydrogen bonded through the pyrrole type (−N−H) nitrogen atoms to the nitrate groups. However, to accommodate hydrogen bonding, there is considerable difference in the orientation of the imidazole rings in the two complexes. Specifically, each ring in one of the two complex cations is rotated, about the Cd-N(1) direction, approximately 130° with respect to its counterpart in the other cation. The bond distances and angles between the atoms of the imidazole molecules are practically identical in the two structures.

Moore, C. E., **Atomic energy levels—As derived from the analyses of optical spectra, Volume II,** *Nat. Stand. Ref. Data Ser., Nat. Bur. Stand. (U.S.), 35/V.II 259 pages (Dec. 1971) $4.25, SD Catalog No. C13.48:35/V.II.*

Key words: Energy levels; H–V.

This series of three volumes is a critical compilation of atomic energy levels prepared at the National Bureau of Standards from the analyses of optical spectra. Volume I contains data on the spectra of hydrogen, deuterium, tritium, helium, lithium, beryllium, boron, carbon, nitrogen, oxygen, fluoride, neon, sodium, magnesium, aluminum, silicon, phosphorus, sulfur, chlorine, argon, potassium, calcium, scandium, titanium, and vanadium (^{1}H to ^{23}V). Volume II covers the spectra of chromium, manganese, iron, cobalt, nickel, copper, zinc, gallium, germanium, arsenic, selenium, bromine, krypton, rubidium, strontium yttrium, zirconium, and niobium (^{24}Cr to ^{41}Nb). Volume III includes the spectra of molybdenum, technetium, ruthenium, rhodium, palladium, silver, cadmium, indium, tin, antimony, tellurium, iodine, xenon, cesium, barium, lanthanum; hafnium, tantalum, tungsten, rhenium, osmium, iridium, platinum, gold, mercury, thallium, lead, bismuth, polonium, radon, radium, and actinium (^{42}Mo to ^{57}La; ^{72}Hf to ^{89}Ac).

O'Connell, J. S., **Electromagnetic multipole transitions in the recoupling picture, or electron scattering without curls,** *Nat. Bur. Stand. (U.S.), Tech. Note 713, 20 pages (Feb. 1972) 30 cents, SD Catalog No. C13.46:713.*

Key words: Electric transitions; electromagnetic operators; electron scattering; magnetic transitions; multipoles; recoupling.

The formation of the multipole operators from the fundamental charge, current, and moment operators of electron-nucleus scattering is carried through as an angular momentum recoupling problem rather than the usual vector algebra derivation. This point of view allows the electric and magnetic transition operators to be obtained in a simple and intuitive manner. The single particle reduced matrix elements of the charge, current, and moment operators are then calculated in the j–j coupling scheme using a flow chart technique developed by Danos.

Okabe, H., **Fluorescence and predissociation of sulfur dioxide,** *J. Amer. Chem. Soc.* **93,** *No. 25, 7095–7096 (1971).*

Key words: Fluorescence; predissociation; quenching; SO_2.

The fluorescence intensity of SO_2 was measured as a function of incident wavelength in the region 2000 to 2300 Å where dissociation is expected to compete with fluorescence.
A sudden decrease of the fluorescence intensity was observed below the incident wavelength 2189 Å, corresponding to the photon energy of 5.66 eV which agrees almost exactly with the thermochemical threshold of 5.65 eV for dissociation. This indicates that the photodissociation starts to compete with the fluorescence above this photon energy. The quenching rate by Ar of the excited SO_2 produced at 2208 Å is 5×10^{-11} cm^3 molecules^{-1}s^{-1} on the basis of the lifetime of 9 ns calculated from the integrated absorption coefficient. The lifetime decreases to 3.2 ns for the excited state at 2189 Å because of the predissociation.

Payne, J. E., Editor, **Care of books, documents, prints and films,** *Consumer Info. Series 5, 19 pages (Dec. 1971) 45 cents, Stock Number 0303–0941.*

Key words: Films; negatives; paper; photographs; preservation of records; prints; records; repair of records; storage of records; slides.

This paper describes what the average person can do to care for the books, documents, films and prints that he hopes to preserve for a long time. It tells (1) what *can* be done with respect to storage and simple repair, (2) what *not* to do, such as storage in hot attics and damp basements, (3) when to seek professional help and (4) where to go to find more detailed information.

Peterson, C., Thomas, J. L., Cook, H., Editors, **Aluminum wire tables,** *Nat. Bur. Stand. (U.S.), Handb. 109, 66 pages (Feb. 1972) 65 cents, SD Catalog No. C13.11:109.*

Key words: Aluminum conductor; aluminum wire cables; conversion factors; electrical conductivity; electrical conductor; electrical resistivity; standard values; temperature coefficient.

This handbook of aluminum wire tables is a companion publication to NBS Handbook 100, Copper Wire Tables, a review of which is contained in Part I, Sections 1 and 2. Data are presented on the conductivities and resistivities of both solid and stranded wires of various sizes and composition, together with a variety of other data of interest to the designer of electrical equipment and installations. Values are expressed in both U.S. Customary and International System (SI) Units. Wire sizes involved are based on and restricted to those manufactured and typically used in the United States. American Wire Gage sizes are used for the smaller range of conductors from 56 gage through 4/0. Larger conductors are sized on the basis of circular mil area. The alloy compositions included in these tables are EC–0 (annealed), EC–H19, 5005–H19, and 6201–T81; values are given over a temperature range of 0 to 100 °C.

Peterson, W. K., Beaty, E. C., Opal, C. B., **Measurements of energy and angular distributions of secondary electrons produced in electron-impact ionization of helium,** *Phys. Rev.* **A 5,** *No. 2, 712–723 (Feb. 1972).*

Key words: Electron scattering; helium; ionization; secondary electrons.

The energy and angular distributions of electrons produced in the ionization of helium by electrons with energies between 100 eV and 2 keV have been measured in a crossed beam apparatus consisting of a fixed hemispherical energy analyzer and a rotatable electron gun. Distributions of secondary electrons (those electrons departing with energies less than one-half that of the incident primary electrons) were obtained for a wide range of energies and for angles between 30° and 150° with respect to the direction of the incident primary electron beam. The observed angular distributions were significantly different from the results of two early electron impact measurements; however, they agreed to the extent expected with more recent results and with similar proton impact data. For secondary energies above 50 eV and for primary energies greater than 300 eV, the energy distributions (the cross sections integrated over angle) were observed to be very equal to the distribution given by the Mott formula for free-free electron scattering multiplied by the number of electrons in the target.

Phelan, R. J., Jr., Mahler, R. J., Cook, A. R., **High D* pyroelectric polyvinylfluoride detectors,** *Appl. Phys. Letters* **19,** *No. 9, 337–338 (Nov. 1, 1971).*

Key words: Detector; infrared; polyvinylfluoride; pyroelectric.

Polyvinylfluoride plastic films exhibit a normalized detectivity, D* (500 K, 1, 1), of 3×10^8 cm $Hz^{1/2}/W$. This value for the infrared-detector figure of merit is close to the highest available from other pyroelectric materials. A pyroelectric coefficient of 1 nC/cm² K was obtained from the optical response, and a material figure of merit of 1.3×10^{-9} C cm/J was determined.

Powell, R. L., Wagner, P., **Irradiation effects on low temperature thermal and electrical conductivities of two graphites,** *Carbon Letters to Editor* **8,** *690–692 (1970).*

Key words: Electrical conductivity; graphite; neutron irradiation damage; thermal conductivity.

Experiments to determine the effect of radiation on the low temperature (6–100 K) thermal conductivities and electrical resistivities of two commercially available graphites have been performed. Two specimens of H4LM grade graphite with sample axes oriented parallel and perpendicular to the grain respectively and one specimen of Graph-i-tite G with the sample axis oriented parallel to the grain were used for the experiments. The specimens were irradiated in the core of the reactor at a power level of five megawatts for a total exposure of 120 megawatt-hours. Integrated neutron dose was computed to be 1.73×10^{18} nvt and total gamma 3×10^9 rads. The irradiation treatment reduced the thermal conductivity by a factor of about eight at 100 K and was also effective in reducing the temperature coefficient of the thermal conductivity. Similarly, the irradiation caused an increase in the electrical resistivity.

Radebaugh, R., Siegwarth, J. D., **Anomalous thermal resistance between sintered copper powder and dilute He^3-He^4 solutions,** *Phys. Rev. Letters* **27,** *No. 12, 796–799 (Sept. 20, 1971).*

Key words: Copper; cryogenics; dilution refrigerator; helium 3-helium 4; Kapitza resistance; phonon-electron interaction; powder.

The thermal resistances between seven samples of sintered copper powder and a nearly saturated dilute He^3-He^4 solution were measured between 14 mK and 200 mK. All samples showed the anomalously high thermal resistances seen in metal foils, and the values are higher than that given by recent calculations of Seiden. Reproducibility of samples was found to be excellent and room temperature formed oxide layers had no detectable effect.

Rasmussen, A. L., **Measurement of laser energy of linear components of polarization at 1.060 μ,** *Rev. Sci. Instr.* **42,** *No. 11, 1590–1593 (Nov. 1971).*

Key words: Laser calorimeter; laser energy; laser polarization; laser power; reflectivity measurement.

A double reflecting plate calorimeter, described in a previous publication, was used to evaluate the energy components of a pulsed 1.060 μm neodymium laser light beam entering the calorimeter polarized parallel (E_H) and perpendicular (E_V) to a horizontal plane. The relationship between these components varied from $E_H = 0.94\ E_V$ to $E_H = 1.25\ E_V$. Estimated error of E_H and E_V is 2.3%. As a check on the accuracy of polarization component measurements at 1.060 μm, an intercomparison of data was made between this calorimeter and an NBS liquid cell calorimeter. The agreement was about 0.2%.

Reed, R. P., **Materials at low temperatures (A series of review papers) introduction,** *Cryogenics* **11,** *No. 5, 347–348 (Oct. 1971).*

Key words: Cryogenics; material properties; survey.

We intend to present a number of review papers critically evaluating research on particular materials (for example, aluminum) or groups of materials (for example, composites) to assist in appraisal for cryogenic use. Well-qualified experts have been asked to contribute to this series during the next several years.

Reed, R. P., Clark, A. F., Schramm, R. E., **Defect annealing (4 to 295K) after martensitic phase transformation in an Fe-29 Ni alloy,** *Scripta Met.* **5,** *No. 6, 485–488 (June 1971).*

Key words: Electrical resistivity; iron-nickel alloys; martensite; point defects.

It has long been suggested that martensitic phase transformations introduce considerable lattice defects into both the product (martensite, bcc) phase and into any retained parent (austenite, fcc) phase (see, for example, Reed and Breedis (1) and Wayman (2)). We report here the results of experimental resistivity measurements of defect annealing after a martensitic phase transformation in an Fe-29 wt. % Ni alloy. Recovery stages similar to those in iron are identified and we conclude that about 0.5 at. % of point defects are produced by the transformation.

Reimann, C. W., Zocchi, M., Mighell, A. D., Santoro, A., **Crystal and molecular structure of nitratobis-(2,2′-dipyridyl) cobalt(III) hydroxide nitrate tetrahydrate, $[Co(C_{10}H_8N_2)_2(NO_3)](NO_3)(OH) \cdot 4H_2O$,** *Acta Cryst.* **B27,** *Part 11, 2211–2218 (Nov. 1971).*

Key words: Dipyridine and nitrate ligands; hydrogen bonding; monoclinic symmetry; octahedral coordination; transition metal-Co(III)-coordination complex.

The structure of nitratobis-(2,2′-dipyridyl)cobalt(III) hydroxide nitrate tetrahydrate, $[Co(C_{10}H_8N_2)_2(NO_3)](NO_3)(OH) \cdot 4H_2O$, has been determined by single-crystal x-ray diffraction techniques. Crystals of this complex are monoclinic with $a = 10.923(2)$, $b =$

464-124 OL - 72 - 4

15.998(4), $c = 14.442(2)$Å, $\beta = 101.93(2)°$, space group C/2c, $\rho_c = 1.57$ g.cm^{-3}, $\rho_o = 1.54$ g.cm^{-3}, and $Z = 4$. The structure was solved by Patterson and Fourier methods. The cobalt atom is octahedrally coordinated by two molecules of 2,2′-dipyridyl and by a bidentate nitrate group. Water molecules, nitrate groups, and the hydroxide ions are involved in hydrogen bonds which extend continuously in the *a* and *c* directions. The final refinement of the structure by full-matrix anisotropic least-squares analysis resulted in an R value of 6.2%, based on 2995 observed reflections.

Reneker, D. H., Colson, J. P., **Annealing and melting of polyoxymethylene crystals polymerized within irradiated trioxane crystals,** *J. Appl. Phys.* **42,** *No. 12, 4606–4614 (Nov. 1971).*

Key words: Polymerization; polymer annealing; polyoxymethylene; solid state polymerization; trioxane.

Morphological changes produced by the annealing and melting of the polyoxymethylene crystals that polymerize inside irradiated trioxane crystals were observed. The crystals in which the polyoxymethane chains were oriented parallel to the threefold axis of the trioxane underwent major reorganization when held at 184 °C for 30 s. The polyoxymethylene crystals in which the chain axis was inclined at a large angle with respect to the threefold axis of the trioxane transformed and melted at temperatures approximately 5 °C lower.

Robertson, B., **Wyler's expression for the fine-structure constant α,** *Phys. Rev. Letters* **27,** *No. 22, 1545–1547 (Nov. 29, 1971).*

Key words: Conformal group; fine structure constant; relativistic quantum theory; symmetric spaces.

Wyler's expression for α in terms of the Euclidian volumes of certain bounded spaces agrees with experiment only if the radius of these spaces is arbitrarily chosen to equal one. However, the relationship between these spaces and the invariance group $O(n, 2)$ of the *n*-dimensional wave equation is independent of the radius. There is no known reason for setting the radius equal to one.

Romberg, E. F., Wall, N. S., Blum, D., Lightbody, J. W., Jr., Penner, S., **Elastic scattering of 60–120 MeV electrons from ^{46,48,50}Ti,** *Nucl. Phys.* **A173,** *124–128 (1971).*

Key words: Elastic electron scattering; isotopes; radius; ratios; skin thickness; titanium.

The elastic electron scattering from the isotopes ^{46,48,50}Ti has been measured at an angle of 127.5°. The ratios of the cross sections were analysed with a partial-wave analysis for a Fermi-shaped charge distribution and the parameter variations were deduced. Some consequences of these results are discussed.

Sappenfield, K. M., Marinenko, G., Hague, J. L., **Standard Reference Materials: Comparison of redox standards,** *Nat. Bur. Stand. (U.S.), Spec. Publ. 260–24, 97 pages (Jan. 1972)* ***$1.00,*** *SD Catalog No. C13.10:260–24.*

Key words: Analytical procedures; arsenic-iodine method; comparison; effective purity; oxidimetric standards.

The methods described in this publication are those that have been used at the National Bureau of Standards for the comparison of the current oxidimetric standard reference materials with each other and for the determination of the effective purity of these standard reference materials. The methods, which are modifications of well-established and previously published methods, were selected or designed for their accuracy and dependability. An accurate method was devised for the determination of the effective purity of the arsenic trioxide standard SRM 83c by adding solid iodine and determining the excess iodine photometrically.

Schooley, J. F., Soulen, R. J., Jr., **Superconductive transitions suitable as thermometric fixed points,** *Eizo Kanda, Ed., Proc. XII Conf. Low Temperature Physics, Kyoto, Japan, Sept. 3–10, 1970, pp. 833–834 (Keigaku Publishing Co., Tokyo, Japan, March 1971).*

Key words: Low temperature; pure elements; superconductivity; thermometric fixed points.

We have shown that annealed wire samples of Pb, In, Al, Ga, and Zn, when simply prepared and mounted, exhibit superconductive transitions using A.C. susceptibility techniques which are sharper than one millikelvin. These transitions are reproducible to a millikelvin after many thermal cycles over a 20-month period, suggesting their use as thermometric fixed points.

Schroeder, L. W., de Graff, L. A., Rush, J. J., **Neutron diffraction study of the trigonal and cubic phases of NaSH,** *J. Chem. Phys.* **55,** *No. 11, 5363–5369 (Dec. 1, 1971).*

Key words: Crystal structure; ion orientation; libration; neutron diffraction; phase transition; reorientation; sodium hydrosulfide.

Neutron diffraction powder patterns have been measured for the trigonal and cubic phases of NaSH at 296 and 379 K, respectively. Several possible models describing the orientations of the SH^- ion in the trigonal phase were compared with the experimental results. A model in which the SH^- ions are aligned along the trigonal axis gave the best agreement between calculated and observed structure factors. Thus the transition from the cubic to trigonal phase apparently results from the alignment of the SH^- ions along one of the cube diagonals which then becomes shorter than the others resulting in the less symmetric trigonal structure. Several structural models were also considered for the cubic phase. The isotropic, free rotator mode describing the SH^- orientations can be rejected in favor of a less randomly disordered model by comparison with preliminary neutron inelastic scattering data. The limited diffraction data in this phase, however, do not enable a distinction to be made between disordered models. The preliminary inelastic scattering results also indicate that the librational frequencies of the SH^- ions are similar in both phases, but that reorientations of the SH^- ion between equivalent directions occur at a much faster rate ($\sim 10^{12}$ s^{-1}) in the cubic phase.

Selby, M. C., **Bolovac systems for measuring electrical quantities from 0.5 MHz through microwaves,** *Nat. Bur. Stand. (U.S.), Monogr. 123, 24 pages (Jan. 1972)* ***30 cents,*** *SD Catalog No. C13.44:123.*

Key words: BOLOVAC; calibration of current meters through microwaves; calibration of power meters through microwaves; calibration of voltmeters through microwaves; current measurement; disk-type bolometer evaluation; frequency-domain pulse evaluation; measurement of microwave current; measurement of microwave power; measurement of microwave voltage; mismatch error; picosecond rise-time pulse evaluation; power measurement; pulse-rise-time standardization; sampling oscilloscope standardization; spectrum analyzer standardization; termination mismatch error elimination; thin-film bolometers; voltage measurement.

A novel device—the BOLOVAC—is employed in measurement systems that furnish known voltages and currents up to 18 GHz, remove serious difficulties in power measurements, and are applicable in impedance, attenuation and other measurements. Typical of such measurements are the evaluation of rf power sources; calibration of power meters; measurement of net and incident power flow in a system; calibration of signal generators, voltmeters, current meters, picosecond-rise-time pulse-display oscilloscopes, spectrum analyzers; determination of insertion loss of components; and calibration of directional couplers. The Bolovac also serves as an accurately known resistive termination for match or mismatch applications from LF through microwaves.

Sharp, K. G., Coyle, T. D., **Synthesis and some properties of trifluoro(trifluoromethyl)silane,** *J. Fluorine Chem.—Short Communication* **1,** *249–251 (1971).*

Key words: Difluoroiodo(trifluoromethyl)silane; fluorine; fluoroalkylsilanes; silicon; silcon difluoride; trifluoro(trifluoromethyl)silane.

The simplest member of the perfluoroalkylfluorosilane series, CF_3SiF_3 has been prepared in high yield from CF_3SiF_2I and has been definitively characterized. The compound decomposes at 78° to form SiF_4, C_2F_4, and cyclo-C_3F_6. The thermal lability of CF_3SiF_3

can account for equivocal reports in the existing literature regarding synthesis from perfluoroalkyl halides and Si/Cu alloy at high temperatures.

Sullivan, D. B., **Resistance of a silicon bronze at low temperatures,** *Rev. Sci. Instr.* **42,** *No. 5, 612–613 (May 1971).*

Key words: Alloy; bronze; magnetoresistance; resistance; temperature coefficient.

A specially prepared silicon bronze is shown to be quite insensitive to magnetic field and temperature change at liquid helium temperatures. The temperature coefficient of resistance is of the order of a few parts per million per degree over the range 2–10 K and the change in resistance at a flux density of 1 T (10^4 G) is about 10 ppm.

Taylor, J. K., Editor, **Microchemical Analysis Section: Summary of Activities, July 1970 to June 1971,** *Nat. Bur. Stand. (U.S.), Tech. Note 585, 77 pages (Jan. 1972) 70 cents, SD Catalog No. C13.46:585.*

Key words: Air pollution analysis; sulfur dioxide; carbon monoxide; ozone; nitrogen dioxide; fire research; microchemical analysis; particulate analysis.

This report describes the scientific program of the Microchemical Analysis Section of the Analytical Chemistry Division of the National Bureau of Standards, Institute for Materials Research during July 1970 to June 1971. General activities are reported in the areas of air pollution measurement standards including both gases and particulates, in the field of microchemical analysis, in fire research and in electrochemical analysis performed under an international research grant program. A sulfur dioxide standard reference material for use in monitoring ambient atmosphere, and the initial work on a similar standard for stationary sources are described. Research activities on potential standard reference materials for ozone, nitrogen dioxide, and carbon monoxide are also described.

Tsang, W., **Thermal decomposition of 3,4-dimethylhexane, 2,2,3-trimethylpentane, tert-butylcyclohexane, and related hydrocarbons,** *J. Phys. Chem.* **76,** *No. 2, 143–156 (1972).*

Key words: Bond energy; cyclohexyl radical; 3,4-dimethylhexane; heats of formation; *n*-propyl radical; *s*-butyl radical; shock tube; *t*-butyl radical; thermal decomposition; 2,2,3-trimethylpentane.

3,4-Dimethylhexane, 2,2,3-trimethylpentane and tert-butyl cyclohexane have been decomposed in a single pulse shock tube. Rate expressions for the main bond breaking steps are: $k(sC_4H_9 - sC_4H_9 \rightarrow 2sC_4H_9\cdot) = 10^{16.34} \exp(-37{,}900/T)s^{-1}$, $k(sC_4H_9 - tC_4H_9 \rightarrow sC_4H_9\cdot + tC_4H_9\cdot) = 10^{16.30}$ exp $(-36{,}400/T)s^{-1}$, and $k(tC_4H_9 - cC_6H_{11} \rightarrow tC_4H_9\cdot + cC_6H_{11}\cdot) = 10^{16.31} \exp(-37{,}300/T)s^{-1}$. They lead to ΔH_f^{300} $(sC_4H_9\cdot) = 55$ kJ/mol (13.2 kcals/mol), ΔH_f^{300} $(tC_4H_9\cdot)$ kJ/mol (9.3 kcals/mol) and ΔH_f^{300} $(cC_6H_{11}\cdot) = 66$ kJ/mol (15.8 kcals/mol). Rate expressions for the decomposition of all hydrocarbons formed from s-butyl or cyclohexyl radicals and methyl, ethyl, isopropyl, t-butyl, t-amyl, allyl, 1-methylallyl, propynyl, and benzyl radicals have been calculated. Estimates are given for the rates of decomposition of hydrocarbons formed from n-propyl radicals and any of the compounds listed above. The accumulated single pulse shock tube data can now give quantitative information on the initial cracking patterns of almost all aliphatic hydrocarbons. The A-factors determined in this study provide striking confirmation for the earlier observation that this value, per c-c bond, for alkanes is a constant. On this basis, it appears that $D(tC_5H_{11} - H) - D(tC_4H_9 - H) = 5.4$ kJ/mol, $D(sC_4H_9 - H) - D(iC_3H_7 - H) = 3.5$ kJ/mol, and $D(nC_3H_7 - H) - D(C_2H_5 - H) \sim -1.5$ kJ/mol. The absolute magnitude of the A-factors are all at least a factor of 10 lower than expected. It is demonstrated that recent chemical activation and very low pressure pyrolysis studies completely support the shock tube results.

Velapoldi, R. A., Menis, O., **Formation and stabilities of free bilirubin and bilirubin complexes with transition and rare-earth elements,** *Clin. Chem.* **17,** *1165–1170 (1971).*

Key words: Bilirubin degradation; lanthanides; photooxidation; solvent effects; spectral shifts.

We investigated complexes formed between bilirubin and transition or rare-earth elements, and their relative stabilities. Relative rates of complex formation were analogous to metalloporphyrin and metal complex stabilities, according to the Irving-Williams series. Transition metals that formed strong, square planar complexes caused rapid bilirubin degradation. Iron(II) was oxidized to iron(III) in the bilirubin complex. Of the lanthanide complexes, only samarium(III) showed covalent bonding tendencies. Comparative molar absorptivities were calculated for several of the metal-bilirubin complexes. The stability of bilirubin in several solvents and under various experimental conditions is reported. At room temperature, bilirubin photooxidizes to biliverdin on exposure to laboratory light.

Viezbicke, P. P., **NBS frequency-time broadcast station WWV, Fort Collins, Colorado,** *Nat. Bur. Stand. (U.S.), Tech. Note 611, 29 pages (Oct. 1971) 35 cents, SD Catalog No. C13.46:611.*

Key words: High frequency; standard radio frequencies; time-frequency broadcasts; time signals; WWV.

This report describes the design and construction of the National Bureau of Standards frequency-time broadcast station located at Fort Collins, Colorado. The principal function of the station is to broadcast basic standards of frequency and time signals on frequencies of 2.5, 5, 10, 15, 20, and 25 MHz. These high frequency transmissions, which can be received on the simplest of equipment, provide the necessary accuracy required to fulfill some of the needs of industry, Government, and the public. The technical and administrative supervision of the station is under the Time and Frequency Division, Frequency-Time Broadcast Services Section, National Bureau of Standards, Boulder, Colorado.

Wagner, H. L., **Standard reference materials for polymer characterization at the National Bureau of Standards,** *Polymer Preprints, ACS* **12,** *No. 2, 770–774 (1971).*

Key words: Characterization; gel permeation chromatography; light scattering; molecular weight; molecular weight distribution; osmometry; SRM 705; SRM 706; SRM 1475; SRM 1476.

The National Bureau of Standards now has available a total of four Polymer Standard Reference Materials, designed for use in the calibration of instruments employed in polymer characterization. Polystyrene is available in narrow (SRM 705) and broad (SRM 706) molecular weight distributions, while polyethylene whole polymers are available in both high density linear (SRM 1475) and low density branched (SRM 1476) materials. After careful measurements of sample homogeneity, these materials were characterized with respect to weight and number average molecular weight, limiting viscosity number in several solvents, and for the polyethylenes, A.S.T.M. density and A.S.T.M. flow rate. The molecular weight of the branched material has not been certified. In addition, the molecular weight distribution of the linear polyethylene was carefully determined; consequently it is well suited for calibration of gel permeation chromatographs at high temperatures in the molecular weight range of 10^3 to 10^6.

Waynant, R. W., Ali, A. W., Julienne, P. S., **Experimental observations and calculated band strength for the D_2 Lyman band laser,** *J. Appl. Phys.* **42,** *No. 9, 3406–3408 (Aug. 1971).*

Key words: Adiabatic approximation; band strengths; D_2 Lyman emission; emission wavelengths; traveling wave excitation; vacuum ultraviolet laser.

Experimental observations have been made of vacuum ultraviolet laser emission in the Lyman band of D_2. Fourteen lines from 1568 to 1614 Å have been measured to have a total peak power of nearly 1 MW in a short (~1 ns) pulse. To facilitate identification of the laser wavelengths, optical functions were calculated using the adiabatic correction to the usual Born-Oppenheimer approximation. The theory predicts the most probable transitions and these wavelengths agree with experiment to within 0.1–0.2 Å.

Wegstein, J. H., **Manual and computerized footprint identification,** *Nat. Bur. Stand. (U.S.), Tech. Note 712, 13 pages (Feb. 1972) 25 cents, SD Catalog No. C13.46:712.*

Key words: Computerized-footprint-identification; footprint; pattern recognition.

Part 1 describes a manual footprint classification system that utilizes the ridge patterns adjacent to the toes on the sole of the right foot. This system is an extension of the FBI footprint classification system. Part 2 describes a method of coding minute details of these prints for storage in a computerized file. The computer can then search a similarly coded unknown print against this file and identify the most likely matching prints from the file.

Wells, T. E., Gard, E. F., **An integrated system for the precise calibration of four-terminal standard resistors,** *Proc. Conf. Electronic and Electrical Measurements and Test Instrument Conference, Ottawa, Canada, June 1–3, 1971, IEEE Trans. Inst. Meas.* **IM–20,** *No. 4, 253–257 (Nov. 1971).*

Key words: Ampere-turn balance; flux balance; standard resistor; voltage balance.

A description is given of the system currently in use at the National Bureau of Standards for measurements of 1-ohm standard resistors of the Thomas type. A tenfold improvement in accuracy over the former method has been realized. Resistors of this type are now reported to eight decimal places with a total uncertainty of 0.08 ppm. The latter figure includes a three-standard-deviation limit for random errors plus an estimate of systematic errors.
The new system is not only more rapid in operation than the old one (fewer man hours required), but has consistently produced data of superior resolution while operating with a lower test power in resistors. A dc current-linkage balance is used to determine the standard-unknown differences while both are connected in series and totally immersed in a specially designed circular oil bath, which remains completely covered during all tests. Bath temperature is maintained constantly at 25,000 °C (± 0.003 °C) in a unique manner.

White, H. S., Jr., Standards Coordinator, **Guidelines for registering data codes,** *Nat. Bur. Stand. (U.S.), Fed. Info. Process. Stand. Publ. (FIPS Pub.) 19, 7 pages (1972) 20 cents, SD Catalog No. C13.52:19.*

Key words: Data codes; data elements; data processing systems standards; Federal Information Processing Standards; Management Information systems; United States Government.

Office of Management and Budget Circular No. A–86, Standardization of data elements and codes assigns to the National Bureau of Standards responsibility for maintaining registers of data elements and codes and to Federal departments and agencies the responsibility for registering program and agency codes with NBS. This publication provides guidelines for registering data codes with NBS and for reporting the use of the codes to maintaining agencies for purposes of receiving changes.

White, H. S., Jr., Standards Coordinator, **Guidelines for describing information interchange formats,** *Nat. Bur. Stand. (U.S.), Fed. Info. Process. Stand Publ. (FIPS Pub) 20, 11 pages (1972) 25 cents, SD Catalog No. C13.52:20.*

Key words: Data processing systems standards; Federal Information Processing Standards; formatted records; information interchange; United States Government.

This publication provides guidelines which identify and describe the various characteristics of formatted information that should be considered whenever formatted information is interchanged. The objective is to clarify and improve the documentation necessary to effectively provide, process, or use the information involved. The guidelines provided are to be used throughout the Federal Government as a checklist for preparing effective documentation of formatted information interchange.

Wiederhorn, S. M., Johnson, H., **Effect of pressure on static fatigue of glass,** *J. Amer. Ceram. Soc.—Discussions and Notes* **54,** *No. 11, 585 (Nov. 1971).*

Key words: Fracture; glass; high pressure; static fatigue; strength.

The static fatigue behavior of glass at elevated pressures was studied using fracture mechanics techniques. Stress time-to-failure data were obtained on three different glass compositions exposed to high pressure water, 7 kbar. The fracture behavior of glass in water was observed to be insensitive to pressure. It is suggested that this insensitivity resulted from compensating mechanisms in which the increase in fracture resistance arising from a positive activation volume for stress corrosion cracking is balanced by a decrease in fracture resistance due to increased hydroxyl ion concentration at the crack tip.

Wollin, H. F., Compiler and Editor, **National Bureau of Standards Handbook 44–4th Edition–1971, Specifications, Tolerances, and other technical requirements for commercial weighing and measuring devices,** *Superseding Handbook 44–3rd Edition, Nat. Bur. Stand. (U.S.), Handb. 44–Fourth Edition, 207 pages (1971) $2, SD Catalog No. C13.11:44/4.*

Key words: Specifications; tolerances; technical requirements; commercial weighing and measuring devices.

NBS Handbook 44, Fourth Edition, "Specifications, Tolerances, and Other Technical Requirements for Commercial Weighing and Measuring Devices," is a revision of the Third Edition of Handbook 44. This Fourth Edition adopted by the National Conference on Weights and Measures is given legal status in practically every state in the United States.

Yokel, F. Y., Somes, N. F., **Performance criteria for innovation housing systems,** *J. Am. Soc. Eng. Ed.* **61,** *No. 2, 105–107 (Nov. 1970).*

Key words: Building code; building systems; housing; performance criteria; performance testing.

A philosophy for the application of the performance concept to the evaluation of innovative housing systems is evolved, and its application to Operation BREAKTHROUGH is illustrated by examples.

Zalewski, E. F., Keller, R. A., **Tunable multiple wavelength organic-dye laser,** *Appl. Opt.* **10,** *No. 12, 2773–2775 (Dec. 1971).*

Key words: Dye; dye laser; laser.

A technique for simultaneously tuning a dye laser at two different wavelengths has been developed. The apparatus consists of an optical cavity formed by two partially transparent, broad-band mirrors. A diffraction grating is placed along the optical axis outside of each mirror to form a secondary cavity. When the gratings are at the proper angle, there is enough optical feedback through the partially transparent mirrors to cause the laser to emit only at the wavelengths corresponding to the grating angles. Two wavelength outputs with each wavelength separately tunable were obtained from a rhodamine 6G-organic-dye laser using this technique.

Zimmerman, J. E., Frederick, N. V., **Miniature ultrasensitive superconducting magnetic gradiometer and its use in cardiography and other applications,** *Appl. Phys. Letters* **19,** *No. 1, 16–19 (July 1, 1971).*

Key words: Cardiography; gradiometry; instrumentation; Josephson effect; magnetocardiography; magnetometry; superconducting devices.

A portable magnetic gradiometer was built using an rf-biased point contact device as a sensor and a superconducting flux transformer 2.5 cm in diameter by 10 cm long to couple to the gradient of the external field. The instrument is limited by fluctuations which are probably associated with an uneven boiling of the cryogenic liquids and by environmental fluctuations in some locations. It is shown that the inherent sensitivity can be increased by an order of magnitude by increasing the bias frequency from 30 to 300 MHz. A possible use of the instrument as a magnetocardiograph in an unshielded environment was demonstrated.

Zimmerman, J. E., **Sensitivity enhancement of superconducting quantum interference devices through the use of fractional-turn loops,** *J. Appl. Phys.* **42,** *No. 11, 4483–4487 (Oct. 1971).*

Key words: Instrumentation; Josephson effect; Magnetometry; superconducting devices.

A new "fractional-turn" configuration for superconducting quantum interference devices provides enhanced sensitivity, with large loop area and low loop inductance. By operating the new configuration at optimum bias frequency (300 MHz or higher), inherent field sensitivities of 10^{-15} (10^{-11} G) or better can reasonably be expected. The operational sensitivity of an instrument using such a device would probably be limited by externally generated noise in most applications. The configuration is readily adaptable to measurements of both diagonal and off-diagonal components of the field gradient.

Other NBS Publications

J. Res. Nat. Bur. Stand. (U.S.), 76B (Mathematical Sciences), No. 1 & 2 (January–June 1972) SD Catalog No. C13.22/sec.B:76/1&2, $1.25.

Pseudo-random numbers: permutations of triplets. U. Dieter.
Minimax-based selection, adjustment and disaggregation for incompletely specified univariate distributions. A. J. Goldman.
Three results for trees, using mathematical induction. W. A. Horn.
Abstract groups as doubly transitive permutation groups. R. Merris.
Covariances of two sample rank sum statistics. P. Tryon.
Efficient techniques for unbiasing a Bermoulli generator. J. Lechner.
Checks of the algebraic matrices for the configurations $(d+s)^n p$. C. Roth.

Allan, D. W., Gray, J. E., Comments on the October 1970 Metrologia paper "The U.S. Naval Observatory clock time reference and the performance of a sample of atomic clocks," Metrologia **7,** No. 2, 79–82 (April 1971).

Andrews, J. R., An interfacing unit for a 28 psec feedthrough sampling head and a random sampling oscilloscope, Rev. Sci. Instr. **42,** No. 12, 1882–1885 (Dec. 1971).

Andrews, J. R., Horizontal time base sweep generator for a traveling wave oscilloscope, IEEE Trans. Nucl. Sci. **NS-18,** No. 5, 3–8 (Oct. 1971).

Bates, R. G., Paabo, M., Measurement of pH, Handbook of Biochemistry, H. A. Sober, Ed., 2nd Edition, pp. J227–J233 (Chemical Rubber Company, Cleveland, Ohio, Jan. 1971).

Chumas, S. J., Tabulation of voluntary national standards, industry standards, international recommendations and certification programs for consumer products, Nat. Bur. Stand. (U.S.), Tech. Note 705, 74 pages (Dec. 1971) 70 cents, SD Catalog No. C13.46:705.

Eisenhart, C., Youden's Burette Experiment, J. Quality Technol. **4,** No. 1, 20–23 (Jan. 1972).

Ellerbruch, D. A., Microwave methods for cryogenic liquid and slush instrumentation, IEEE Trans. Instr. Meas. **IM-19,** No. 4, 412–416 (Nov. 1970).

Fey, L., Time dissemination capabilities of the Omega system, Proc. 25th Annual Frequency Control Symp., Atlantic City, N.J., April 26–28, 1971, pp. 167–170 (Electronic Industries Association, Washington, D.C., April 1971).

Foote, W. J., A new flange design for O-ring seals, Rev. Sci. Instr. **41,** No. 8, 1237 (Aug. 1970).

Hanson, D. W., Hamilton, W. F., One-way time synchronization via geostationary satellites at UHF, IEEE Trans. Instr. Meas. **IM-20,** No. 3, 147–153 (Aug. 1971).

Kushner, L. M., Technology, product performance, and the consumer, Sci. Teacher **38,** No. 8, 22–26 (Nov. 1971).

Page, C. H., The International System of Units (SI), Phys. Teacher **9,** No. 7, 379–381 (Oct. 1971).

Proctor, T. M., Jr., A passive analyzer for ultrasonic shear waves, J. Acoust. Soc. Amer. **50,** No. 5, 1379–1381 (Nov. 1971).

Radebaugh, R., Siegwarth, J. D., Dilution refrigerator technology, Cryogenics **11,** No. 5, 368–384 (Oct. 1971).

Siegwarth, J. D., Raderbaugh, R., Analysis of heat exchangers for dilution refrigerators, Rev. Sci. Instr. **42,** No. 8, 1111–1119 (Aug. 1971).

**Publications for which a price is indicated are available by purchase from the Superintendent of Documents, U.S. Government Printing Office, Washington, D.C. 20402 (foreign postage, one-fourth additional). The NBS non-periodical series are also available from the National Technical Information Service (NTIS), Springfield, Va. 22151, which was formerly the Clearinghouse. Reprints from outside journals and the NBS Journal of Research may often be obtained directly from the authors.*

U. S. GOVERNMENT PRINTING OFFICE : 1972 OL - 464-124

UNITED STATES
GOVERNMENT PRINTING OFFICE
PUBLIC DOCUMENTS DEPARTMENT
WASHINGTON, D.C. 20402

OFFICIAL BUSINESS
PENALTY FOR PRIVATE USE, $300

POSTAGE AND FEES PAID
U.S. GOVERNMENT PRINTING OFFICE

U.S.MAIL

JOURNAL OF RESEARCH of the National Bureau of Standards
A. Physics and Chemistry

Vol. 76A, No. 4 July–August 1972

Contents

Page

The emf-temperature coefficient of "acid" standard cells of the saturated cadmium sulfate type from 15 to 40 °C. Walter J. Hamer, Anna Skapars, and Bruce F. Field. 321

Pulse radiolysis of neopentane in the gas phase. R. E. Rebbert and P. Ausloos. 329

Anatomy and thermal history of laser self-focusing damage tracks in glass. Wolfgang Haller and Joseph H. Simmons. 337

Normal emissivity of an isothermal, diffusely reflecting cyclindrical cavity (with top) as a function of inside radius. W. B. Fussell. 347

Lattice vibrations of antiparallel chain sheet structures. Bruno M. Fanconi. 351

Publications of the National Bureau of Standards. 361

UNIVERSITY MICROFILMS INC
ATTN SERIALS SECTION
300 NORTH ZEEB RD
ANN ARBOR MICH 48106

Library of Congress Catalog Card Number: 62–37059

For sale by the Superintendent of Documents, U.S. Government Printing Office, Washington, D.C. 20402. (Order by SD Catalog No. C 13.22/sec.A:76/4). Single copy price varies. This issue $1.25. Subscription price $9.50 a year; $2.25 additional for foreign mailing.

UNITED STATES GOVERNMENT PRINTING OFFICE, WASHINGTON : 1972